THE OXIDATION PROPERTIES OF IRON - NICKEL ALLOYS IN CARBON DIOXIDE -CARBON MONOXIDE ATMOSPHERES AT 1000°C

BY

LARRY ARTHUR MORRIS, M. Sc.

OXIDATION PROPERTIES OF IRON - NICKEL ALLOYS

THE OXIDATION PROPERTIES OF IRON - NICKEL ALLOYS IN CARBON DIOXIDE - CARBON MONOXIDE ATMOSPHERES AT 1000°C

By

LARRY ARTHUR MORRIS, M.Sc.

A Thesis
Submitted to the Faculty of Graduate Studies
in Partial Fulfilment of the Requirements
for the Degree
Doctor of Philosophy

McMaster University
October 1965

DOCTOR OF PHILOSOPHY (1965)
(Metallurgy)

McMASTER UNIVERSITY
Hamilton, Ontario

TITLE: The Oxidation Properties of Iron - Nickel Alloys in Carbon Dioxide - Carbon Monoxide Atmospheres at 1000°C

AUTHOR: Larry Arthur Morris, B.A. (McMaster University)
M.Sc. (McMaster University)

SUPERVISOR: Professor W. W. Smeltzer

NUMBER OF PAGES: xi, 148

SCOPE AND CONTENTS:

In this thesis, the results of oxidation tests carried out on iron-nickel alloys in carbon dioxide - carbon monoxide atmospheres at 1000°C are presented. Linear oxidation kinetics were observed for the formation of wustite on alloys containing up to 50 weight % nickel. Spinel oxides appear on alloys containing greater than 50% nickel. A subscale developed in all alloys investigated. An oxidation model is presented for the constant uptake of oxygen based on detailed balancing of the individual reaction steps, assuming that dissociation of carbon dioxide is the rate controlling process. The subscale formation mechanism is based on the principles of diffusion in multicomponent metallic systems. Theoretical relationships are presented which adequately account for the experimental observations.

ACKNOWLEDGEMENTS

Grateful acknowledgement is made to Dr. W. W. Smeltzer for direction and encouragement throughout all stages of this research project.

The author is indebted to Dr. J. S. Kirkaldy for assistance regarding the development of the internal oxidation model and resultant expressions, and to Dr. G. R. Purdy and Mr. H. Walker, Dept. of Metallurgy and Metallurgical Engineering for many helpful discussions concerning electron probe micro analyses. Dr. L. Baker kindly supplied information concerning the problem of gaseous diffusion.

The chemical analyses of the alloys used in this investigation, obtained through the offices of Dr. W. D. Bennett and W. Ott, Falconbridge Nickel Mines Metallurgical Laboratory, Thornhill, Ontario, are appreciated.

This project was supported by grants from the U. S. Air Force Office of Scientific Research, Air Research and Development Command, the Defense Research Board, Ottawa, Canada, to Dr. W. W. Smeltzer, and Steel Co. of Canada Fellowships in Metallurgy awarded the author in 1963 and 1964.

TABLE OF CONTENTS

LIST OF ILLUSTRATIONS

LIST OF TABLES

CHAPTER I

INTRODUCTION

Advances in science and technology have increased the demand for materials capable of withstanding the effects of aggressive environmental conditions. As a result, a wide variety of alloy systems have been developed to overcome the inadequacies of pure metals. In the field of metal oxidation, however, complications arise since the mechanisms of alloy oxidation are more complex and not as well understood as those for pure metals. Numerous oxidation mechanisms are described in the literature, but very few have been formulated on a mathematical basis. Advances in the latter situation are mainly associated with the subject of internal oxidation.

Wagner has attempted to theoretically describe, on a mathematical basis, the mechanism of oxidation for alloys in which one component is or behaves as a noble element. Interesting oxide morphologies may develop~~s~~ if diffusion in the alloy phase is the rate controlling process. Consequently, in the present investigation, experiments were initiated to selectively oxidize iron to wustite from iron - nickel alloys.

Since the diffusive flux of iron in wustite is extremely rapid at elevated temperatures, it was hoped that diffusion in the alloy phase would be rate controlling. Other oxides, in addition to wustite, will form on iron - nickel alloys in air or oxygen; however, these were suppressed by using CO_2 - CO atmospheres as the oxidizing gas. Preliminary tests revealed the formation of subscale in the alloy phase, and that most of these alloys oxidized at linear rates. These observations violate the basic assumptions of present theory. Subsequently, experiments were carried out in order to determine the mechanisms associated with these phenomena.

In the following sections, the results of these experiments are presented. The constant rate of uptake of oxygen from the gas phase is theoretically described in terms of a rate limiting phase boundary reaction, and the internal oxidation process is qualitatively explained on the basis of the principles of diffusion in multicomponent systems. These sections are preceded by a review of metal oxidation theory and publications pertinent to this study.

CHAPTER II

REVIEW OF THE LITERATURE

2.1 Introduction

A metal or alloy in a gaseous environment constitutes a very complex chemical system, and in many cases a concise interpretation of experimental data can only be formulated with difficulty. A few decades ago, many investigators thought that the mechanism of metal oxidation was one of simple diffusion of metal or non-metal ions through the oxide lattice. However, a marked increase in the number of publications in the field of metal oxidation has significantly contributed to the understanding of this complex subject. It is generally accepted that many other factors may influence the reaction process, such as metal and oxide structures and oxide compositions, oxygen solution in the metal phase, nucleation, and mechanical properties of the oxides.

It is the purpose of this chapter to present a summary of metal and alloy oxidation principles incorporating properties of metal oxides, general concepts of metal - gas reactions, empirical and theoretical rate equations and the theories of internal oxidation. A complete description may be had on consulting one of the standard works in this field [1,2,3,4].

2.2 Oxidation of Metals

2.2.1 Oxide Structures

Phenomena in metal - gas reactions may be related to the different zones of activity, namely, the gas phase, the oxide - gas interface, the oxide phase, the metal - oxide interface and the metal phase. In the gas phase, there exists the possibility of gaseous diffusion, whereas adsorption, desorption and solution of gases at the gas - oxide interface may accompany the formation of oxide. In the oxide phase, the diffusion of metal or non - metal ions and the migration of electrons are the most important processes. Electron transfer, formation of oxide, and the solution of metal or non - metal ions into the oxide are predominant at the metal - oxide interface. In the metal phase, a number of processes may occur, such as the solution of various ions with the possible precipitation of oxide, (internal oxidation).

It is necessary to understand the nature of oxide layers before discussing oxidation mechanisms. Practically all oxides are semiconductors, and electrical conduction may occur either by electron holes, (p-type semiconduction), or by electrons, (n-type semiconduction). Wagner(5) et al. proposed that oxide semiconductors are not of exact stoichiometric composition, but may contain an excess of either cations or anions. This excess is accomplished by having cation or anion vacancies or ions in interstitial positions in the lattice. Thus, the model for semiconducting oxides, using a metal deficient oxide as an example, (p-type), is one in which the cation lattice contains vacant sites, and electrical neutrality is maintained by the formation of cations of higher valency or electron holes, as shown in Fig. 1. Electrical conductivity occurs by the movement of electron holes, and ions via cation vacancies.

The model for a metal excess or n-type oxide is one in which there are metal ions and electrons in interstitial positions or anion vacancies in the lattice. Several methods may be employed to test the

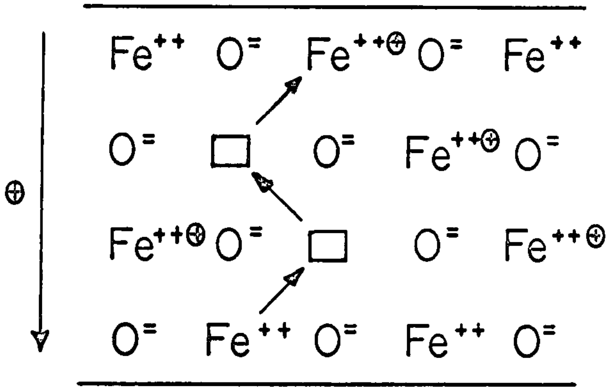

$$1/2\ O_2 = FeO + Fe\overset{++}{\square} + 2\oplus$$

$$Fe + Fe\square + 2\ominus = NIL$$

Fig.1. Model for p-type semiconducting oxide

validity of these models, the most successful being the measurement of electrical conductivity of an oxide as a function of oxygen pressure. The p-type oxide Cu_2O and the n-type oxide ZnO offer good examples to demonstrate the good agreement between conductivity measurements and prediction based on the defect models. Wagner[6,7] predicted and observed that the electrical conductivity of Cu_2O increased with the 8th root of the oxygen pressure. It is assumed that oxygen adsorbed on the oxide reacts with Cu^+ ions to form Cu_2O and a vacancy in the lattice. Cu^+ ions and electrons then migrate from the interior forming new oxide and new defects. One oxygen molecule would lead to the formation of four vacancies and four electron holes;

$$(O_2) = 4Cu^{+}_{\square} + 4\oplus + 2Cu_2O \qquad 2\text{-}1$$

where $Cu^{+}_{\square}$ denotes a cation vacancy and $\oplus$ an electron hole. Applying the law of mass action,

$$\frac{P_{O_2}}{\left[Cu^{+}_{\square}\right]^4 \left[\oplus\right]^4} = \text{constant} \qquad 2\text{-}2$$

where $[\ \ ]$ implies concentration. Since $\left[Cu^{+}_{\square}\right] = \left[\oplus\right]$

$$\left[Cu^{+}_{\square}\right] = \left[\oplus\right] = \text{constant } (P_{O_2})^{1/8} \qquad 2\text{-}3$$

Since the conductivity is proportional to the concentration of electron holes, it should be proportional to the 8th root of the oxygen pressure. This was experimentally verified.

In the case of ZnO, a metal excess oxide, an increase in oxygen potential causes interstitial zinc ions to form new oxide,

$$2Zn_i^{++} + 4e + (O_2) = 2ZnO \qquad 2\text{-}4$$

or

$$2Zn_i^{+} + 2e + (O_2) = 2ZnO \qquad 2\text{-}5$$

where Zn_i^{+} represents an interstitial ion. Applying the ideal mass action law as before, the conductivity, K, is found to be proportional to $(PO_2)^{-1/6}$ or $(PO_2)^{-1/4}$. Experimentally, K varies with $(PO_2)^{-1/3.6}$ to $(PO_2)^{-1/5}$.

The variable composition range of oxides is one of the most important factors when considering metal oxidation reactions. The nature of the defect structure of the oxide which occurs in a particular case determines the oxidation rate. For an oxide layer growing on a metal, an oxygen pressure gradient and a defect gradient exists across the oxide. A concentration gradient within a single solid phase causes diffusion of ions via interstitial or vacant lattice sites. Therefore, it is understandable that a knowledge of the defect structure and nature of the diffusing species is necessary in order to understand the oxidation mechanism.

2.2.2. Oxidation Rates

Although compact oxides grow by a diffusion mechanism, other processes, such as those mentioned above concerning the different zones of activity in metal - gas systems, may be rate controlling, giving rise to a number of empirical rate laws. A major consideration of gas - metal reaction studies is to determine an empirical rate equation and, if possible, theoretical rate equations based on physical theory to explain the kinetics of the reaction. Kinetic data obtained from metal - gas studies are most often compiled in the form of weight gain per unit area, $\Delta m/A$, as a function of time, t. In many cases, the increase in weight can be related to the thickness of the oxide film if the density and molecular volume of the oxide are known.

The simplest rate expression is the linear equation, where the thickness of the oxide film has no influence on the rate of uptake of oxygen:

$$\frac{dx}{dt} = K_L \qquad 2\text{-}6$$

or,

$$\frac{d}{dt}\left(\frac{\Delta m}{A}\right) = K_L' \qquad 2\text{-}7$$

which on integration gives,

$$\left(\frac{\Delta m}{A}\right) = K_L' t + A \qquad 2\text{-}8$$

where K_L' is the linear rate constant and A is a constant. Ideally, $\left(\frac{\Delta m}{A}\right) = 0$ when $t = 0$, therefore, $A = 0$. However, in many cases, only part of a kinetic curve may be described by the linear rates as a result of mixed reaction control during the initial stages of oxidation. In all rate equations which do not pass through the origin, a constant must be added, but, for the sake of simplicity, will be omitted.

If the oxide is non-protective offering no barrier between the gas phase and metal surface, the linear law is expected to hold. Porous or cracked oxides are formed on a number of metals which show a strong tendency to oxidize at a linear rate. These metals generally have a low or high volume ratio of oxide to metal consummed. A low volume ratio suggests that the metal is always exposed to the gas phase. This was suggested by Pilling and Bedworth[8], and become known as the Pilling and Bedworth rule: if the volume ratio of oxide to metal consumed is less than unity, a porous non-protective layer will be formed, and if greater than unity, a compact oxide will be formed. The rule can only be used as a rough guide since there are a number of exceptions. Other rate controlling interface reactions mentioned above and gaseous diffusion of reactants or products may also yield a linear reaction rate.

Tammann[9], and in an independent investigation, Pilling and Bedworth[8], formulated the parabolic rate law. This law is based on rate control by either cation or anion diffusion. The rate of oxidation is inversely proportional to the film thickness:

$$\frac{dx}{dt} = \frac{k}{X} \qquad 2\text{-}9$$

or, on integration,

$$x^2 = 2kt \qquad 2\text{-}10$$

In terms of weight increase,

$$\left(\frac{\Delta m}{A}\right)^2 = k_p t \qquad 2\text{-}11$$

where k_p is the parabolic rate constant.

In some cases, it has been found that kinetic data for metals exposed to oxygen at intermediate temperatures, 300° - 600°C, obey a cubic law,

$$\left(\frac{\Delta m}{A}\right)^3 = k_c t \qquad 2\text{-}12$$

However, the same data often can be approximated by other rate laws.

Finally, thin film formation may be described by a logarithmic relationship,

$$\left(\frac{\Delta m}{A}\right) = k_1 \log(at + t_o) \qquad 2\text{-}13$$

where k_1, a, and t_o are constants, or its alternative, the inverse logarithmic relationship,

$$\frac{1}{(\Delta m/A)} = A - k_{i1} \log t \qquad 2\text{-}14$$

The oxidation rates of metals and alloys rarely agree with a given rate law over a wide range of conditions. The oxidation rates can quite often be divided into definite regions, such as, a linear region followed by a parabolic region. A combination of rate laws is often required. Copper, at low oxygen pressure, oxidizes linearly, then gradually changes to a parabolic rate. This may be written as,

$$\left(\frac{\Delta m}{A}\right)^2 + k_1\left(\frac{\Delta m}{A}\right) = k_2 t \qquad 2\text{-}15$$

which indicates that two processes are rate controlling. In the early stages, $\left(\frac{\Delta m}{A}\right)^2$ is small, and the rate is essentially linear. At a later stage, $\left(\frac{\Delta m}{A}\right)$ is small compared to the first term, and the rate is essentially parabolic.

2.2.3 Effect of Gas Flow, Temperature, Pressure

The major effect of gas flow is to increase the supply of reactant gas and to remove gaseous reaction products. Gas flow affects the transition between interface control and gaseous diffusion control.

The effects of gas pressure and temperature often aid in the interpretation of a reaction mechanism. In many cases, when stable oxides are formed, and at high pressures, (> 1mm), there is no pressure effect or only a very small effect. However, at low pressure, an effect is often observed. The rate of gaseous diffusion to the reaction surface may be rate controlling, and the flux of gaseous molecules is directly proportional to the pressure. If an interface reaction is rate controlling, such as/ the dissociation of a diatomic molecule, one would expect the rate to increase with the square root of the gas pressure. If a diffusion process in the oxide is rate controlling, the oxidation rate-pressure relationship can be quite different depending on the diffusion mechanism. Since the value of the diffusion constant depends upon the concentration of lattice defects, a pressure dependency is expected when the gas pressure has an effect on the defect structure of the oxide, as was illustrated above in the case of Cu_2O.[10]

The effects of temperature may be of assistence for interpretation of reaction mechanisms. Surface reactions may be expected to obey an Arrhenius relation,

$$k = A\, e^{-Q/RT} \qquad 2\text{-}16$$

where k is the oxidation rate constant, A is a constant having the same units as k, and Q is the activation energy required for oxidation. Rates controlled by interface reactions are expected to vary exponentially with temperature. The temperature dependence of diffusion rates can be expressed in the same manner, and therefore, an exponential temperature dependence is expected.

The following summary may be made, in view of four main rate controlling processes,

(1) gas diffusion rate controlling: time has no affect on the rate; a linear pressure dependency is expected; and the effect of temperature is small. The latter effect is a result of the insensitivity of the parameters determining gas diffusion rates to temperature;

(2) interface reaction control: there is no time dependence; a linear or square root of pressure dependence is expected; and the rates are exponentially related to temperature.

(3) diffusion process: this process requires a square root of time dependence and an exponential variation with temperature; however, the effect of pressure depends on the diffusion mechanism;

(4) physical processes, such as mechanical failure of oxides, are complicated; time, pressure and temperature dependencies are unknown.

2.2.4 Oxidation Mechanisms: Thin Films

Several mechanisms have been suggested concerning thin film formation. The processes are less understood than those of scale growth. No attempt will be made to completely describe the theories since descriptions are available in the literature.[1,2,3,4] A division between thin and thick films may be made on the basis of the nature of the concentration gradient providing the driving force for the reaction. Thin films are formed by ion migration under the influence of an electric field across the oxide, whereas thick films are formed by a thermally activated diffusion process in an electrically neutral oxide. A film greater than 10^{-4} cm. is a thick film, since field effects are minimal at this thickness.

Cabrera and Mott[11] proposed a mechanism for thin film formation by assuming that a chemisorbed film exists on the oxide surface, and that ions and electrons move independently in the film. Electrons are able to pass from the metal phase to the adsorbed oxygen atoms, either by thermionic emission or by the quantum mechanical tunnel effect. However, ions cannot readily diffuse through the film at low temperatures. Accordingly a strong electric field is developed across the film which is capable of causing ion migration through the oxide.

In the case of an n-type oxide, Cabrera and Mott derived a parabolic rate equation for films less than 1000 Å for the condition that the diffusion rate was proportional to the field strength. For a p-type oxide, a cubic rate equation was derived. For very thin films, less than 80 Å, the electric field strength is so large that the rate of ion migration is not directly proportional to the field strength. Under these conditions, the drift velocity was exponentially related to the field strength, and an inverse logarithmic rate equation was derived. Evidence for the validity of these equations can be found in the literature.

For formation of oxide films less than 50 Å thick, Hauffe and Ilschner[12] have assumed that electron transfer by the tunnel effect is rate controlling and exponentially related to the field strength. A logarithmic rate equation was derived. Other attempts have been made to derive expressions valid for thin film formation. Grimley and Trapnell[13] suggested that the adsorbed layer of oxygen atoms could be saturated even at low temperatures and pressures. Electrons may be provided by cations at the oxide - gas interface, which undergo a change in valency. In this case, the field is localized to the ion pair. Adsorbed oxygen atoms attract positive holes in p-type oxides, and could form neutral pairs. Dissociation of these neutral pairs by electron transfer from the metal would produce field creating ions. Considerations based upon equilibrium states between neutral pairs and such ions lead to the development of logarithmic, cubic, and linear rate equations. Uhlig[14] also derived logarithmic, and cubic rate equations for formation of films in the thickness range of 10^4 Å by assuming that electron transfer from the metal to the oxide phase determines the oxidation rate.

Since the theoretical derivations are difficult to confirm, many additional detailed investigations are necessary to clarify thin film mechanisms, and the validity of the oxide film models.

2.2.5 Oxidation Mechanisms: Oxide Scales

As oxide formation proceeds to the extent that electron field effects in the film can be neglected, the parabolic rate law is often obeyed by a number of metals and alloys. The mechanism for scale growth according to this law has been described by Wagner.[15] The mechanism is based on the model of a semiconducting oxide. The rate of film growth is controlled by the diffusion of the reactants on a concentration gradient existing across the scale. Wagner derived an expression for the rate of scale growth in terms of the specific conductivity of the scale, K, the transport numbers of the cations, anions, and electrons, and the free energy decrease of the oxidation reaction, quantities that can be measured independently. This expression is,

$$\frac{d\eta}{dt} = \left\{ \frac{300\ A}{96500\ Ne} \int_{\mu_x(m)}^{\mu_x(S)} (\tau_c + \tau_x)\tau_e K \frac{1}{Z_x} \quad du_x \right\} \frac{1}{\xi} \qquad \text{2-17}$$

where $\frac{dn}{dt}$ is the number of gram equivalents of oxide formed per unit time, A is the cross sectional area, N is Avogadro's number, e is the electronic charge, τ_c, τ_a, τ_e are the transport numbers of cations, anions, and electrons respectively. Z_x is the anion valency, $\mu_x(s)$ and $\mu_x(m)$ are the chemical potentials of the anions at the oxide - gas and metal - oxide interfaces, and ξ is the film thickness. The portion of the equation in brackets is called the rational rate constant, k_r.

Wagner[16] also obtained an alternate expression utilizing ion mobilities which can be expressed in terms of the self diffusion constants of the ions, namely,

$$k_r = c_i \int_{a_c(s)}^{a_c(m)} \left(D'_c + \frac{Z_x}{Z_c} D'_x \right) d \ln a_c \qquad 2\text{-}18$$

or,

$$k_r = c_i \int_{a_x(m)}^{a_x(s)} \left(D'_c \frac{Z_c}{Z_x} + D'_x \right) d \ln a_x \qquad 2\text{-}19$$

where $c_i = z_c c_c = z_x c_x$ is the concentration of metal or non - metal ions, a_c and a_x are the thermodynamic activities, and D'_c and D'_x are the self diffusion constants of the metal and non - metal ions respectively.

Equation 2-17 has been experimentally verified for a number of cases[15,17,18] and most rigorously for the oxidation of copper to Cu_2O.[10] Equation 2-18 has been successfully tested for the oxidation of cobalt[19] and iron[20]. Other investigators, notably Hoar and Price[21] Jost[22], have derived special forms of the Wagner relationship using analagous models.

Several other mechanisms have been introduced; in general, they are associated with rate laws other than the parabolic law or deviations from this relationship. Smeltzer et al.[23] noted that titanium, zirconium and hafnium, in the range 300 - 600° C, oxidized too rapidly for the mechanism to be explained by a normal diffusion process. It was postulated that short circuit diffusion paths such as, grain boundaries and dislocations, may exist in the oxide. Two parallel reactions occur, normal lattice migration with a diffusion constant V_L, and short circuit diffusion with constant D_B. They assumed that the fraction of total sites, f, available for the diffusing species within short circuit paths, decreased exponentially with time. The rate equation is as follows:

$$x^2 = k_p \left[t + \frac{f^o \alpha}{k} \left\{ 1 - \exp(-kt) \right\} \right] \qquad 2\text{-}20$$

where x is the film thickness, t is time, k_p the parabolic rate constant, $\alpha = D_B/D_L$ and k is a constant. Excellent agreement was obtained between theory and experimental data.

Mechanisms have been advanced to account for the occurrence of paralinear (parabolic followed by linear) and linear rate laws.[24] These models are usually based on the formation of porous non - protective scales. However, under special conditions, the growth of a compact, pore free scale may follow a linear rate law. For example, owing to the exceptionally high concentration of vacant lattice sites in wustite, iron can diffuse rapidly to the oxide - gas interface, and the surface reaction becomes controlling when the oxidizing potential of the gas phase is low. This behavior would be confined to an oxide of high defect concentration. The proposed mechanisms for this type of oxidation are pertinent to the present investigation, and will be presented in detail in a later section.

2.3 Oxidation of Alloys

2.3.1 General Features

It is not yet possible to predict the oxidation effects to be expected from the addition of an alloying element to a pure metal by a unified theory. A number of factors must be considered; for example, the affinity of the alloy constituents for the components of the reactant gas, the solubility limits of the phases, the diffusion rates of atoms in alloys and in the oxides, the formation of ternary compounds, the relative volumes of the various phases, all of which may be functions of temperature and pressure. Several limiting cases of alloy oxidation have been theoretically treated, and it is hoped that advancements in knowledge will permit the derivation of a more universal theory.

In considering the oxidation of a binary alloy, it is useful to determine if one constituent will behave as a noble element. The free energies of formation and the resultant dissociation pressures of the oxides can be used as a guide. If the oxygen potential is less than that required to form the oxide of one element but exceeds that of the other, the oxide of the latter will be stable and grow. This type of reaction is known as selective oxidation. However, if the oxygen potential is high and exceeds the oxidation potential of both elements, a number of possibilities exists. In very high oxygen potentials, only the presence of a noble element, such as gold, platinum, silver, etc., will permit selective oxidation. Consideration of free energy data will not allow one to speculate concerning the distribution of reaction products.

Some insight may be gained on the distribution of phases if the ternary phase diagram for a binary alloy A-B and oxygen is known for the conditions of diffusive growth of phases and rapid interface reactions as described by Clark and Rhines[25] and Kirkaldy[26]. Once the existance of the more noble element has been determined, it is usually beneficial to consider the possible modes of oxidation.

Moreau and Bènard[27] have presented a very general classification of these different modes based on experimental observations. The classes are illustrated diagramatically in Fig.2. Class I refers to the case of selective oxidation. This classification can be divided into two subgroups, I_A and I_B, where the former concerns the selective oxidation of the minor addition and the latter to the major component. In each case, there appears two possibilities. The oxide of the minor more reactive element may be nucleated and precipitate within the matrix of the major element. The formation process is called internal oxidation, (I_A^1). Another possibility is the formation of an oxide film of the minor element, (I_A^2).

Again two possibilities exist in the case of the selective oxidation of the major element. A thick oxide layer may be formed on the alloy surface, which contains entrapped globules of the addition element, (I_B^1), or the more noble element may concentrate at the metal - oxide interface, and subsequently diffuse back into the metal phase, (I_B^2).

Class II deals with the simultaneous oxidation of both elements. Again it is possible to subgroup the various modes of oxidation. In Class II_A, the oxides are insoluble, and either the minor or the major element has a greater affinity for oxygen. If the minor element has a

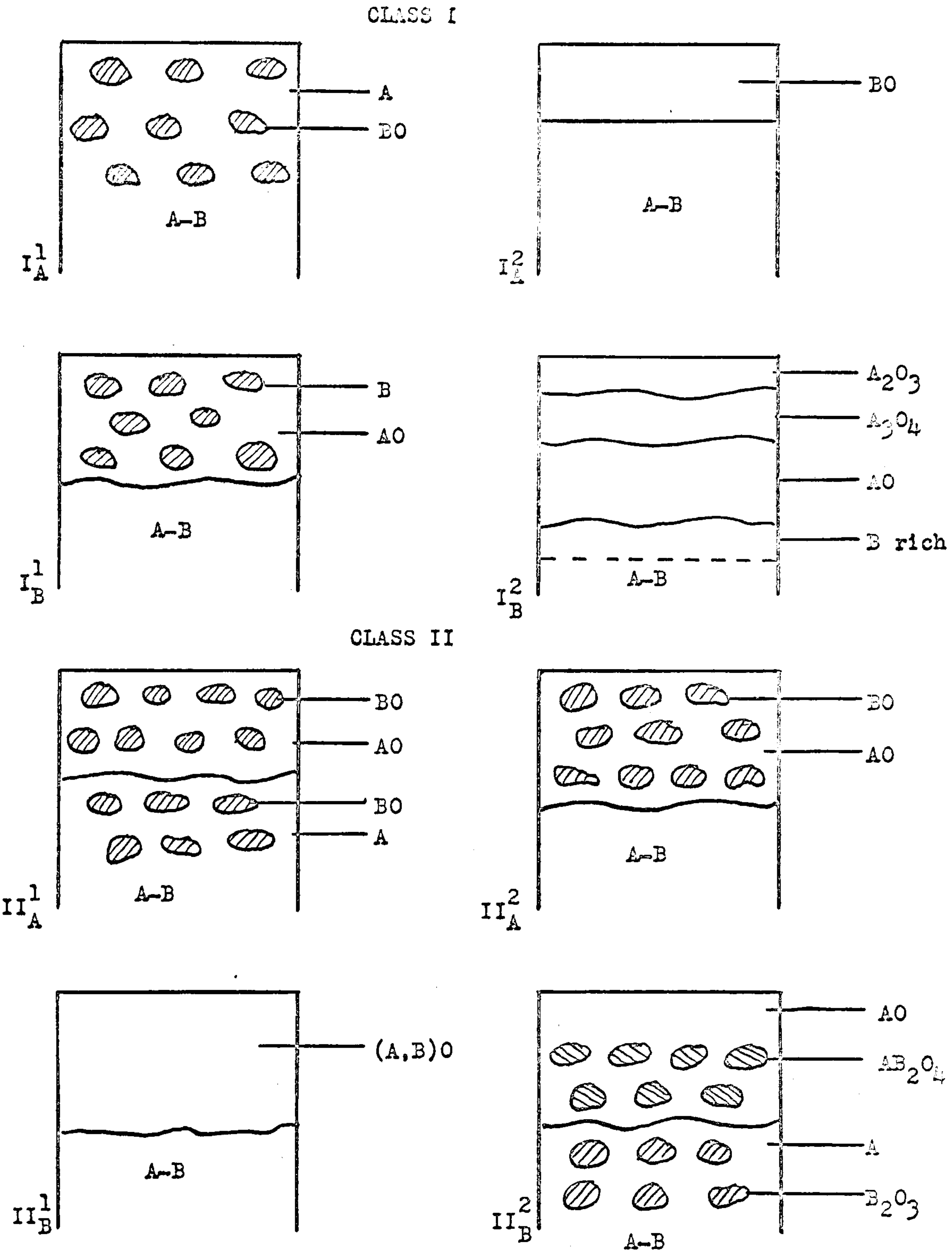

Fig.2. Oxidation Modes of Alloys

higher affinity, its oxide may nucleate on the surface or precipitate as internal oxide. Since the oxide of the major element can form, it will entrap these nuclei or precipitates as the metal - oxide interface recedes. The end result is a dispersion of one oxide in the other and internal precipitates of the former in the metal phase, (II_A^1). If the major element has a greater affinity for oxygen, the process of internal oxidation does not occur as above. Therefore, the reaction product consists of a dispersion of oxide particles in the oxide of the major element, (II_A^2).

The second subgroup refers to mixed oxides, that is oxides in which the two alloying elements are associated. These oxides occur most frequently at high temperatures and oxygen potentials. The simplest case to describe is the formation of a solid solution of one element in the oxide of the other, (II_B^1). The other case concerns the formation of oxides which approach stoichiometric composition, (II_B^2). The most frequent reaction gives rise to a spinel oxide, AB_2O_4.

It can be seen that the above classification is quite general, and introduces some clarity to the complex problem of alloy oxidation. It is unfortunate that variations from these simple cases may occur as a result of mechanical stresses, coalescence of oxides, and other factors often characteristic of particular system.

In the above classification, Moreau and Bènard also considered the additional factor of the appearance of multilayered scales. If a metal exhibits several stable oxides, they may appear in various proportions, depending on conditions of temperature and pressure. The oxide richest in metal will be located adjacent to the metal phase, whereas that richest in oxygen will be nearest the gas phase. Even under conditions of high oxidation potentials, where only the appearance of the most stable oxide is expected, the potential at the metal - oxide interface favours the formation of the other oxides, and these will grow. Examples illustrating these effects are copper base alloys which form cuprous and cupric oxides, and iron base alloys which form wustite, magnetite, and hematite . Valensi[28] has derived an expression for the relative thickness for two oxide layers formed on a metal for ideal and simplified conditions.

2.3.2 Alloy Oxidation Rates

It is necessary to mention that the empirical relationships suggested in section 2.2.2 apply equally as well to alloy oxidation. However, the kinetic data obtained from alloy oxidation experiments often deviate from these ideal rate laws.

The conditions necessary for the parabolic law to hold in alloy systems are as follows. The sequence of reaction layers must not change with time and secondary alteration of the scale structure, such as cracking and phase transformations, must not occur. Interface reactions must be sufficiently rapid for establishment of local thermodynamic equilibrium. In order to define boundary conditions, the composition of the alloy at some point must be the initial composition, and the diffusion constants of the various species should not be a function of concentration.

It is obvious that the overall number of kinetic factors to be considered in any theoretical description of alloy oxidation is rather large. Nevertheless, several attempts have been made to theoretically describe the oxidation mechanism for a few limiting cases.

2.3.3 Alloy Oxidation Mechanisms

2.3.3. (a) Ternary Metal Oxides

Since the oxides formed on alloys are ternary semiconducting layers, the effect of the dissolution of solute metal ions into the oxide layer of the solvent element at least qualitatively may be predicted by the defect models described above. The rate of growth of these compounds depends on their defect concentration which, according to this mechanism, may be increased or decreased by the addition of solute ions.

Consider for example the metal deficit p-type oxide NiO, and the equilibrium,

$$1/2\ O_2 = Ni_{\square}^{++} + 2\oplus + NiO \qquad 2\text{-}21$$

the mass action constant is given by,

$$\left[Ni_{\square}^{++}\right]\left[\oplus\right]^2 = \text{Constant}\ (P_{O_2})^{\frac{1}{2}} \qquad 2\text{-}22$$

the notation being the same as above. If a solute ion of higher valency than 2 is added, it will substitute for nickel ions in the oxide lattice in a higher valence state than nickel, and decrease the concentration of positive holes. The concentration of vacancies increases, and since the oxide grows by diffusion via vacant cation sites, the rate of oxidation is expected to increase. On the other hand, if an ion of lower valancy is added, the concentration of positive holes will increase and the number of vacant sites is reduced on being filled by the solute ion. Therefore, the oxidation rate will be decreased. Those effects have been experimentally verified.[1,2,3,4] Similarily, it can be shown for metal - excess oxides, the addition of ions of higher valency decreases the rate of oxidation, whereas additions of ions of lowervalency increases the rate.

A special case of alloy oxidation, involving diffusion processes within the alloy and external scale, concerns the oxidation properties of a noble metal - base metal system. This situation has been amenable to theoretical analysis and is of particular interest to the present research on the iron - nickel system.

2.3.3. (b) Oxidation of Alloys With Noble Metals

Wagner[29] discussed the oxidation process for a binary alloy in which one component is a noble metal, and for the case of uniform scale formation. The treatment was carried out for the system nickel - platinum where nickel oxide is formed over the entire concentration range, containing only very small amounts of platinum in solid solution. From this analysis, the ratio of the rate of formation of nickel oxide on the alloy to pure nickel for a given thickness of the oxide layer is,

$$\alpha = \frac{1 - (N_{A(e)}/N_{A(i)})^{1/3}}{1 - (N_{A(e)})^{1/3}} \tag{2-23}$$

Here, $N_{A(e)}$ is the equilibrium mole fraction of nickel at the metal - oxide interface coexisting with the oxide and ambient gas, and $N_{A(i)}$ is the equilibrium mole fraction coexisting with the oxide and gas when the gas pressure equals the dissociation pressure of pure nickel oxide. Since concentration gradients exist in the alloy phase as a result of the formation of oxide, impoverishment is relieved by diffusion of nickel from within the bulk alloy to the metal - oxide interface. Applying the proper boundary conditions to the solution of Fick's laws for the model illustrated in Fig.3, an expression was obtained containing the parameters α and $N_{A(i)}$. The theory was compared with experiment by simulteneous solution of the two equations, since the values for the remaining parameters are available in the literature. Reasonable agreement was observed for platinum rich alloys. In order to explain deviations at higher nickel content, several arguments were advanced, including the fact that impurity additions or platinum affect the diffusivity of nickel in the oxide, and the observation by Thomas[30] that these alloys oxidize internally.

The above analysis was based on the premise that a planar metal-oxide interface is stable in noble - base metal alloy systems. Wagner[31] has demonstrated that under certain conditions a planar alloy - oxide interface is not stable. The interface was assumed to be slightly perturbed and take the form of a sine wave profile. Applying Fick's law with appropriate boundary conditions the local drift velocity, u_x, of the metal-oxide interface was calculated in terms of the diffusive flux of the non-noble element. The difference between this velocity and the average velocity of the interface, u_x^A, was determined to be,

$$u_x - u_x^A = - u_x^A (2\pi b \gamma' / \lambda) \sin (2\pi y / \lambda) \qquad 2\text{-}24$$

where b = the amplitude of the sin wave

λ = wave length

y = distance parallel to metal oxide interface

and $\gamma' = (q-1) / (q+1)$

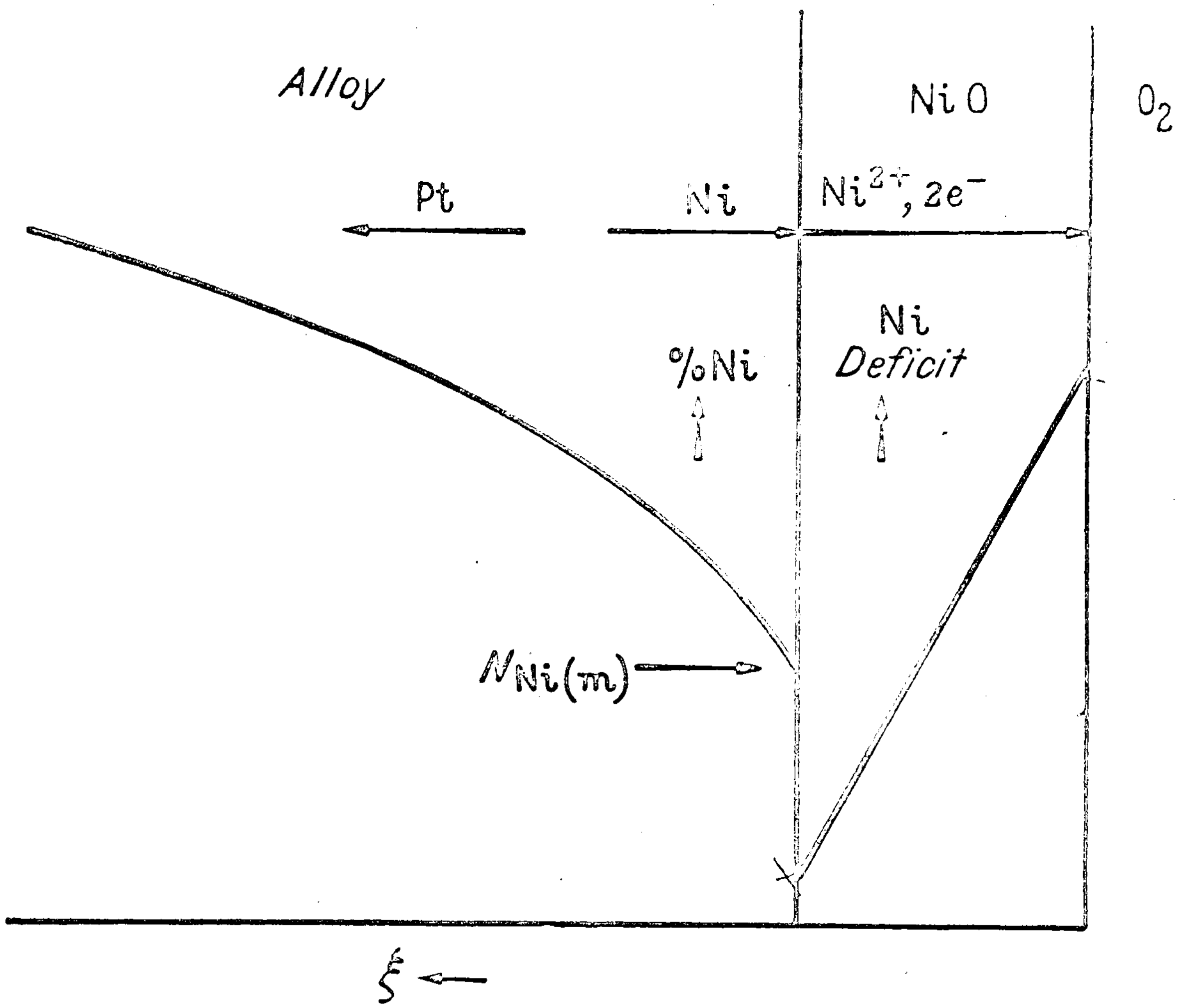

Schematic representation of diffusion processes during the oxidation of nickel–platinum alloys.[29]

Fig.3

In this latter expression,

$$q = \frac{N_A}{1-N_A} \cdot \frac{D'V'}{D''/V''} \qquad 2\text{-}25$$

where N_A = the average mole fraction of less noble element at the average plane interface (x^*).

V', V'' = molar volumes of alloy and oxide respectively,

D' = interdiffusion coefficient in alloy,

D'' = self diffusion coefficient in oxide.

Thus, if diffusion in the oxide is rate controlling, N_A does not differ from the bulk, and $D' > D''$. Therefore, $q > 1$ and deviations from a plane will tend to disappear, that is a planar interface will be stable. If diffusion in the alloy is rate controlling, the value of N_A will be decreased, and $D'' > D'$, therefore, variations in the alloy-oxide interface will be amplified giving rise to a non-planar interface. In the limit, as shown in Fig.4, an interface will be developed where protruding sections of the oxide of the less noble component will alternate with slender trunks of the alloy enriched in the noble element. For this condition of diffusion control in the alloy phase, expressions were derived for the thickness of the oxide film, the thickness of the two phase layer consisting of oxide columns alternating with slender trunks of oxide and the overall rate of oxidation. A purpose of this investigation was to test these idealized mechanisms for the iron-nickel system.

Another interesting situation studied by Wagner[29] concerns an alloy consisting of two components, one of which, A, forms a highly protective oxide compared to that of the other, Class $I_{\underline{A}}^2$, Fig.2. In

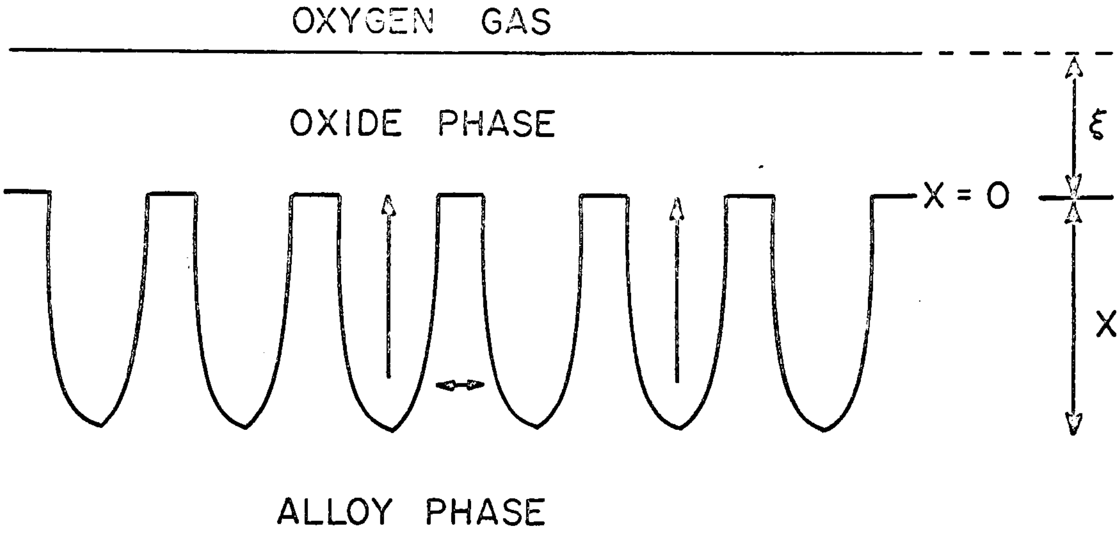

Fig.4. Non - planar interface morphology after Wagner[31]

this case, it is desirable to know the minimum concentration of A required for exclusive formation of a highly protective film, AO. The necessary requirement is that the diffusive supply of A to the metal-oxide interface is at least greater than the consumption of metal. A relationship for the minimum value may be obtained by setting the diffusive flux equal to the rate of consumption. This amount is,

$$N_{\underline{A}}(\text{min}) = \frac{1}{16 Z_{\underline{A}} C} \left(\frac{\pi k_p}{D} \right)^{\frac{1}{2}} \qquad 2\text{-}26$$

where $Z_{\underline{A}}$ = the valency of A

D = diffusivity of A is the metal

k_p = parabolic rate constant

C = concentration of A in the bulk in g-atoms/cm^3

A number of systems, iron - aluminium, iron - chromium, iron - silicon, show qualitative agreement with theory. Rapp[32] found agreement with theory in his investigation of the silver - indium system whereas Mack[33] did not find agreement for copper-beryllium alloys.

2.3.3. (c) Internal Oxidation

A number of investigators [34,35,36] observed that copper alloyed with baser elements such as silicon, manganese, tin, etc., formed a layer of alloy enriched in copper containing oxide particles of these less noble elements beneath an outer scale of cuprous oxide. Smith[34] referred to this layer as a subscale and the formation mechanism as internal oxidation. A very extensive study on the internal oxidation of copper base alloys has been carried out by Rhines[37] and studies on silver base alloys by Rhines and Grobe[38], Leroux and Raub,[39] and Norbury.[40] There are numerous observations reported in the literature concerning subscale formation in iron-base alloys.[41]

Initially, it was thought that internal oxidation would occur if alloys contained small amounts of a more reactive element, which preferentially oxidized within the alloy as a result of oxygen diffusion into the alloy. Rhines and co-workers have stated that it is entirely possible for the oxygen supply to the subscale to originate from the thermal dissociation of an external oxide film at the alloy - oxide interface. It is not necessary for an external scale to be present, since oxygen can be adsorbed from the gas phase and subsequently diffuse into the alloy. When the concentrations of the two reacting species reach values exceeding the equilibrium saturation values of the oxide in question, this oxide may be randomly nucleated and grow.

Rhines described the following conditions necessary for internal oxidation; a relatively high solubility of oxygen in the alloy, appreciable diffusivity of oxygen, possibility of formation by an alloying element of an oxide more stable than the solvent metal, a low solubility of the oxide in the alloy and, the constitution of the system, regarded as a ternary, must be such that a quasi-binary equilibrium may occur between the solid solvent and the precipitating oxide at temperature.

However, objections may be raised concerning the above description of internal oxidation and especially Rhines' third condition as pointed out by Thomas.[30] Oxidation tests, carried out on binary copper-platinum, copper - palladium, nickel - platinum alloys, demonstrated that the oxide of the solvent or host element may constitute the subscale. Therefore, the conditions and description of internal oxidation must be given more generality.

The degree of internal oxidation is dependent on the amount of oxygen fluxed into the alloy interior, which is a function of oxygen solubility and diffusion rate, neglecting the flux of the solute element to the surface. In cases where the oxygen diffusion rate is fast, the oxide particle size is small and the penetration depth is large. Increasing temperature and reacting metal concentration promote a large particle size. In general, the particles are randomly distributed within the alloy matrix and may aquire a variety of shapes. Regarding distribution, Smith[34] has reported an interesting exception. In certain alloys, rows of precipitates were formed parallel to the surface, referred to as Liesegang ring formation. This type of precipitation has been observed, for example, in gels whereby a solute salt is precipitated by the inward diffusion of a suitable reagent. For occurrence of this phenomenon, nucleation can only occur if there is supersaturation of the reactants. Upon precipitation, the growth process depletes the region of the reacting element ahead of the precipitate, thus, further nucleation may occur only at a front at a discrete distance ahead of the previous one.

Theoretical determinations of subscale penetration rates have been carried out for several specific cases. Rhines et al,[42] Darken[43] and Meijering and Druyvesteyn[44] have considered the case when no external scale is formed. These investigators assumed that oxygen saturates the alloy surface and diffuses into the interior, and the oxidizable alloying element diffuses independently outwards forming its oxide with the counter-diffusing oxygen. Applying Fick's laws, expressions were developed for the continuous penetration of the subscale front, which corresponded to a parabolic time dependence. In order to test their expression, Rhines et al. found it necessary to assume the concentration of oxygen and the alloying element went to zero at the subscale-alloy interface. The simplified expression was used to calculate the subscale penetration for a number of copper base alloys[42] and silver base alloys.[38] The agreement with experiment was generally good; however, appreciable deviations occurred with some alloys.

Wagner[45] and Böhm and Kahlweit[46] have adopted a different approach to the same problem. In each case, the subscale front was assumed to obey a parabolic dependence, that is, the thickness of the subscale region is directly proportional to the square root of time. Fick's laws were solved to obtain an expression for the proportionality constant in terms of the oxygen solubility at the surface, the bulk concentration of the alloying element, and the diffusivities of oxygen and alloying element.

In a more extensive analysis, Rhines et al.[42] have derived expressions for the rates of both external scale and subscale growth. The two expressions were of parabolic form. Each equation contained the parabolic rate constants for subscale and external scale growth indicating the interdependencies of the growth rates. The theoretical rate laws were not quite satisfactory for interpretation of several copper base alloys, although disagreement was not too serious. The authors indicated that the assumption that the presence of internal oxide did not interfere with the growth process probably was a source of error.

The third case, where the external and internal oxide consist of the same metal, is of particular interest because similar observations have been made on the iron-nickel system in the present investigation.

Thomas[30] considered the oxidation properties of the copper-platinum, copper-palladium, and nickel-platinum systems at elevated temperatures, and found that all the alloys investigated oxidized internally as well as externally. Also, the same oxides, cuprous and nickel oxide, constituted the external scale and the subscale. Basically, the fundamental problem in this situation was to obtain a satisfactory mechanism to account for internal oxidation. If one component oxidizes preferentially to form an external scale, the oxygen potential or pressure at the metal-oxide interface is equal to the dissociation pressure of that oxide. For an ideal solution, the oxygen pressure, everywhere in the metal phase, would be lower than that required to precipitate oxide. Therefore, Thomas proposed that a small amount of noble metal dissolved in the oxide increases the dissociation pressure of the oxide. To confirm this hypothesis, it was demonstrated experimentally that a very small amount of platinum or palladium was in solid solution in cuprous oxide. The noble metal concentration was highest at the alloy-oxide interface, and decreased with distance from this interface. Therefore, the partial pressure of oxygen at the subscale-alloy interface is less than that at the alloy-oxide interface, and this pressure gradient represents the driving force for diffusion of oxygen across the subscale.

The model presented by Thomas is shown in Fig. 5. Copper diffuses through the subscale on the concentration gradient $(N_{Cu(i)} - N_{Cu(m)})/\xi_i$ and enters the scale as ions. These ions diffuse through the oxide on the gradient $(N_{+(m)} - N_{+(s)})/\xi_e$ to react with oxygen. At m, cuprous oxide dissociates into copper and oxygen atoms, and oxygen diffuses through the subscale on the concentration gradient $(N_{O(m)} - N_{O(i)})/\xi_i$

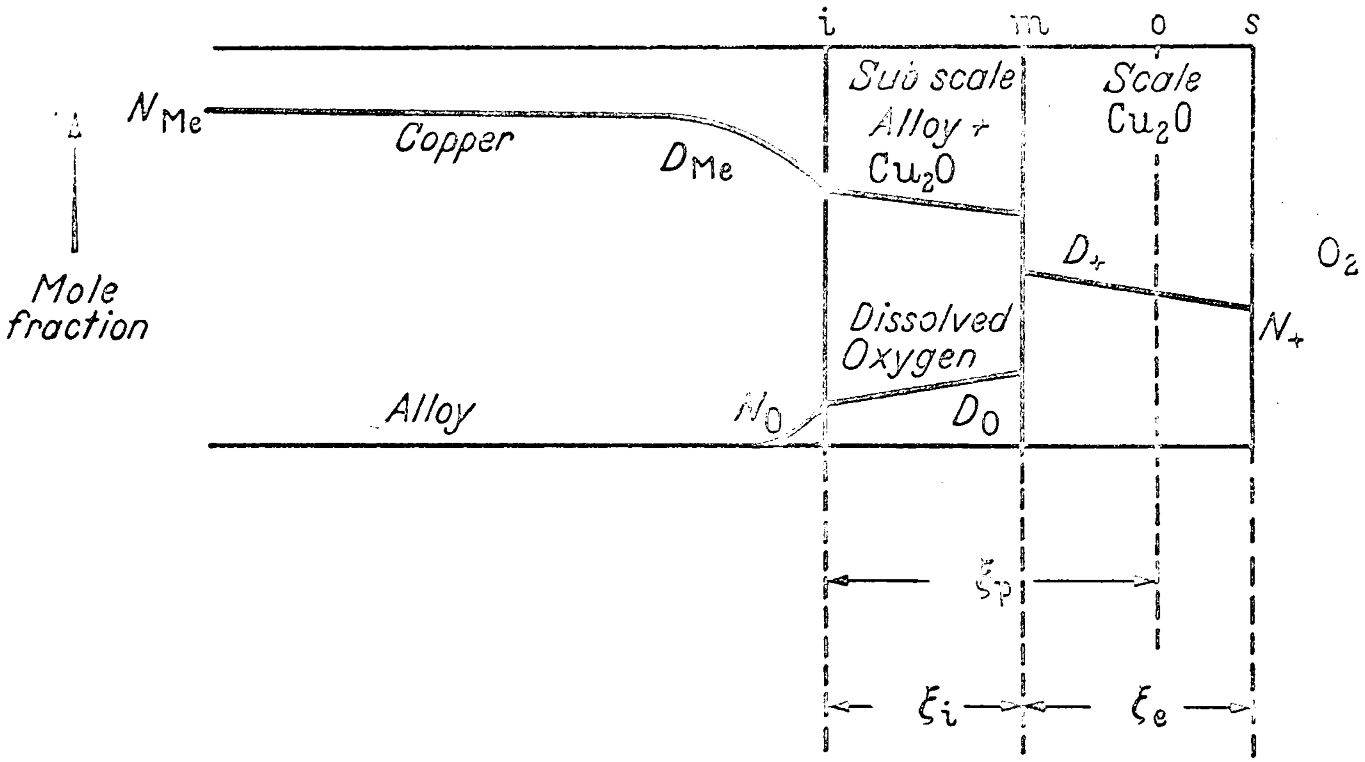

Fig.5 Internal Oxidation Model after Thomas[30]

It was assumed that the concentration gradients were linear, the oxide precipitation did not interfere with diffusion processes, the diffusivity of oxygen in the alloy is independent of composition and that the solubility of oxygen increases with increasing noble metal content. The value of $N_{O(i)}$ was taken to be zero, and all other concentrations were assumed to be independent of time for fixed external conditions. Furthermore, the subscale and scale growth rates were assumed to be parabolic, that is,

$$\xi^2 = K_B t \quad \text{and} \quad \xi_i^2 = K_S t \qquad 2\text{-}27$$

Considering the original alloy-gas interface as the distance origin, Thomas derived the following equations from Fick's laws:

$$(K_B)^{\frac{1}{2}} = \frac{D_+ \; (N_+(m) - N_+(s)}{\frac{2M_{Cu}}{M_o} \cdot \frac{N_O(m) D_O}{(K_S)^{\frac{1}{2}}} + \frac{N_{Cu}(m)}{2} \; (K_B \varphi)^{\frac{1}{2}}} \qquad 2\text{-}28$$

$$(K)^{\frac{1}{2}} = \frac{2D_+ \; (N_+(m) - N_+(s))}{(K_B)^{\frac{1}{2}} \; (N_{Cu(b)} - N_{Cu(i)})} \; \left(1 - \frac{2D_{Cu}}{K}\right) \qquad 2\text{-}29$$

$$(K)^{\frac{1}{2}} = \varphi \; (K_B)^{\frac{1}{2}} + (K_S)^{\frac{1}{2}} \qquad 2\text{-}30$$

where $K = \xi_i^2/t$, D_+ = diffusion constant of copper ions in cuprous oxide, D_{Cu} = diffusion rate of Copper in the alloy, φ = volume ratio of oxide to metal consumed and $N_{Cu(b)}$ is the bulk mole fraction of copper.

If all the terms are known, the equations can be solved simultaneously for K_S. However, Thomas found it necessary to treat the first expression, 2-28, as a quadratic in K_B and substitute in experimental values of K_S to test the relation. The agreement was good. Equation 2-29 could not be tested on the same basis, since $N_{Cu(i)}$ was unknown, However, using experimental data in the equation, calculated estimations of this unknown parameter seemed reasonable. According to this analysis, the rate constant for external scale formation was primarily governed by the diffusion of copper in the subscale, whereas the subscale rate constant was largely determined by the diffusion of oxygen to the subscale-alloy interface.

CHAPTER III

OXIDATION PROPERTIES OF IRON, NICKEL AND IRON-NICKEL ALLOYS

3.1 Oxidation of Iron

Numerous investigations have been reported in the literature concerning the oxidation properties of iron over a wide range of temperatures and reactant gas pressures. This is not surprising when one considers the technological importance of this metal; this fact has stimulated many research projects.

There are peculiarities in the iron-oxygen system, shown in Fig.6, which are not usually characteristic of other materials. Three oxides are stable at temperatures greater than 570°C, namely wustite, FeO, magnetite, Fe_3O_4, and hematite, Fe_2O_3, and these oxides lead to the formation of multilayered scales at elevated temperatures. Photomicrographs of the oxide layers have been published, and excellent examples are given by Paidassi[47]. Below 570°C, bulk wustite is unstable, although it may be present as a thin film adjacent to iron at temperatures as low as 400°C.[48,49]

Results obtained from inert marker and radioactive tracer diffusion studies[50,51,52] and investigations pertaining to the phase limits of the iron-oxygen system[53,54,55] allow one to resolve the defect structure of these scales. Wustite is a p-type oxide of a large composition range which does not include stoichiometry. The defects consist of vacant cation sites and positive holes, (Fe^{3+} ions), and diffusion occurs via cation vacancies.

Magnetite contains an excess of oxygen, however, it is much smaller

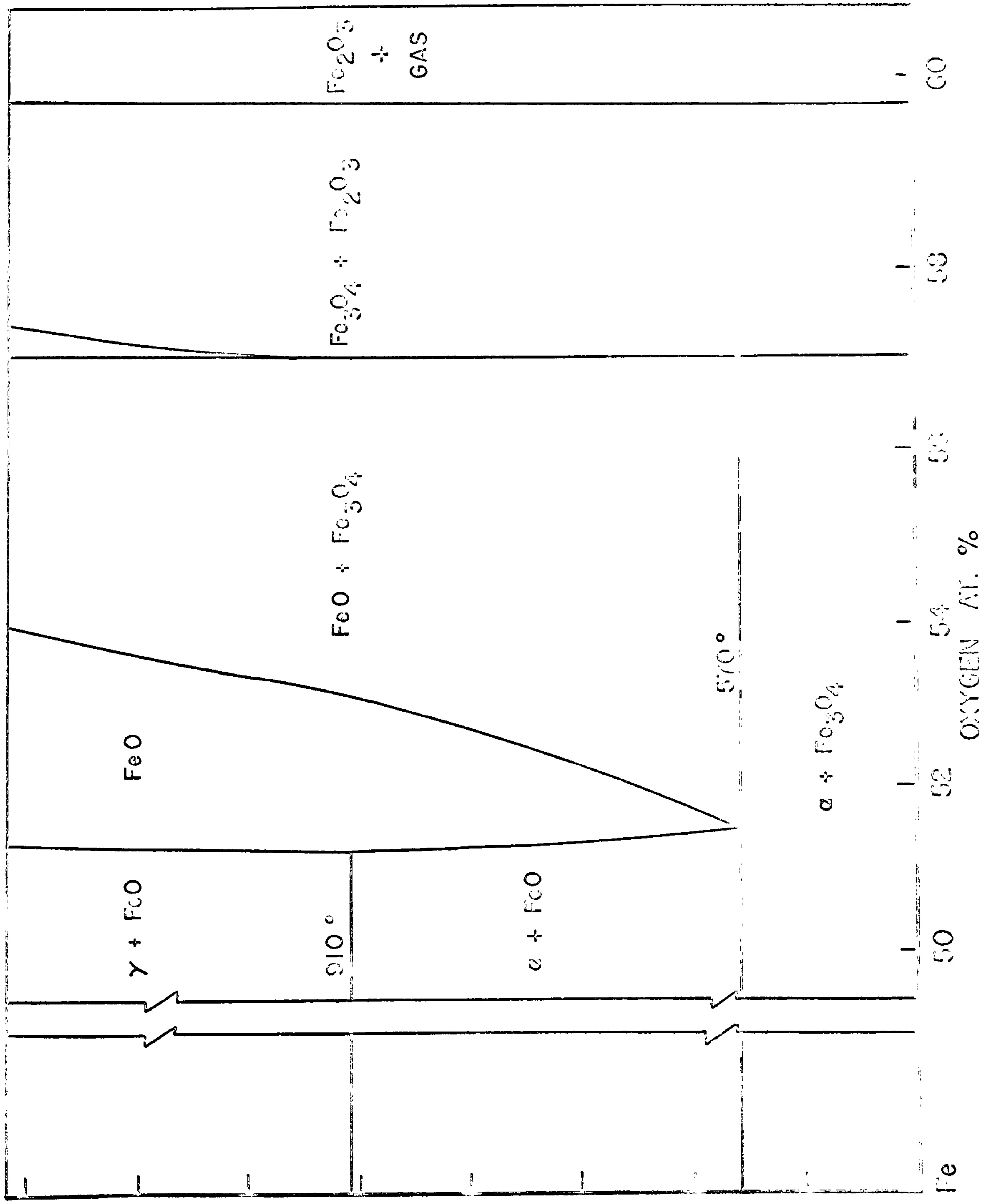

Fig.6. Fe - O phase diagram

than for wustite, and the corresponding defect concentration is smaller. Birchenall et al.[50,51] found that both cations and anions diffuse in magnetite from tracer studies. However, it is generally assumed that diffusion is mainly cationic. Hematite exists with an excess of cations and diffusion is anionic via anion vacancies.

At temperatures below approximately 200°C, a logarithmic oxidation rate has been observed[56,57,58]. Above this temperature, in oxygen or air, the oxidation rate has been reported to obey a parabolic relationship.[8,51,59,60,61,62,63,64]. These results imply that the mechanisms of oxidation are associated with a thin film model in the former case, and diffusion processes in the latter. Indeed, Simnad, Davies and Birchenall[51] determined the oxidation rates of iron to wustite, wustite to magnetite, and magnetite to hematite and found that the parabolic law was obeyed. The self diffusion coefficients of iron in the three oxides were determined by Himmel, Mehl and Birchenall[50] and the experimental oxidation rates were compared with the rates calculated by substitution into Wagner's theoretical rate equation. The agreement was good. Paidassi[59] has metallographically demonstrated that the three oxides thicken at a parabolic rate at temperatures greater than 700°C. The relative thickness of the layers was approximately 100/5/1 for $\tau_{FeO}/\tau_{Fe_3O_4}/\tau_{Fe_2O_3}$ and these values are independent of time.

It was mentioned in the previous section that compact scales can be grown on iron at linear rates in atmospheres of low oxidation potentials. Under special conditions, the oxygen pressures in carbon dioxide and water atmospheres are sufficiently low for iron to exhibit this oxidation behavior. Fischbeck, Neundeubel and Salzer[65] initially observed these linear reaction rates on oxidising iron in carbon dioxide.

Since studies on the oxidation kinetics of iron in atmospheres of low oxidation potential are of specific bearing to the work in this investigation, reported data will be reviewed in some detail.

Hauffe and Pfeiffer[66] oxidized iron in carbon dioxide-carbon monoxide atmospheres at 900° - 1000°C. Wustite was the only oxide formed for kinetic reasons to be described. Again, it was found that the uptake of oxygen was proportional to time suggesting that a phase boundary reaction was rate controlling. Since the reaction rate depended on the gas pressure as follows,

$$K_L = \text{constant } (P_{CO_2}/P_{CO})^{0.71} \tag{3-1}$$

the authors suggested that the overall rate determining reaction was the dissociation of carbon dioxide on the wustite surface producing chemisorbed oxygen ions. That is,

$$CO_2 = O^-_{ad} + CO + \oplus \tag{3-2}$$

followed by the incorporation of the adsorbed species into the wustite lattice,

$$O^-_{ad} = FeO + Fe_{\square} + \oplus \tag{3-3}$$

where $\oplus$ denotes an electron defect and $Fe_{\square}$ a vacant cation site in the wustite lattice. Furthermore, Pfeiffer and Laubmeyer[67] studied the oxidation of iron at very low oxygen potentials, established by the Cu_2O-CuO equilibrium, and linear rates were observed. The following relationship between linear rate constant and oxygen pressure was obtained,

$$K_L = \text{constant } (P_{O2})^{0.7} \qquad 3\text{-}4$$

and, by comparison with equation 3-1, concluded that the oxygen potential resulting from the dissociation reaction was controlling the rate of oxide formation.

In a recent comprehensive investigation, Pettit , Yinger and Wagner[68] studied the oxidation of iron in carbon dioxide-carbon monoxide atmospheres at 925°-1075°C. A chemisorption reaction was assumed to be rate controlling, namely,

$$CO_2 \rightarrow CO + O_{ad} \qquad 3\text{-}5$$

The number of equivalents of oxide formed per unit area per unit time, $\overset{o}{n}$, is given by,

$$\overset{o}{n} = k'P_{CO_2} - k''P_{CO} \qquad 3\text{-}6$$

where k' is the reaction rate constant for the forward reaction and k'' for the reverse reaction in equation 3-5. According to Wagner and Kobayaski[69], the rate of dissociation of carbon dioxide is a function of the concentration of electron defects in the oxide. Since the decomposition reaction was assumed to be rate controlling, the concentration of defects was considered to be given by the equilibrium between iron and wustite. Therefore, this concentration does not appear in the kinetic equation. At equilibrium, $\overset{o}{n} = 0$, and,

$$k''/k' = P^{eq}_{CO_2}/P^{eq}_{CO} = K \qquad 3\text{-}7$$

where K is defined by the equilibrium,

$$Fe + CO_2 = CO + FeO \qquad 3\text{-}8$$

Substitution into equation 3-6 and writing P_{CO_2} in terms of the total pressure P, Pettit et al. obtain,

$$K_L = k'P(1+K)\left(N_{CO_2} - N_{CO_2}(eq)\right) \qquad 3\text{-}9$$

where N_{CO_2} is the mole fraction of CO_2 in the gas phase and the subscript (eq) denotes the mole fraction of CO_2 in the atmosphere in equilibrium with iron and wustite. The results of Hauffe and Pfeiffer[66] are compatible with this expression.

Smeltzer[70] also investigated the mechanism of oxidation of iron to wustite in carbon dioxide-carbon monoxide atmospheres assuming as before that the kinetics were determined by a chemisorption reaction. Furthermore, it was assumed that carbon dioxide was adsorbed irreversibly to form chemisorbed oxygen and carbon monoxide. The elementary steps for the oxidation reaction are as follows,

$$CO_2(g) \rightarrow O^{=}_{ads} + 2\oplus_{(o)} + CO(g) \qquad 3\text{-}10$$

$$O^{=}_{ads} \rightarrow FeO + Fe_{\square(o)} \qquad 3\text{-}11$$

$$Fe_{\square(o)} + 2\oplus_{(o)} \rightleftharpoons Fe_{\square(i)} + 2\oplus(i) \qquad 3\text{-}12$$

$$Fe_{(i)} + Fe_{\square}(i) + 2\oplus(i) \rightleftharpoons nil \qquad 3\text{-}13$$

$$O^{=}_{ads} + 2\oplus(o) \rightarrow \tfrac{1}{2}O_{2(g)} \qquad 3\text{-}14$$

The subscripts (g), (o), (i) refer to the gas phase and lattice defect structure at the oxide-gas interface and metal-oxide interface respectively. Nil refers to the annulment of lattice defects by the solution of iron into the oxide.

Oxidation would obey a parabolic law if the concentration of vacancies and electron holes equalled their equilibrium values. Since linear rates were observed, equations 3-10 and 3-11 were assumed to represent the rate controlling processes. Considering that the surface coverage of adsorbed oxygen, Θ, is constant during oxidation, and that the lattice defects in the oxide are equilibrated with the metal phase, Smeltzer derived the following expression for the surface coverage,

$$\Theta = \frac{k_2}{k_3 + k_6K}(P_{CO_2} - P'_{CO_2}) / 1 + \frac{k_2}{k_3 + k_6K}(P_{CO_2} - P'_{CO_2}) \qquad 3\text{-}15$$

where k_2, k_3 and k_6 are the rate constants for oxygen chemisorption, wustite formation, and oxygen desorption respectively; K is a constant defined by the equilibration of iron with wustite.

Two approximations to equation 3-15 were considered, namely, that Θ approaches zero and the oxidation rate is determined by the dissociation of carbon dioxide, and the rate of incorporation is rate controlling, $0 < \Theta < 1$ and $k_2 << k_3 + k_6K$. The relationships derived for these conditions are,

$$K_L = k_2\,(P_{CO_2} - P'_{CO_2}) \qquad 3\text{-}16$$

and,

$$K_L = \frac{k_3k_2}{k_3 + k_6K}(P_{CO_2} - P'_{CO_2}) \qquad 3\text{-}17$$

respectively. Linear relations were found when K_L was plotted versus the partial pressures of carbon dioxide above the equilibrium value in support of the theory. Since the partial pressures are proportional to the mole fraction of carbon dioxide and the total pressure, the above equations are of the same form as equation 3-9 .

More recently, Turkdogan[20] described the initial rates of oxidation of iron in water-hydrogen atmospheres by applying Eyring's theory of absolute reaction rates. Again, a chemisorption reaction was assumed. The overall phase boundary reaction was represented by,

$$H_2O(g) + 2e \rightarrow O^{=}_{ad} + H_2(g) \qquad 3\text{-}18$$

The wustite surface was considered to contain a fixed number of sites per unit area, fractions of which were occupied by the adsorbed species, H_2O, H_2, $O^{=}_{ad}$, $[H_2O]_{\dagger}$ and vacant sites, denoted by Θ_{H_2O}, Θ_{H_2}, Θ_O, $\Theta_{\dagger}$, $\Theta_{\square}$, respectively. $[H_2O]_{\dagger}$ represents the activated complex. A relation for the fraction of sites occupied by the activated complex was obtained assuming equilibrium between the water vapor in gas phase and the activated complex,

$$\Theta_{\dagger} = K_{\dagger} \frac{k_3}{k_4} \frac{\Theta_o}{a_o} a_{H_2O} \qquad 3\text{-}19$$

where a_o is the activity of oxygen at the oxide-gas interface, $a_{H_2O} = P_{H_2O}$ is the activity of water vapor in the gas phase, and $K_{\dagger}$ is the equilibrium constant for $H_2O = [H_2O]_{\dagger}$. The rate of oxidation was obtained from expressions for the dissociation of the activated complex. The linear oxidation kinetics of iron were represented as,

$$K_L = k' \Theta_O \left(\frac{1}{a_o} - \frac{1}{a_o''}\right) P_{H_2O}\, e^{-E/RT} \qquad 3\text{-}20$$

where k' is an overall constant containing the constants of equation 3-19, and the universal specific rate constant RT/Nh, E is a heat of activation, and a_o'' is the actitty of oxygen at the oxide - gas interface in equilibrium with the gas phase. If Θ_o is constant and a_o is defined as the standard state, $a_o = 1$, the rate of oxidation is,

$$K_L = k'' \left(1 - \frac{1}{a_o''}\right) P_{H_2O} \qquad 3\text{-}21$$

An analogous expression was derived for oxidation kinetics in carbon dioxide - carbon monoxide atmospheres. Data obtained from the literature demonstrated good agreement between theory and experiment.

3.2 Oxidation of Nickel

Nickel oxide is the only oxide observed on pure nickel. This oxide is a metal deficit p-type semiconductor, the oxidation rate exhibiting a sixth-root power dependency on the oxygen pressure.[10] At temperatures in excess of 400°C, the oxidation rate of nickel has been reported to obey a parabolic relationship in accordance with the Wagner mechanism.[71,72,73,74] The oxidation rate is very sensitive to impurity content,[71] and the oxide may exhibit porosity at high temperatures.[75,76]

At temperatures of approximately 400°C, the oxidation rate has been reported as cubic and logarithmic. Engell, Hauffe and Ischner[77] explained the cubic rates by a model whereby the ion flux through the film was a function of the electric field strength and the concentration gradient. Uhlig, Pickett and MacNairn[78] reported logarithmic rates and found the rate changed at the Curie temperature. The proposed mechanism was based on electron transfer from the metal to the oxide, and the observed rate change at the Curie temperature was associated with a change in the electron work function.

3.3 Oxidation of Iron-Nickel Alloys

The oxidation properties of the iron-nickel system have been studied in air and oxygen over a range of pressures and temperatures. Under these conditions, multilayer scales are formed similar to those found on pure iron. Most studies have been associated with phase identification and oxide morphology. A notable exception is the investigation of Brabers and Birchenall[79] in which specimens were oxidized for various time periods in air, and then subsequently brought to equilibrium in an inert atmosphere. Several features of the iron-nickel-oxygen ternary phase diagram were determined at 1050°C. For a complete tabulation of results, Foley[80] has published a survey of the oxidation properties of iron-nickel alloys.

Oxidation is severe with alloys containing low nickel concentrations, (0 - 10 wt.%Ni). Alloy, highly enriched in nickel, is entrapped by the receding metal-oxide interface[52,81,82,83,84]. For oxidation tests in lab air, controlled oxygen-nitrogen and oxygen-nitrogen-water vapor atmospheres, Foley[85,86,87,88,89] has demonstrated parabolic scale growth for alloys containing 30 - 80% Ni. At least for times up to 60 minutes, high nickel additions greatly reduce the rate compared to pure iron. This is a result of the disappearance of the wustite layer, due to the enrichment of nickel at the metal-oxide interface. Diffusion processes are slower in the remaining nickel bearing spinel and hematite layers.

Kennedy, Calvert and Cohen,[90] using a high temperature diffraction apparatus, determined essentially the same scale structure on three iron-nickel alloys in the composition range 25 - 75% Ni at 800°C in oxygen.

The individual oxide layers thickened according to a parabolic law. There was considerable subscale formation especially in the 25% Ni alloy, and this was attributed to scale fracture, allowing the reactant gas to penetrate along the interface and grain boundaries. Yearian, Boren, and Warr[91] also reported a nickel bearing spinel and hematite layers on a 25% Ni alloy as did Koh and Caugherty[92] for a 50% Ni alloy at 1193°C. Basically, reaction rates for alloys containing more than 30% Ni, appear to be controlled by diffusion through a nickel bearing spinel, and diffusion of nickel through the inner nickel oxide layer for nickel alloys containing small amounts of iron.[80]

The oxidation properties of a series of iron-nickel alloys containing up to 30% Ni were investigated by Benard and Moreau[93] in air at 675° - 950°C. Three surface layers were detected consisting of hematite, magnetite and a mixture of wustite and magnetite adjacent to the metal. Extensive internal oxidation occurred in these alloys. Little nickel and nickel oxide were detected in any of these layers by chemical analyses. Iron was selectively oxidized, and nickel was enriched at the metal-oxide interface. In the 30% Ni alloy the surface concentration of nickel was 50% at 850°C, 60% at 950°C, and 82% at 1050°C. There were two distinct stages in the oxidation - time curves with the exception of that for a 20% alloy at 675°C where parabolic behavior was closely approached. These deviations from parabolic behavior were attributed to the highly selective oxidation of iron, the subsequent enrichment of nickel at the surface, and diffusion of iron through this enriched layer in the initial stages. In the later stages, deviations occurred as a result of a decreased oxygen flux across the oxide to the interior of the alloy.

Internal oxidation was more severe at the grain boundaries than within the grains. The authors suggested that oxygen diffused down these boundaries and precipitated oxide particles which subsequently coalesced and enveloped the metal grains. Oxygen was then transported through the oxide and diffused into the metal lattice and precipitated oxide within the grains similar to the process occurring at the metal-oxide interface.

Birchenall et al.[79,94] oxidized iron-nickel alloys of several compositions at 1050°C in oxygen, then allowed the specimens to come to equilibrium by annealing in an inert atmosphere. Equilibration occurred mainly by the dissolution of oxide and oxygen diffusion into the alloy phase. Several details of the iron-nickel-oxygen ternary phase diagram were deduced from the results as shown in Fig.7. Based on previous reports and the equilibrium data, the authors proposed the following oxidation mechanism. Iron is selectively oxidized from an alloy when placed in a highly oxidizing potential. Although the alloy is enriched in nickel, only minute amounts of this metal reach the outer layers of magnetite and hematite due to formation of an inner wustite layer. Oxygen solubility must be higher in the alloys than pure iron in order to precipitate oxide in the alloy. This causes further nickel enrichment. Concurrently, the wustite composition becomes higher in oxygen and the driving force for metal diffusion is decreased. Thus, rates lower than that required for continuous parabolic behavior are observed.[93] As the nickel concentration exceeds the equilibrium between alloy-spinel-wustite, a nickel bearing spenel consumes wustite from the inside, while a nickel free spinel (Fe_3O_4) consumes it from the outside. As the spinels join, the nickel concentration may be homogenized by diffusion. This results in

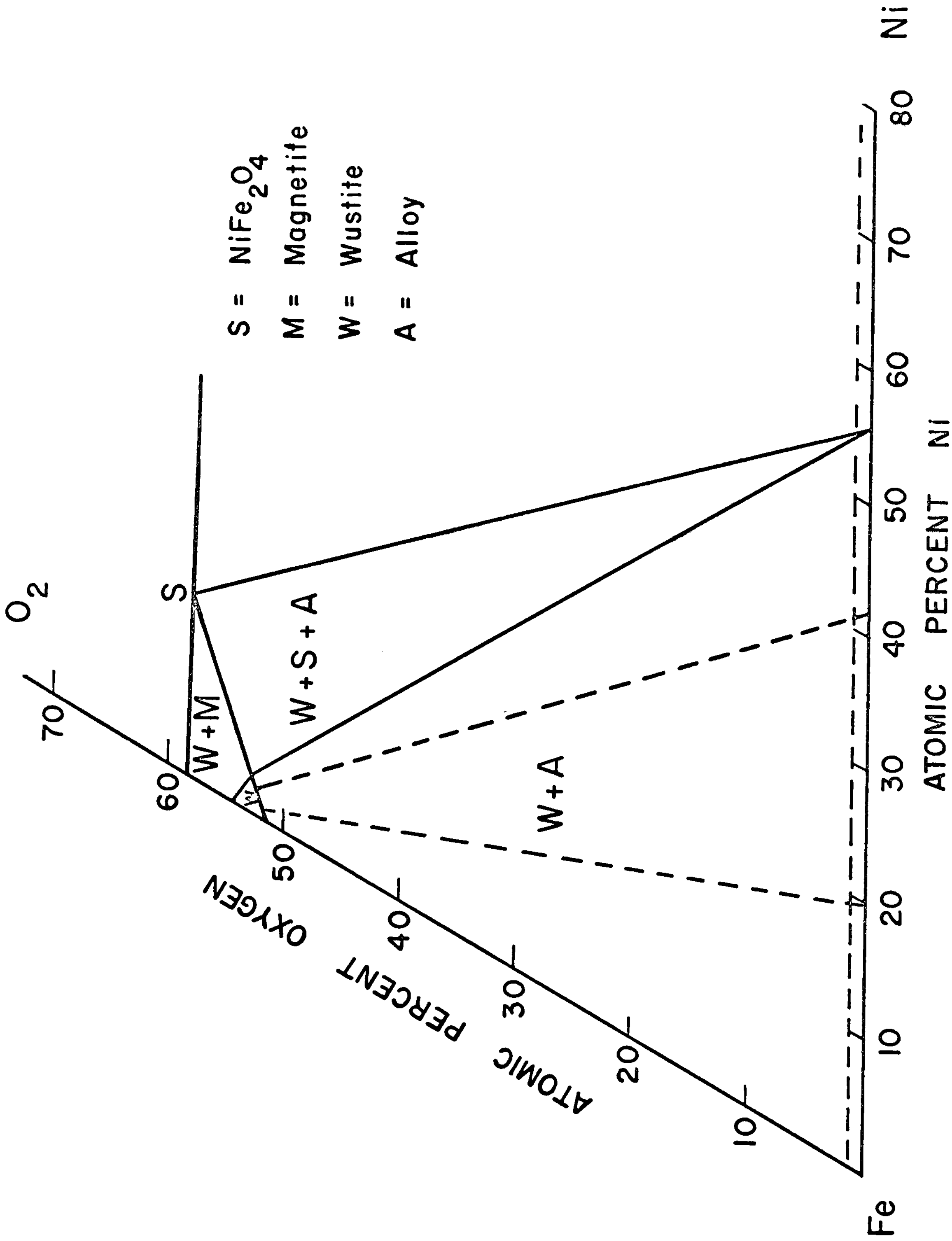

IRON RICH CORNER OF Fe-Ni-O PHASE DIAGRAM AT 1050 °C

Fig.7.

the spinel-hematite layer structure reported above. Upon elimination of wustite, the oxidation rate is greatly reduced.

CHAPTER IV

THEORETICAL CONSIDERATIONS

4.1 Introduction

In the Introduction, it was mentioned that the purpose for employing carbon dioxide - carbon monoxide atmospheres as the oxidizing gas was to reduce the number of oxide layers in the scale formed on the alloy to one, namely, wustite. It is evident from the preceding review on the oxidation properties of iron-nickel alloys that the occurrence of multilayer scales lead to complex oxidation phenomena. Since linear reaction rates were observed under these conditions, the oxidation mechanism at least appears similar to that of iron. Therefore, in this section, an attempt will be made to expand some of the oxidation concepts outlined above for iron, in order to derive a theoretical rate expression applicable to iron-nickel alloys.

It has been established that subscales are formed in alloys in which one component is a noble element, for example, copper-platinum, copper-palladium, nickel-platinum.[30] Although nickel is not a noble element per se, under the oxidation conditions used in the present investigation, it behaves as a noble element. Recently, advances have been made in the field of diffusion in multicomponent systems. Internal oxidation occurs in a ternary system, hence the first attempt will be made to interpret this type of oxidation on the basis of ternary diffusion. theory. A simple model will be presented to account for oxygen diffusion in the alloy and the appearance of a subscale, based on recent developments in ternary diffusion.

4.2 Linear Oxidation Rates

The basic premise of Hauffe and Pfeiffer[66] is accepted in the development of the oxidation rate expression, for iron-nickel alloys exposed in atmospheres containing carbon dioxide. That is, the formation of wustite is determined by a chemisorption reaction. Transfer of oxygen from the gas phase to the oxide may be represented by detailed balancing of the elementary reaction steps,

$$CO_2 \underset{k_2}{\overset{k_1}{\rightleftharpoons}} O^{=}_{ads} + CO(g) + 2\oplus \tag{4-1}$$

$$O^{=}_{ads} \underset{k_4}{\overset{k_3}{\rightleftharpoons}} (Fe,Ni)O + Fe_{\square} \tag{4-2}$$

$$Fe_{\square} + 2\oplus + Fe_{Alloy} \rightleftharpoons nil \tag{4-3}$$

$$Ni_{alloy} \rightleftharpoons Ni_{oxide} \tag{4-4}$$

where the subscript (g) refers to the gas phase, nil refers to the annulment of lattice defects by the solution of iron into the oxide, and k_1, k_2, k_3, k_4, are reaction rate constants dependent on temperature. (Fe, Ni)O refers to wustite with less that 2 atomic % nickel. These processes are represented in Fig.8.

In the following derivation, it is assumed that the concentration of electron defects, cation vacancies and the oxygen activity in wustite at the metal-gas interface are equal to their equilibrium values. The rate of formation of wustite per unit time is given by.

$$\frac{d(FeO)}{dt} = k_3 \Theta_o - k_4 \Theta_v \, a_o \, [\square] \tag{4-5}$$

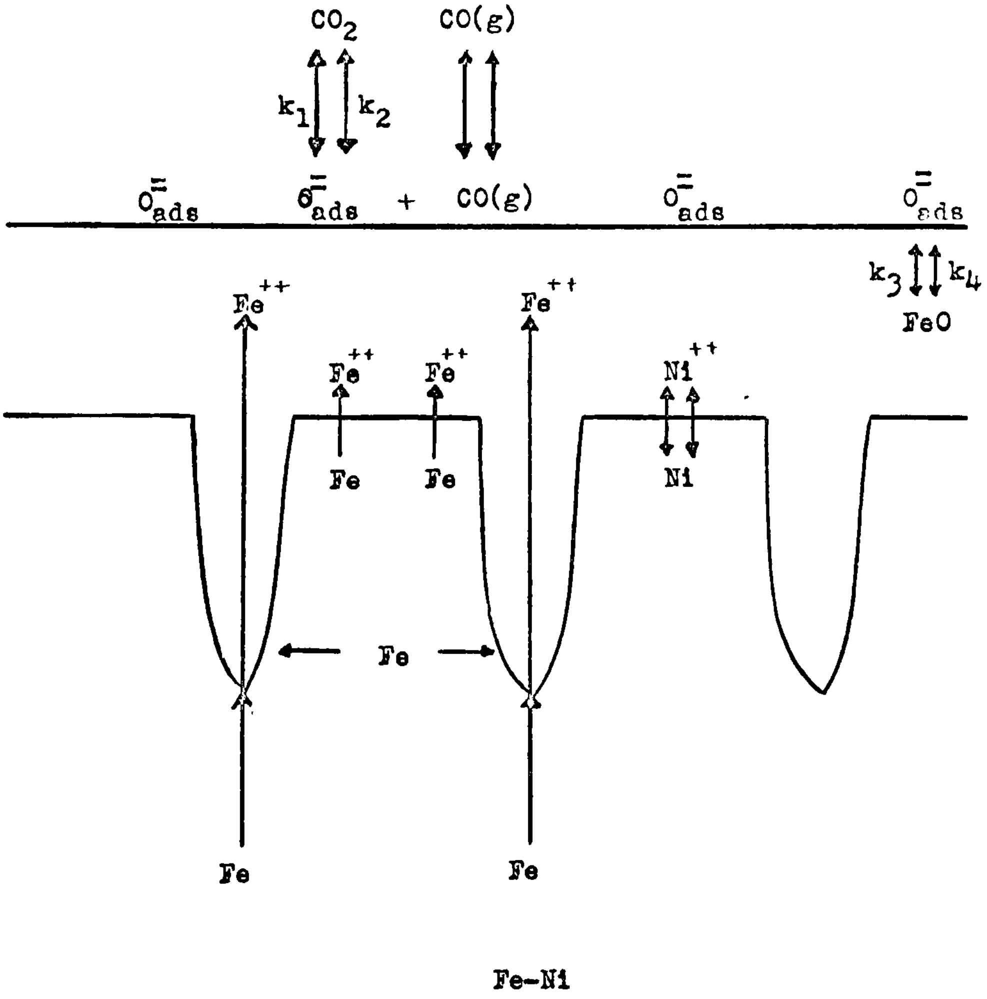

Fig. 8. Linear oxidation model

where Θ_o, Θ_v are fractions of surface sites for an energetically homogenious surface covered with adsorbed oxygen ions and vacant sites respectively, $[\square]$ is the vacancy concentration, and a_o is the oxygen activity in wustite at the metal-oxide interface. Assuming Θ_o, Θ_v are constant for given conditions, this is $d\Theta_o/dt = 0$,

$$\frac{\Theta_o}{\Theta_v} = k_1 P_{CO_2} + k_4 a_o [\square] / k_2 P_{CO} [\oplus]^2 + k_3 \qquad 4\text{-}6$$

At equilibrium, d FeO/dt = 0, therefore,

$$\frac{\Theta_o'}{\Theta_v'} = \frac{k_4}{k_3} a_o [\square] = \frac{k_1 P_{CO_2}'}{k_2 P_{CO}' [\oplus]^2} \qquad 4\text{-}7$$

where ' denotes the equilibrium value. Equation 4-5 may be written as,

$$\frac{d\ FeO}{dt} \doteq K_L = k_3 \Theta_v \left[\frac{\Theta_o}{\Theta_v} - \frac{k_4}{k_3} a_o [\square] \right]$$

$$= \frac{k_3 \Theta_v}{k_2 P_{CO} [\oplus]^2 + k_3} \left[k_1 P_{CO_2} + k_4 a_o [\square] - \frac{k_4}{k_3} a_o [\square] (k_2 P_{co} [\oplus] + k_3) \right]$$

$$= \frac{k_3 \Theta_v}{k_2 P_{CO} [\oplus]^2 + k_3} \left[k_1 P_{CO_2} - \frac{k_4}{k_3} k_2 a_o [\square] [\oplus]^2 P_{CO} \right]$$

$$= \frac{k_3 k_1 \Theta_v}{k_2 P_{CO} [\oplus]^2 + k_3} \left[1 - \frac{k_4 k_2}{k_3 k_1} a_o [\square] [\oplus]^2 \frac{P_{CO}}{P_{CO_2}} \right] P_{CO_2} \qquad 4\text{-}8$$

Substituting from equation 4-7 yields,

$$K_L = \frac{k_3 k_1 \Theta_v}{k_2 P_{CO} [\oplus]^2 + k_3} \left[1 - \frac{P_{CO_2}'}{P_{CO}'} \frac{P_{CO}}{P_{CO_2}} \right] P_{CO_2}$$

or,

$$K_L = \frac{k_3\, k_1\, \Theta_v}{k_2 P_{CO} [\oplus]^2 + k_3} \left[1 - \frac{a_o}{a_o^g}\right] P_{CO_2} \qquad 4\text{-}9$$

The activities of oxygen are readily calculated from the equilibrium

$$CO_2 \rightleftharpoons CO + O$$

Accordingly, $a_o = K\, P'_{CO_2}/\, P'_{CO}$, $a_o^g = K\, P_{CO_2}/P_{CO}$, the activity of oxygen in the gas phase. Equation 4-9 is the general form of the rate expression. If the assumption is made that $k_3 \gg k_2\, P_{CO}\, [\oplus]^2$, equation 4-9 becomes,

$$K_L = k_1 \Theta_v \left[\, 1 - a_o/a_o^g \right] P_{CO_2} \qquad 4\text{-}10$$

This is a particular form of the expression valid when the rate of incorporation of oxygen into the oxide is greater than the desorption of adions.

It is immediately apparent that, for the case of pure iron, this expression is equivalent to that of Turkdogen et al.,[20] equation 3-21. It is also equivalent to that of Smeltzer, equation 3-16, and to the expression of Wagner, equation 3-9, if it can be proven that,

$$(1 - a_o/a_o^g)\, P_{CO_2} = (1+K) \quad (P_{CO_2} - P'_{CO_2})$$

Manipulation of the L. H. S. gives,

$$(1 - a_o/a_o^g)\, P_{CO_2} = P_{CO_2} - \frac{P'_{CO_2}}{P'_{CO}}\, \frac{P_{CO}}{P_{CO_2}}\, P_{CO_2}$$

$$= P_{CO_2} - \frac{P'_{CO_2}}{P'_{CO}} \quad (1 - N_{CO_2})\, P$$

where N_{CO_2} is the mole fraction of carbon dioxide in the carbon dioxide-carbon monoxide atmosphere and $P = P_{CO} + P_{CO_2}$. Therefore,

$$(1 - a_o/a_o^g)\, P_{CO_2} = P_{CO_2} - \frac{P'_{CO_2}}{P'_{CO}}\, P + \frac{P'_{CO_2}}{P'_{CO}}\, P_{CO_2}$$

$$= \left[\left(1 + \frac{P'_{CO_2}}{P'_{CO}}\right) P_{CO_2} - \frac{P'_{CO_2}}{P'_{CO}}\, P \right]$$

$$= \left(1 + \frac{P'_{CO_2}}{P'_{CO}}\right) \left[P_{CO_2} - \frac{P'_{CO_2}}{P'_{CO}} \; \frac{P}{\left(1 + \frac{P'_{CO_2}}{P'_{CO}}\right)} \right]$$

$$= \left(1 + \frac{P'_{CO_2}}{P'_{CO}}\right) \left[P_{CO_2} - \frac{P'_{CO_2}}{P'_{CO}} \; \frac{P'_{CO}}{P}\, P \right]$$

$$= (1 + K) \; (P_{CO_2} - P'_{CO_2})$$

that is,

$$K_L = k_1 \Theta_V \, (1 + K) \; (P_{CO_2} - P'_{CO_2}) \qquad \text{4-11}$$

The validity of the above expressions for the kinetics of iron-nickel alloy oxidation will be established in this investigation.

4.3 Internal Oxidation

To date, the process of internal oxidation has been treated using binary diffusion equations in which the effects of a concentration gradient of one component on the diffusive flux of another are neglected. It is apparent from the review of alloy oxidation that a component in an alloy may be concentrated at the metal-oxide interface as a result of external and internal scale formation. This is readily apparent for alloys containing an element which has a very low solubility in the oxidation products.

Steep concentration gradients may exist at the metal - oxide interface. As confirmation for these considerations regarding the iron - nickel system, Brabers and Birchenall[79] and Roeder and Smeltzer [95] have demonstrated that the solubility of nickel in wustite is less than 2 wt.%. Interaction between the inward flux of oxygen and concentration gradients in the metal phase may be of importance in internal oxidation of a binary alloy and can only be introduced by employing ternary diffusion equations. Furthermore, if an oxide scale is formed on a binary alloy, the oxygen concentration in the alloy at the metal - oxide interface will be the saturation value in order to obtain interfacial equilibrium. For internal oxidation to occur in a system which forms the same oxide internally as well as externally, for example, copper - platinum, copper palladium, and iron - nickel, the oxygen concentration must exceed the saturation valu e in order to establish the system in the two phase alloy plus oxide region of the ternary phase diagram and provide supersaturation for oxide nucleation. In the following theoretical developments, an internal oxidation model will be presented for the iron - nickel system based on the principles of diffusion in multicomponent systems.

For a complete description of diffusion in multicomponent metallic systems, one may consult contributions by Onsager[96] and Kirkaldy.[97]

Diffusion in ternary systems may be described by utilizing Onsager's extension of Fick's first law[96], in which the flux of each component is assumed to be a linear function of all the concentration gradients. For example, the flux of one component may be written as,

$$J_i = - \sum_{k=1}^{3} D_{ik} \nabla C_k \tag{4-12}$$

By appropriate choice of a reference system,[97] and considering unidirectional diffusion only, equation 4-12 becomes,

$$J_i = -\sum_{k=1}^{2} D_{ik} \nabla C_k = - D_{11} \frac{\partial C_1}{\partial x} - D_{12} \frac{\partial C_2}{\partial x} \tag{4-13}$$

The D_{12} coefficient or off-diagonal diffusion coefficient represents the diffusivity of component one on the concentration gradient of component two. Combining 4-13 with the continuity equation,

$$\mathrm{div}\, J_1 + \frac{\partial C_1}{\partial t} = 0 \qquad 4\text{-}14$$

the generalized ternary diffusion equation is obtained,

$$\frac{\partial C_1}{\partial t} = D_{11}\frac{\partial^2 C_1}{\partial x^2} + D_{12}\frac{\partial^2 C_2}{\partial x_2} \qquad 4\text{-}15$$

assuming constant D's. Similarily for component two,

$$\frac{\partial C_2}{\partial t} = D_{21}\frac{\partial^2 C_1}{\partial x^2} + D_{22}\frac{\partial^2 C_2}{\partial x_2} \qquad 4\text{-}16$$

It is now necessary to describe a model for subscale formation in iron - nickel alloys in order to define the boundary conditions for solution of equation 4-15. Since iron is selectively oxidized, nickel is rapidly enriched at the alloy surface. The nickel concentration at the metal-oxide surface is assumed to be constant for experimental times. Oxygen saturation of the alloy surface is maintained by the presence of an oxide film. For formation of internal oxide precipitates, the alloy must become supersaturated relative to its stability condition by inward diffusion of oxygen. The initial concentration profile in the alloy phase is shown schematically in Fig.9. For the considerations to be advanced, it is unnecessary to specify the metal gradients in the oxide scale. Components one and two refer to oxygen and nickel respectively, C_{11}, C_{21} and C_{10}, C_{20} are their initial concentrations for $x < 0$, to $x > 0$, respectively, where x is measured from the alloy-oxide interface.*

A solution for equation 4-15, satisfying the boundary conditions,

---

*see Appendix II

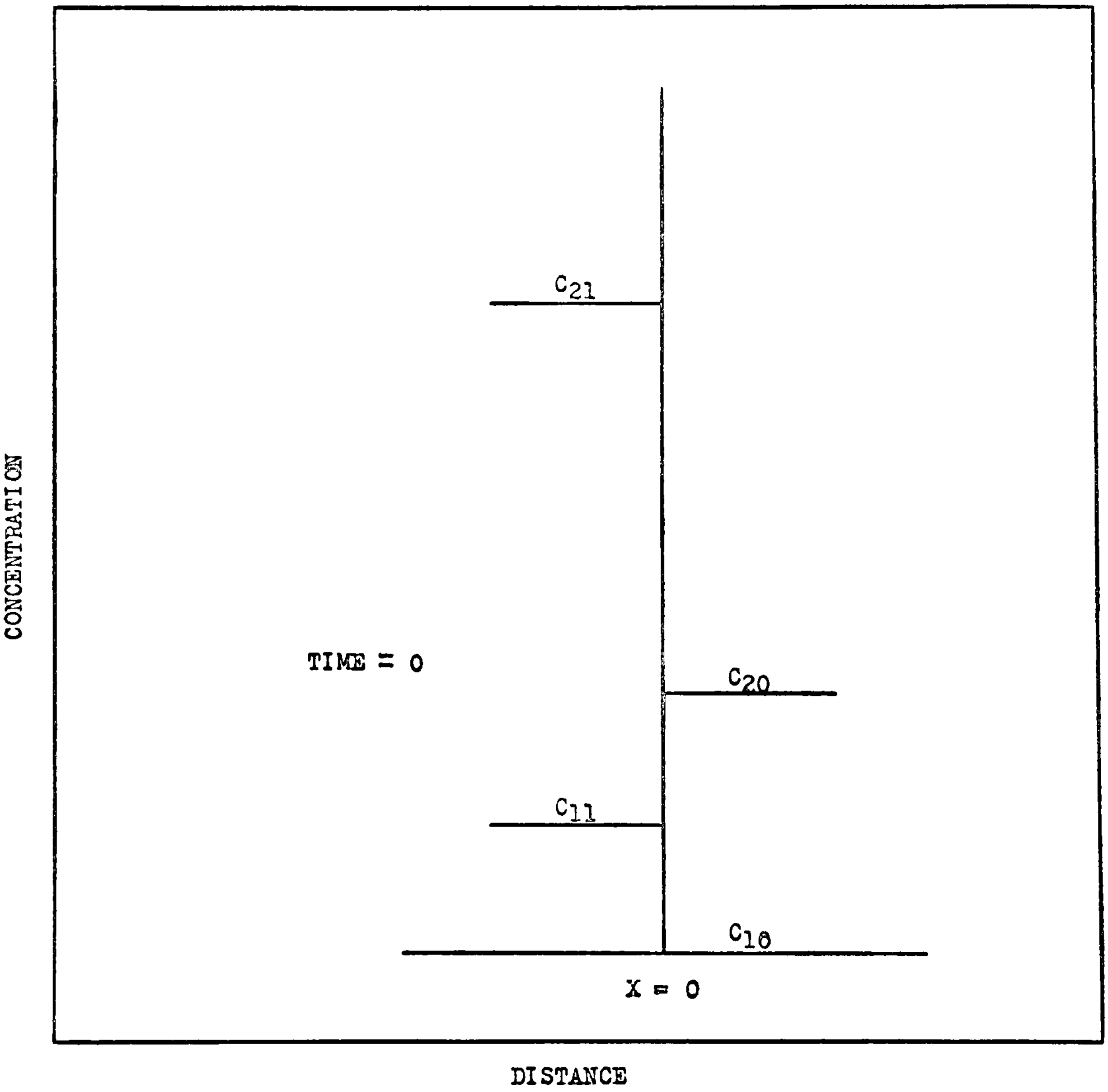

Fig.9. Concentration profile for t = 0.

is as follows,[98,99]

$$C_1 = C_{10} + \left\{\frac{D_{12}}{D_{11}} (C_{21} - C_{20}) + (C_{11} - C_{10})\right\} \operatorname{erfc} \frac{x}{2\sqrt{D_{11}t}} - \left\{\frac{D_{12}}{D_{11}} (C_{21} - C_{20})\right\} \operatorname{erfc} \frac{x}{2\sqrt{D_{22}t}} \qquad 4\text{-}17$$

where D_{11} and D_{22} are the diffusion constants of oxygen and nickel in the alloy respectively, and C_1 is the oxygen concentration. Since the concentration of oxygen in the alloys is very small compared to the nickel concentration, it is assumed that the product $D_{21} \frac{\partial^2 C_1}{\partial x^2}$ is negligible. The solution to equation 4-16 under this restriction is [22];

$$C_2 = C_{20} + (C_{21} - C_{20}) \operatorname{erfc} \frac{x}{2\sqrt{D_{22}t}} \qquad 4\text{-}18$$

The consequences of equations 4-17 and 4-18 with respect to the degree of oxygen supersaturation in the alloy phase for precipitation of internal oxide particles will be demonstrated in a later chapter.

An accurate mathematical description of the precipitation kinetics would indeed be a difficult if not impossible task. A distribution function would be required to determine the relative fluxes of metal and oxygen in the alloy and oxide phases. A qualitative interpretation of the subscale formation mechanism may be obtained as follows. When sufficient oxygen supersaturation is present in the alloy to initiate oxide precipitation, growth of oxide particles will then reduce the concentration of oxygen in the metal phase to its saturation value. If the variation of oxygen saturation with alloy composition is small, the oxygen concentration gradient in the subscale region during oxidation will be very small. The solubility of oxygen in iron rich alloys is estimated to be approximately 0.005 wt.% as the solubility of oxygen in gamma iron is 0.003 ± 0.003.[41,100] Thus, the driving force for diffusion of oxygen by its concentration gradient is negligible. Therefore, the oxygen flux through the alloy surface is given by equation 4-13 where diffusion of oxygen on its own concentration gradient is neglected. That is,

$$J_1 = - D_{12} \left. \frac{\partial C_2}{\partial x} \right|_{x = o} \qquad 4\text{-}19$$

Since the amount of oxygen dissolved in the alloy matrix is negligible, oxygen in the subscale region is present as internal oxide. This amount, W_o, for time t is,

$$W_o (t) = \int_o^t J_1 dt = - \int_o^t D_{12} \left. \frac{\partial C_2}{\partial x} \right|_{x = o} dt \qquad 4\text{-}20$$

From equation 4-18,

$$\left. \frac{\partial C_2}{\partial x} \right|_{x = o} = - \frac{(C_{21} - C_{20})}{\sqrt{\pi D_{22}}} t^{\frac{1}{2}} \qquad 4\text{-}21$$

Therefore, assuming D_{12} is not a function of concentration, equation 4-20 becomes,

$$W_o (t) = D_{12} \frac{(C_{21} - C_{20})}{\sqrt{\pi D_{22}}} t^{\frac{1}{2}} \qquad 4\text{-}22$$

The off - diagonal coefficient, D_{12}, can be eliminated from equation 4-22.

Kirkaldy and Purdy[101] have derived an expression applicable to dilute ternary solutions, namely,

$$\frac{D_{12}}{D_{11}} \simeq \varepsilon_{12} N_1 \qquad 4\text{-}23$$

where ε_{12} is the nearest - neighbour pair interaction energy defined by,

$$\varepsilon_{12} = \frac{\partial \ln \gamma_1}{\partial N_2} \qquad 4\text{-}24$$

where γ_1, is the oxygen activity coefficient. The assumption is made that equation 4-23 is valid for large nickel concentrations. Substituting into 4-22,

$$W_o\ (t) = \frac{D_{11}\ \varepsilon_{12}\ N_1\ (C_{21} - C_{20})}{\sqrt{\pi\ D_{22}}}\ t^{\frac{1}{2}} \qquad 4\text{-}25$$

N_1 represents the saturation value of oxygen of the metal - oxide interface. These values are unknown for the iron - nickel system, however, an approximate functional relation between oxygen saturation and nickel content can be obtained utilizing the Gibbs - Duhem expression. Considering an alloy saturated with oxygen (designated α phase), in equilibrium with wustite, (β phase), one can write,[110]

$$N_1^{\alpha}\ d\ln a_1 + N_2^{\alpha}\ d\ln a_2 + N_3^{\alpha}\ d\ln a_3 = 0 \qquad 4\text{-}26$$

were subscripts 1, 2, 3 refer to oxygen, nickel and iron respectively.

Also,

$$N_1^{\beta}\ d\ln a_1^{\alpha} + N_2^{\beta}\ d\ln a_2^{\alpha} + N_3^{\beta}\ d\ln a_3^{\alpha} = 0 \qquad 4\text{-}27$$

Multiplying 4-26 by N_3^β and 4-27 by N_3^α and equating the relations,

$$(N_3^\beta N_1^\alpha - N_3^\alpha N_1^\beta)\,d\ln a_1^\alpha + (N_3^\beta N_2^\alpha - N_3^\alpha N_2^\beta)\,d\ln a_2^\alpha = 0 \qquad 4\text{-}28$$

Wagner[107] has demonstrated that the activities may be expanded in terms of the pair interaction energies, that is,

$$\ln a_1^\alpha = \ln N_1^\alpha + \mathcal{E}_{11} N_1^\alpha + \mathcal{E}_{12} N_2^\alpha \qquad 4\text{-}29$$

and

$$\ln a_2^\alpha = \ln N_2^\alpha + \mathcal{E}_{12} N_1 + \mathcal{E}_{22} N_2 \qquad 4\text{-}30$$

Substituting into 4-28, and multiplying by $\dfrac{N_2^\alpha}{N_3^\beta N_2^\alpha - N_3^\alpha N_2^\beta}$,

$$\frac{(N_3^\beta N_1^\alpha - N_3^\alpha N_1^\beta)}{N_1^\alpha} \cdot \frac{N_2^\alpha}{(N_3^\beta N_2^\alpha - N_3^\alpha N_2^\beta)} (dN_1^\alpha + \mathcal{E}_{11} N_1^\alpha dN_1^\alpha + \mathcal{E}_{12} N_1^\alpha dN_2^\alpha)$$

$$+ dN_2^\alpha + \mathcal{E}_{12} N_2^\alpha dN_1^\alpha + \mathcal{E}_{12} N_2^\alpha dN_2^\alpha = 0 \qquad 4\text{-}31$$

It is necessary to consider a dilute solution in order to obtain a manageable expression, that is, N_2^α and N_2^β approach zero. Define γ as,

$$\gamma = \lim_{N_2, N_2 \to 0} \frac{N_3^\beta N_1^\alpha - N_3^\alpha N_1^\beta}{N_1^\alpha} \quad \frac{N_2^\alpha}{N_3^\beta N_2^\alpha - N_3^\alpha N_2^\beta}$$

$$= \lim_{N_2, N_2 \to 0} \frac{\left(1 - \dfrac{N_3^\alpha N_1^\beta}{N_3^\beta N_1^\alpha}\right)}{\left(1 - \dfrac{N_3^\alpha N_2^\beta}{N_3^\beta N_2^\alpha}\right)} \qquad 4\text{-}32$$

Therefore,

$$= 1 - \frac{N_3^{\alpha} N_1^{\beta}}{N_3^{\beta} N_1^{\alpha}} \simeq 1 - \frac{1}{N_1^{\alpha}} \simeq - \frac{1}{N_1^{\alpha}} \qquad 4\text{-}33$$

since $N_3^{\alpha} \to 1$, $N_1^{\alpha} << 1$, and for wustite, $N_3^{\beta} \simeq N_1^{\beta} \simeq 0.5$. Substituting 4-33 into 4-31 for $N_2^{\beta}, N_2^{\alpha} \to 0$, and rearranging the terms,

$$\frac{dN_1^{\alpha}}{dN_2^{\alpha}} = - \frac{1 + \gamma \varepsilon_{12} N_1^{\alpha}}{\gamma (1 + \varepsilon_{11} N_1^{\alpha})} \simeq - (\frac{1}{\gamma} + \varepsilon_{12} N_1^{\alpha}) \qquad 4\text{-}34$$

since $\gamma >> \gamma \varepsilon_{11} N_1^{\alpha}$. From 4-33,

$$\frac{dN_1^{\alpha}}{dN_2^{\alpha}} = (N_1^{\alpha} - \varepsilon_{12} N_1^{\alpha}) \simeq - \varepsilon_{12} N_1^{\alpha} \qquad 4\text{-}35$$

assuming that $\varepsilon_{12} N_1^{\alpha} >> N_1^{\alpha}$

Integrating 4-35,

$$\ln N_1^{\alpha} = - \varepsilon_{12} N_2^{\alpha} + C \qquad 4\text{-}36$$

where C is an integration constant. Since $\ln N_1^{\alpha} = \ln N_1^{Fe}$ for $N_2^{\alpha} \to 0$, where N_1^{Fe} is the solubility of oxygen in pure iron, 4-36 becomes,

$$N_1^{\alpha} = N_1^{Fe} \exp - \varepsilon_{12} N_2 \qquad 4\text{-}37$$

Finally, substitution into 4-25 yields,

$$W_o (t) = \frac{D_{11} \varepsilon_{12} N_1^{Fe} \exp^{- \varepsilon_{12} N_2} (C_{21} - C_{2\theta})}{\sqrt{\pi D_{22}}} \quad t^{\frac{1}{2}} \qquad 4\text{-}38$$

An evaluation of this analysis for the internal oxidation of iron-nickel alloys will be carried out employing the experimental results of this investigation. Specifically, attempts will be made to demonstrate the validity of the equations describing oxygen supersaturation prior to oxide precipitation and the amounts of oxygen present in the subscale.

CHAPTER V

EXPERIMENTAL PROCEDURE

5.1 Introduction

The major portion of this section will concern the preparation of specimens, the oxidation apparatus, electron probe microanalyses, and X-ray diffraction studies.

5.2 Specimens

Electrolytic iron and nickel were used to prepare the alloys. Portions of each material were accu rately weighed to yield alloys containing 0, 10, 20, 30, 40, 50, 60, 70, and 90, weight percent nickel. Approximately 70 - 90 grams of material was placed into the melting chamber of a non-consumable arc furnace. A tungsten electrode was used for the melting operation, carried out under 200 mm pressure of argon. Each charge was melted, inverted, and then remelted, until a total of four melting operations had been completed, in order to prevent any long range segregation. The product was a button approximately 30mm. in diameter and 5-8mm thick. These buttons were hot rolled at 1000°C to a thickness of 3mm. The surfaces of each sheet were cleaned by pickling in dilute hydrochloric acid and by abrasion using 600 grit silicon carbide polishing paper. The sheets were cold rolled to a thickness of approximately 0.75mm.

The test specimens were obtained by cutting the sheets into platelets 1cm x 1.5cm on a precision shear. A suspension hole was drilled in each plate. A hole diameter was selected so that the area removed equalled the area introduced. The plates were then batch annealed in argon at slightly greater than atmospheric pressure at 1050°C for 3 days. The argon was introduced to the furnace assembly through glass columns containing ascarite and magnesium perchlorate. Zirconium plates were placed near the hot zone of the annealing furnace to act as an oxygen getter. The annealing operation eliminated any short range segregation and allowed the specimens to attain an equilibrium grain size.

Prior to oxidation, the specimens were metallographically polished following the procedure suggested by Samuels.[102] The plates were mounted flat in bakelite and polished through 240, 320, 400, 600 grit silicon carbide using water as lubricant followed by final polishing on selvyt cloths impregnated with 6 micron and 1 micron diamond abrasive using kerosene as lubricant. The kerosene was removed with petroleum ether, and the specimens were stored in acetone. Immediately before an experimental test, the specimens were dried, weighed to ± 2 micrograms, and the surface area was computed by measuring the specimen dimensions with a micrometer.

The chemical composition of the test specimens is given in Table I.

5.3 Oxidation Apparatus

The apparatus used for the oxidation tests is shown pictorially in Fig.10. A schematic illustration of the oxidation cell is given in Fig.11.

The vacuum system consisted of an oil diffusion pump backed by a two stage mechanical pump. A vacuum of 5×10^{-6}mm of mercury (Mc Leod gauge) could be achieved in the reaction tube. Liquid air traps were suitably positioned to prevent back diffusion of diffusion pump oil and to collect mercury from the Mc Leod gauge and manometer.

TABLE I

Chemical Analysis of Specimens

Spectrographic Analysis of Base Materials

(in p.p.m.)

	Al	Cd	Cr	Co	Cu	Mg	Mn	Mo	Si	Ti	V
Fe -	*tr	**nd	tr	nd	10	30	tr	tr	30	tr	tr
Ni -	15	5	0.6	400	44	3	4	1	82	10	1

Chemical Analysis of Alloys

***Nominal composition (wt%Ni) -	10	20	40	50	60	70	90
Actual composition (wt%Ni) -	10.2	19.7	41.0	50.1	60.4	70.5	90.0

* trace

** not detected

*** nominal composition used in text

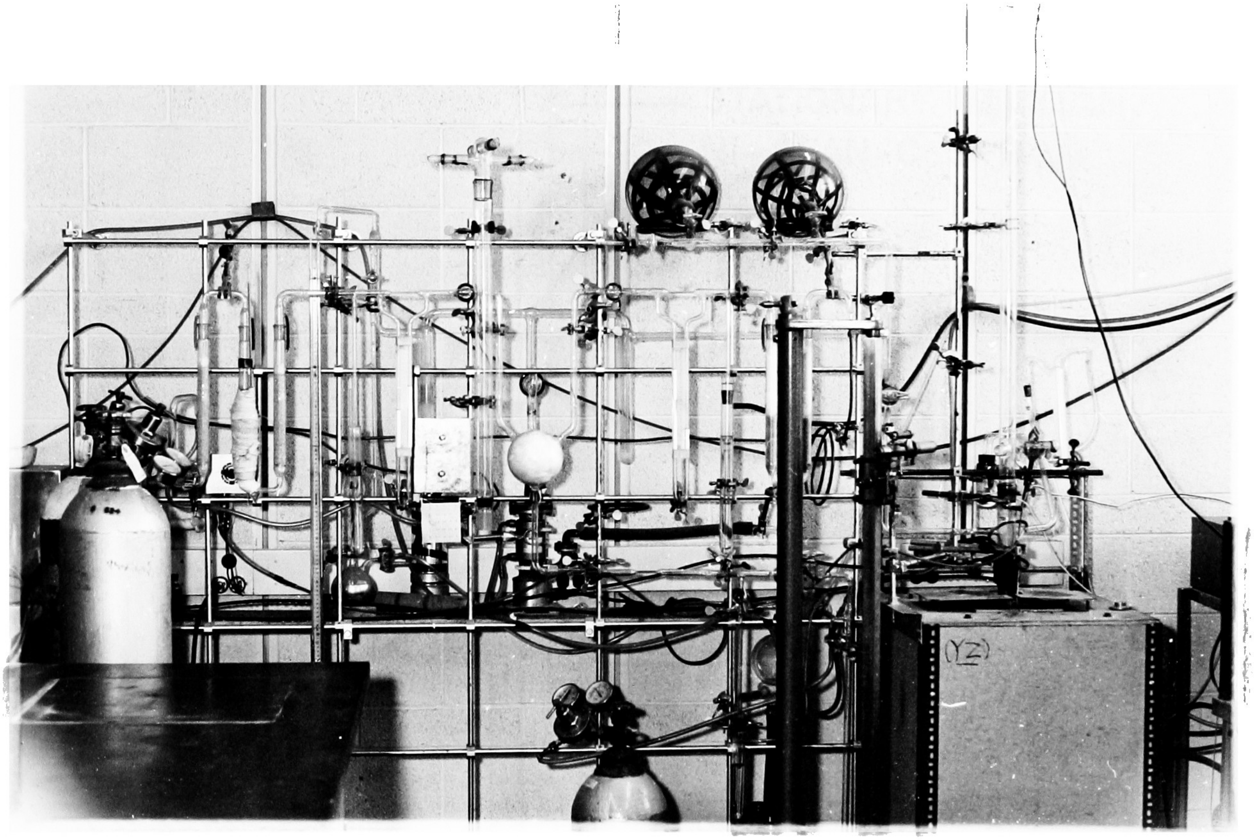

Fig.10 Oxidation Apparatus

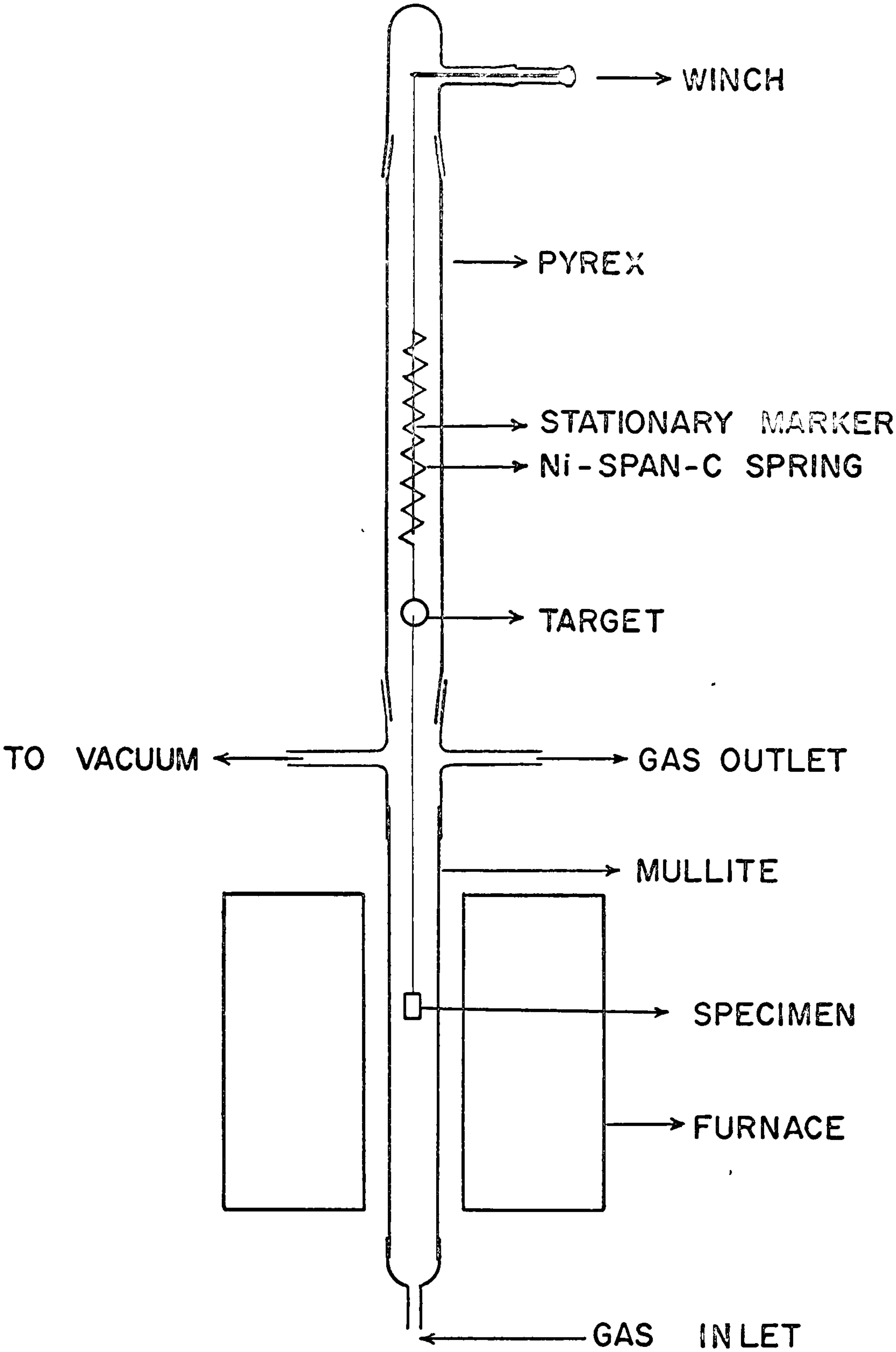

SCHEMATIC DIAGRAM OF KINETIC APPARATUS

Fig.11.

The oxidation tests were carried out in flowing carbon dioxide-carbon monoxide. The ratios of the two gases were accurately controlled by metering the components with simple capillary flowmeters similar to those described by Darken and Gurry.[55] These authors have also demonstrated that linear flow rates should exceed approximately 0.6cm/sec in order to eliminate the undesirable effects of thermal segregation. With this in mind, the capillary dimensions for a suitable flow range were estimated from the relation,

$$-\frac{\Delta p}{l} = \frac{32\,\mu\, V}{g_c\, D^2} \qquad 5\text{-}1$$

where, Δp is the pressure drop across capillary in gm/cm^2, l the capillary length in cm, g_c is 980 cm/sec^2, μ the gas viscosity in gm/cm-sec, D the capillary diameter in cm, and V the velocity of the gas in cm/sec.

The flowmeters were calibrated by measuring the rate of displacement of a soap film up a graduated cylinder. This method agrees quite well with other methods of calibration. The meters were calibrated with the respective gases, that is, carbon dioxide and carbon monoxide. The calibration curves are shown in Fig.12.

The carbon dioxide and carbon monoxide used in the tests were supplied by the Matheson Co. and a typical analysis is given in Table II. The gas cylinders were connected to the pyrex glass assembly through suitable pressure reduction gauges and needle valves via ¼ inch copper tubing. The carbon dioxide passed through columns containing magnesium perchlorate, reduced copper oxide at 400°C and activated alumina, the carbon monoxide through columns containing magnesium perchlorate and

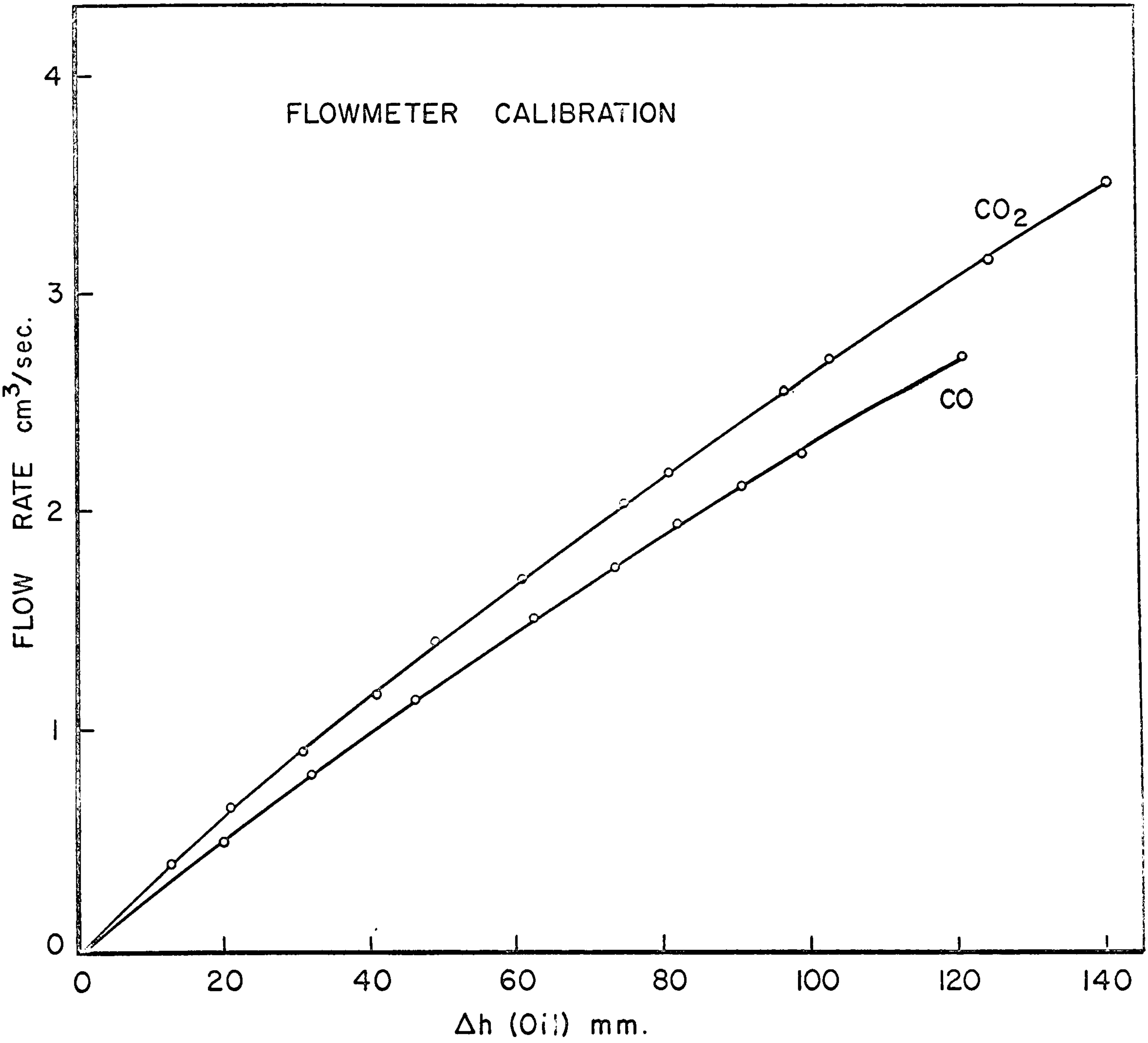
FLOWMETER CALIBRATION
FLOW RATE cm^3/sec.
Δh (Oil) mm.
CO$_2$
CO
0
1
2
3
4
0
20
40
60
80
100
120
140

Fig.12.

TABLE II

Typical Analyses of Carbon Dioxide and Carbon Monoxide Supplied

by

Matheson Co.

Carbon Monoxide: C. P. Grade, 99.5% CO (Min.)

CO_2: 200 p.p.m.

O_2: 20 p.p.m.

N_2: 75 p.p.m.

Dew point: - 60°F

Carbon Dioxide: Bone Dry Grade, 99.95% CO_2 (min)

$N_2 + O_2$: 500 p.p.m.

Dew point: - 30°F

oil content: < 5p.p.m.

ascarite. The gases were mixed in a 1 litre bulb packed with glass wool and were directed through glass tubulation to an inlet at the bottom of the mullite reaction tube. At first, pressure fluctuations in the lines caused severe oscillations of the flowmeter manometers, however, this was corrected by placing a capillary restriction and an oil damping pot between the meters and the furnace. Oscillations were reduced to ± 1mm which was considered adequate.

The furnace assembly consisted of a 20 inch Kanthal element imbedded in insulation which surrounded a 1¼ inch diameter mullite reaction tube. The mullite tube was directly sealed to the pyrex tubing. Power was supplied to the element by means of a 2500 V.A. transformer. The temperature was controlled to ± 2°C by a Philips temperature controller and chromel-alumel thermocouple, which activated a mercury relay in the supply circuit. The control thermocouple was located between the mullite tube and the Kanthal windings, and a measuring thermocouple was placed in the same position at the sample level. It was determined that a 6°C temperature difference existed between the specimen and thermocouple, and this was accounted for in the temperature setting. The temperature variation in the hot zone was 2°C over a distance of four inches. Variation in temperature at the centre of the hot zone was less than ¼°C. It was experimentally verified that a linear gas flow rate of 0.6cm/sec at standard temperature and pressure did not affect the temperature of the specimen.

A schematic diagram of the oxidation cell is shown in Fig.11. A calibrated spring was suspended from a glass winch by a nylon thread which passed through two forks placed at right angles to each other.

The entire suspension could be centered in the cell by manipulation of these forks. The polished specimens were suspended from the spring by a 5 mil platinum wire. The entire assembly could be raised or lowered in order to position the specimen in the center of the hot zone. Weight gains were recorded as a function of time by following the extension of the spring, relative to a stationary marker, with a cathetometer.

The spring was fabricated from 5 mil Ni - Span - C wire by coiling it about a ½ inch stainless steel rod and securely fastening the ends. Ni - Span - C is an age hardening alloy containing chromium, titanium, nickel and iron and exhibits a high elastic limit when in the hardened condition. Another feature of this material concerns the temperature coefficient of expansion. Depending on the age hardening temperature selected, this coefficient may be made positive, negative or zero. Therefore, the coil was annealed in an argon atmosphere for 4.5 hours at 1350°F, resulting in a spring with maximum mechanical properties and a zero coefficient of expansion. The coefficient remains essentially constant over the temperature range 50 - 150°F, and thus, eliminates the need for a constant temperature controlling device in the spring compartment to compensate for room temperature fluctuations.

The spring was calibrated by measuring its extension associated with the addition of short nichrome wires. Each nichrome wire weighed approximately 10 milligrams, and this weight was determined to ± 2 micrograms on a Mettler micro balance. The resultant calibration curve is shown in Fig.13. The sensitivity of the spring is 36 mg/cm. The value remained constant throughout the course of the investigation.

In a typical experiment, a polished specimen was suspended from

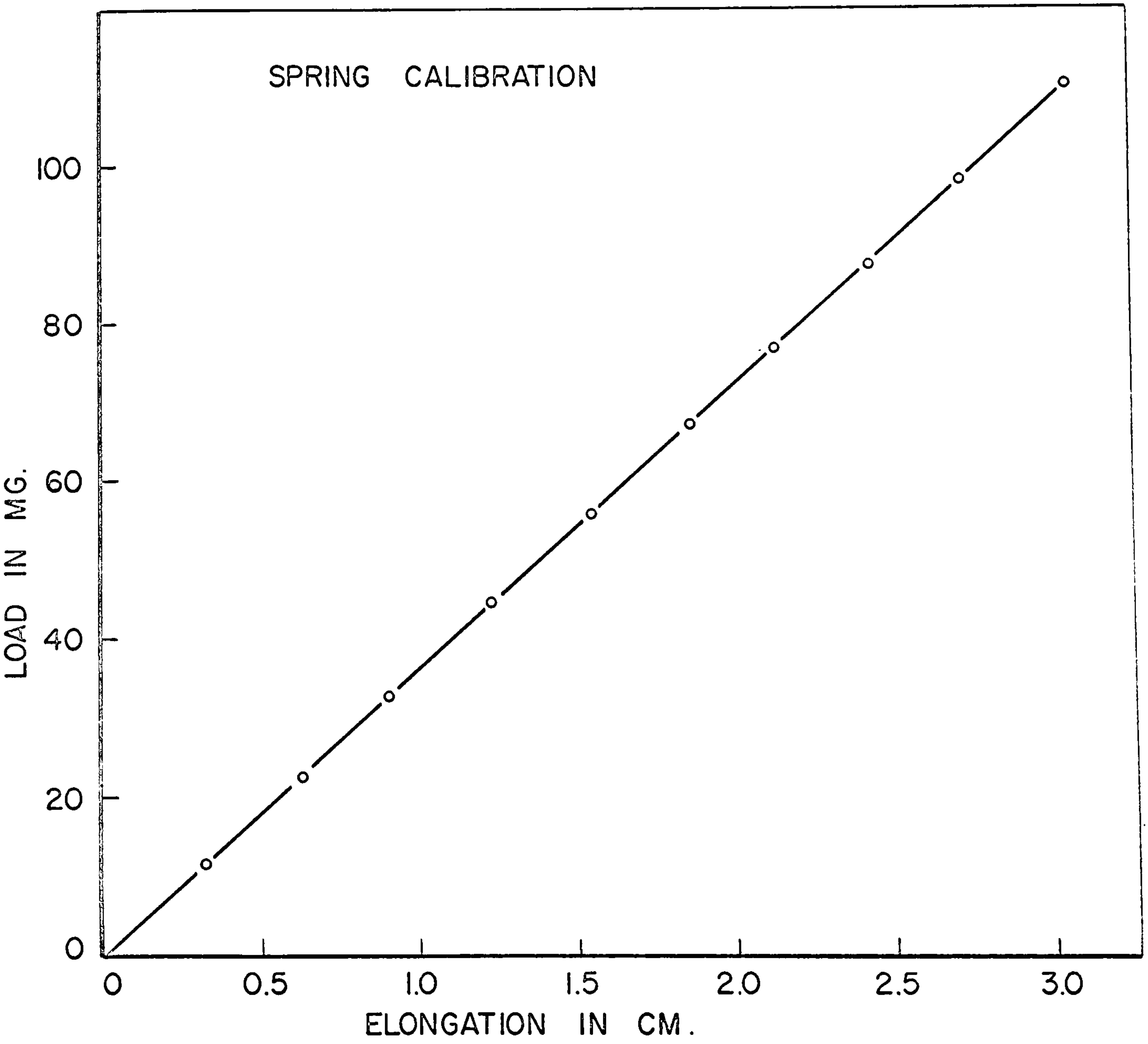
SPRING CALIBRATION
LOAD IN MG.
0
20
40
60
80
100
0
0.5
1.0
1.5
2.0
2.5
3.0
ELONGATION IN CM.

Fig.13.

the spring, and the assembly was coupled to the reaction tube by means of a ground glass joint. The apparatus was evacuated with the mechanical pump, and the furnace was adjusted to test temperature. The system was returned to atmospheric pressure after a period of one hour by filling with nitrogen. Then the reaction gas, mixed in the proper proportions, flowed through the apparatus for a minimum of one hour. The spring assembly was lowered with the glass winch until the specimen was centered in the hot zone. Weight gains were recorded after 5 minutes in order to allow steady state to be attained. After the test, the specimen was quickly raised to the cooler portions of the tube in approximately 20 seconds, and allowed to cool to room temperature in the flowing gas. The oxide surface was examined under the microscope, and then the specimen was mounted vertically in epoxy resin. The mount was then polished in cross section,in a manner similar to that used for surface preparation, and stored in a desiccator until required.

5.4 Electron Probe Microanalysis

No attempt will be made to describe the theory associated with probe microanalysis. A complete description may be had by refering to the text by L. S. Birks.[103] A photograph of the probe assembly is shown in Fig.14. The apparatus was designed by Dr. G. R. Purdy, faculty member, and constructed from a Philips EM-100 electron microscope by Mr. H. Walker, technician, Dept. of Metallurgy and Metallurgical Engineering. A 2 - 3 micpon diameter beam of electrons is focused on the surface of the specimen to be analized. The electrons are sufficiently energetic to generate characteristic X-radiation from the elements present. Spectrometers, at a take off angle of 50° from the horizontal plane of the specimen, diffract

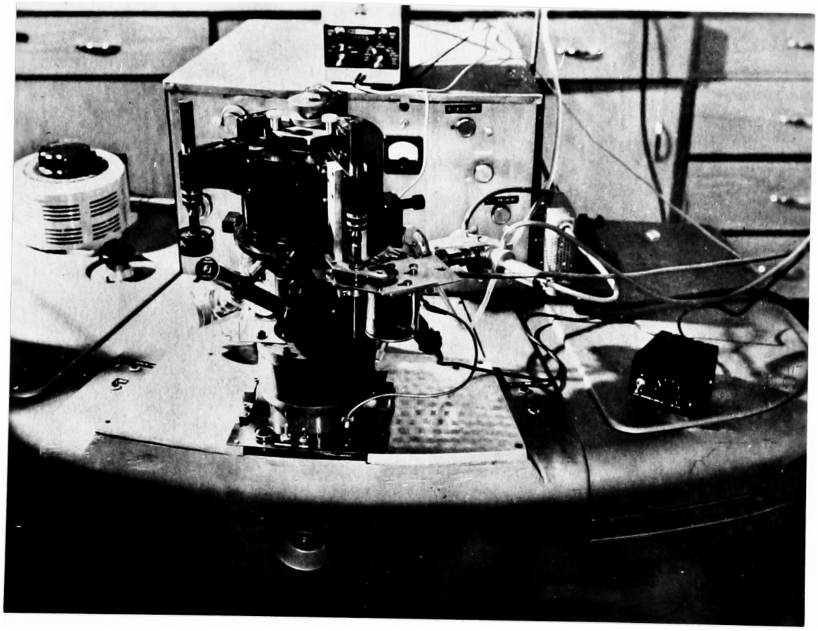

Electron probe assembly

Fig.14.

the radiation of interest into proportional gas counters. The intensity of the radiation is then displayed by an electronic counter or a strip chart recorder.

In order to use the probe for quantitative analysis it is necessary that it be calibrated for the elements of interest. If standards containing a homogeneous distribution of the two elements in various known proportions can be obtained, the calibration is relatively a simple process. Such is the case for the iron-nickel system. The X-ray intensity from a given element, minus the background intensity, is directly proportional to the amount of the element present. The background intensity is determined by counting with the spectrometer set a few degrees off-peak or, as in the case of iron-nickel, by setting the spectrometer for nickel and counting on pure iron. It is not sufficient to plot the observed intensity as a function of composition since this intensity will vary from day to day. Therefore a relative intensity or an intensity ratio is plotted versus composition. A convenient ratio is obtained by using the observed intensity from an alloy, minus the background, and the intensity from the pure element of interest, minus background. Although characteristics of the probe may vary, the intensity ratio will be constant for a given system.

The probe was calibrated for iron-nickel alloys in the above manner. Small alloy plates 2mm square of known composition were mounted in bakelite with pure iron and nickel. A thin film of carbon was evaporated on the polished surface in order to make the mount conducting. Intensity ratios were computed from an average of four determinations for alloys containing 20, 30, 40, 50, 60, 70, and 90 wt. % Ni. The calibration curves are shown in Fig.15.

The composition of an unknown specimen may then be determined by comparing the measured intensity ratio with the curves. Attempts were made to measure the degree of enrichment of nickel in the metal phase at the metal-oxide interface and the concentration gradients in the subscale region. The latter proved to be quite difficult due to the close proximity of the precipitated oxide particles. The few results obtained are considered to be of qualitative value. As the investigation became more advanced, it was noted that the density of internal precipitates was quite low in a band adjacent to the metal-oxide interface. Therefore, the interface concentrations could be more accurately determined by remounting the specimens flat and polishing through the external scale on a very low angle taper section. The metal-oxide interface is thus enlarged and appears free of precipitation. The results were more easily obtained and are considered to be more accurate than the previous method.

5.5 X-Ray Diffraction

X-ray powder diffraction techniques were employed for the purpose of phase identification on a number of specimens. The phases in the remainder of the alloys were determined metallographically.

X-ray powder diffraction patterns were obtained using both large and small Debye - Scherrer cameras in conjunction with a Philips X-ray generator. Iron filtered cobalt radiation was used in all cases. Oxide was mechanically removed from the specimens and ground with an agate pestle and mortar. A base coat nailpolish was added to the powder and, just prior to setting, a quartz rod was inserted into the viscous mixture

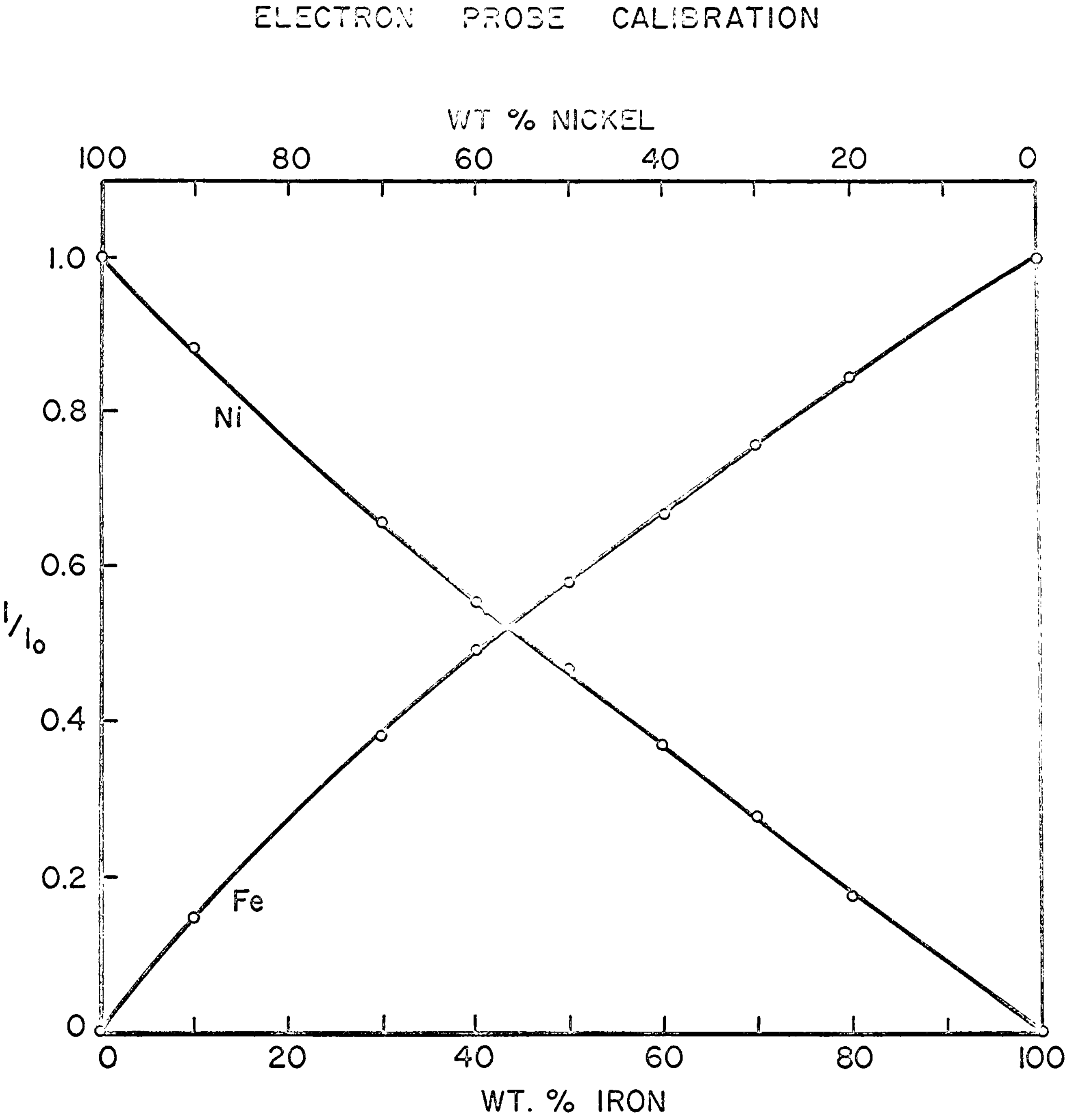
ELECTRON PROBE CALIBRATION
WT % NICKEL
100
80
60
40
20
0
1.0
0.8
0.6
0.4
0.2
0
I/I_0
Ni
Fe
0
20
40
60
80
100
WT. % IRON

Fig.15..

and slowly withdrawn. This produced an approximately 0.2 - 0.4mm diameter filament of oxide powder on the tip of the rod. The filaments were dried and mounted in the X-ray cameras.

5.6 Oxide Morphology

The specimens were examined and photographed using standard metallographic techniques. In several cases, the rates of scale growth and subscale penetration were determined. These results were obtained by measuring the thickness of the scales and subscales as functions of time using a calibrated filar eyepiece with a Reichert metallograph at a suitable magnification. Unfortunately, the scale-gas and subscale-alloy interfaces were quite rugged and, therefore, these measurements were confined to planar regions of the interfaces.

CHAPTER VI

EXPERIMENTAL RESULTS

6.1 Introduction

The data obtained from the various experimental tests will be presented in this section in the usual manner, that is, in the form of graphs, tables and photomicrographs. With the exception of two experiments at 900° and 950°C, all tests were carried out at 1000°C.

6.2 Oxidation Kinetics

The kinetic data, obtained by recording the increase in specimen weight as a function of time, are illustrated graphically in Figs. 16 to 27 for the materials investigated. In all cases, the weight gains are expressed in mg/cm^2 and the time is in hours. The specimen compositions and the experimental conditions are indicated on the graphs. The alloy concentrations are in weight per cent and the gas compositions are expressed in volume per cent, carbon dioxide/ volume per cent carbon monoxide. The results for the iron - 30% nickel alloy, oxidized at 900° and 950°C in a 50% carbon dioxide atmosphere, are shown in Fig. 21. The total gas pressure was 1 atmosphere in all tests.

It is apparent that the data for the 20, 30, and 40% nickel alloys are best described by straight lines, excepting the initial portions of the curves. In some instances, as in the case of pure iron, iron - 10% nickel, and iron - 50% nickel, linear behaviour is observed over a limited range of the data. The linear regions are indicated on the graphs. The rate constants were determined from the slopes of the best straight lines

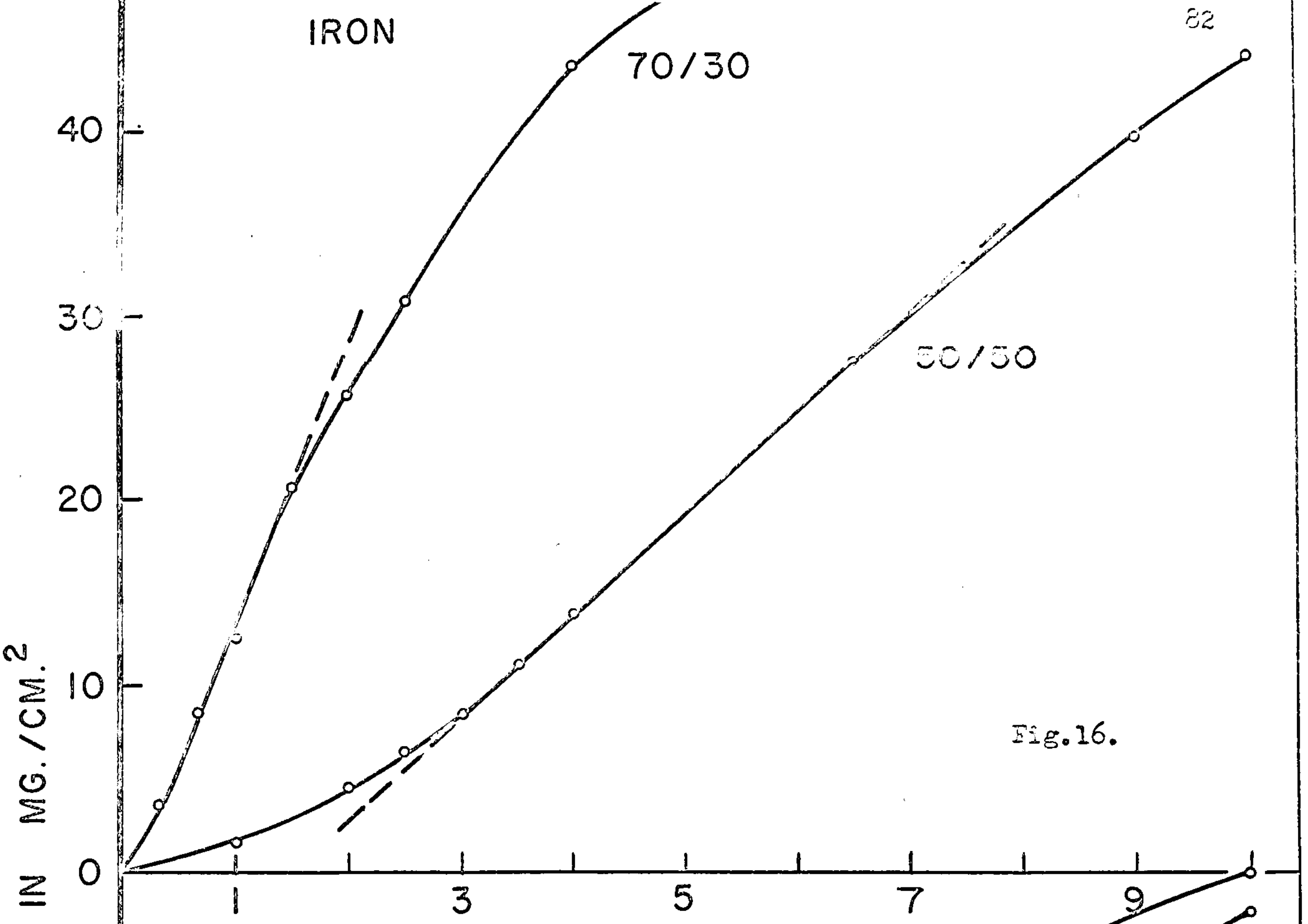
IRON
70/30
50/50
WEIGHT GAIN IN MG./CM.^{2}
0
10
20
30
40
1
3
5
7
9

Fig.16.

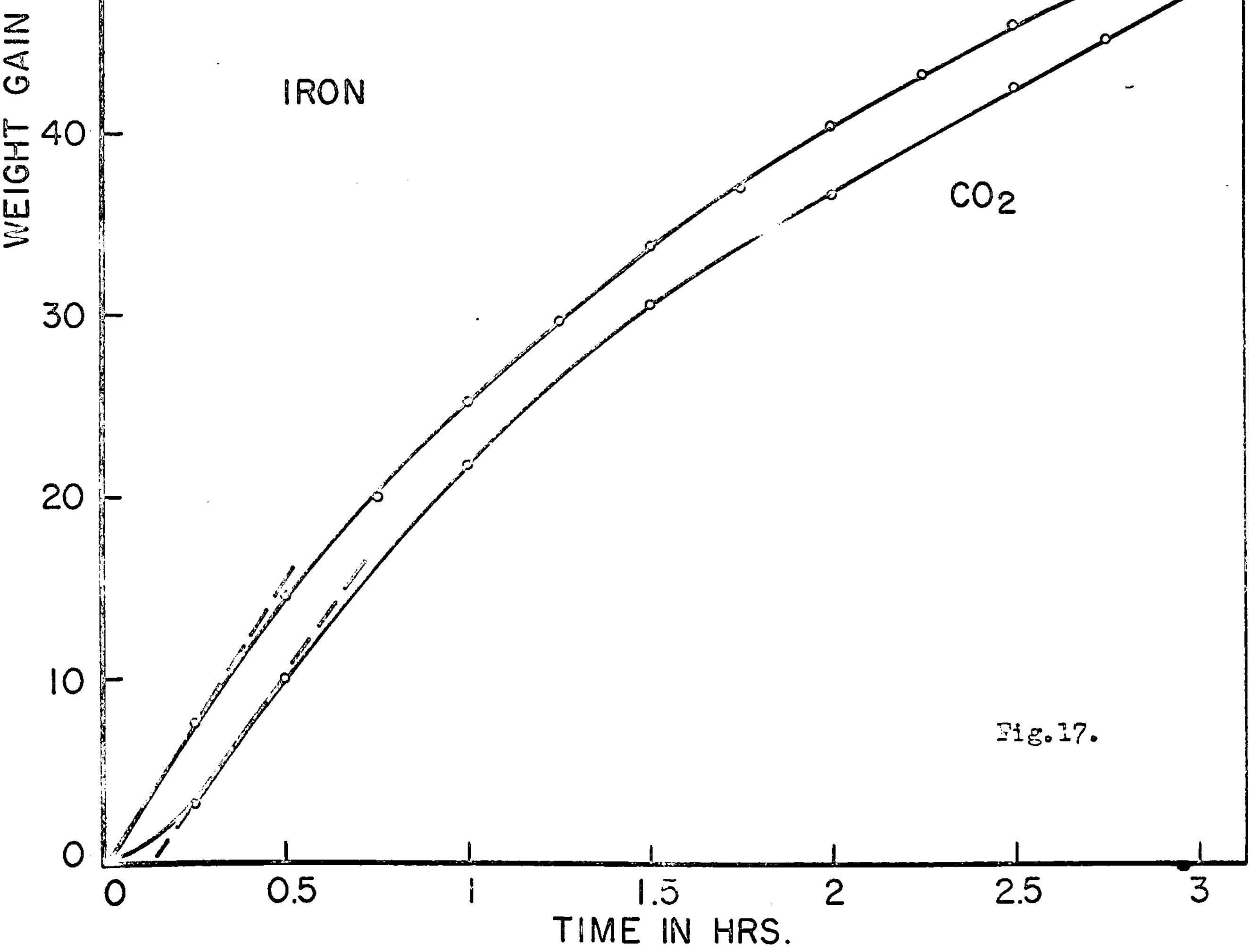
IRON
CO$_2$
0
10
20
30
40
0
0.5
1
1.5
2
2.5
3
TIME IN HRS.

Fig.17.

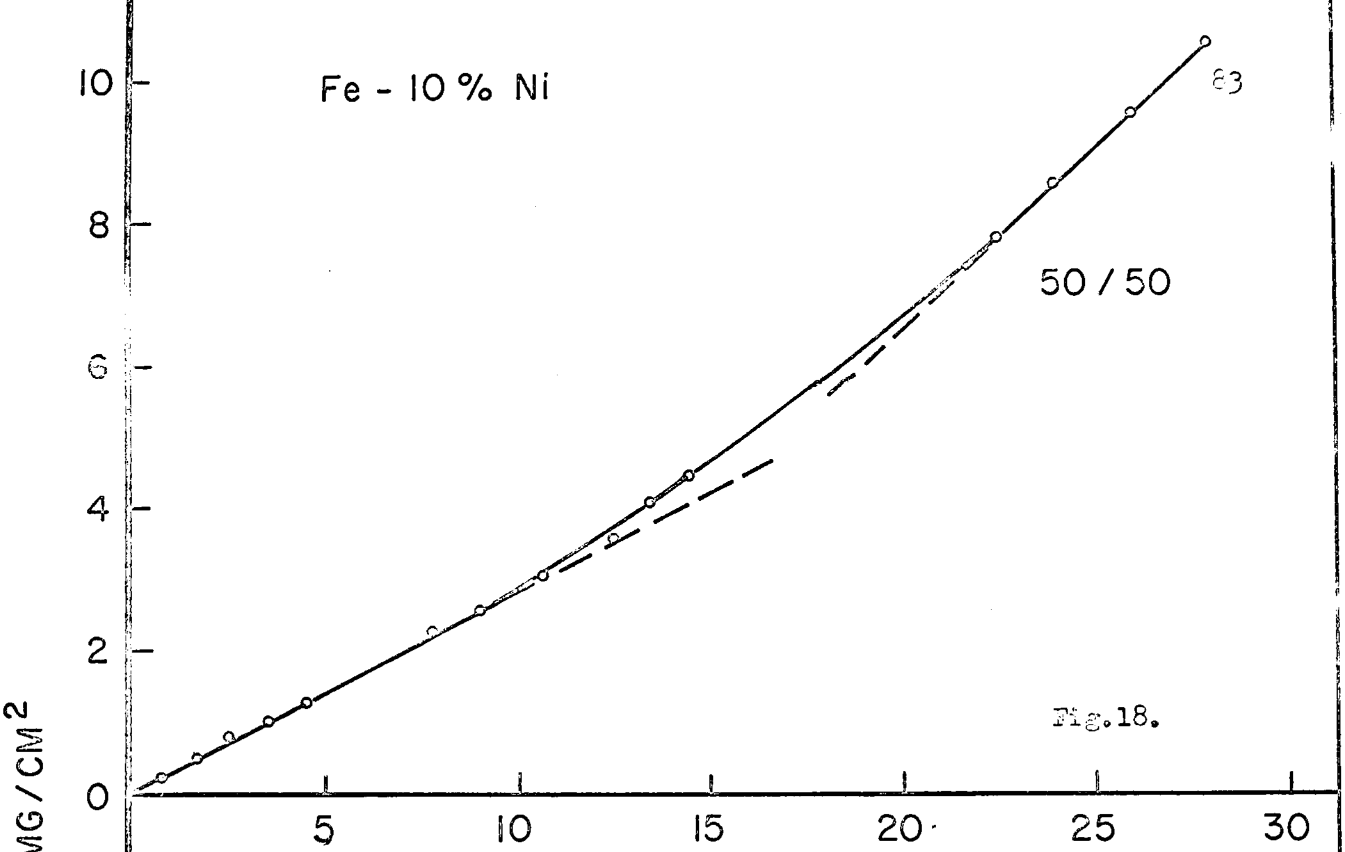
Fe - 10 % Ni
50 / 50
WEIGHT GAIN MG/CM²
0
2
4
6
8
10
5
10
15
20
25
30

Fig.18.

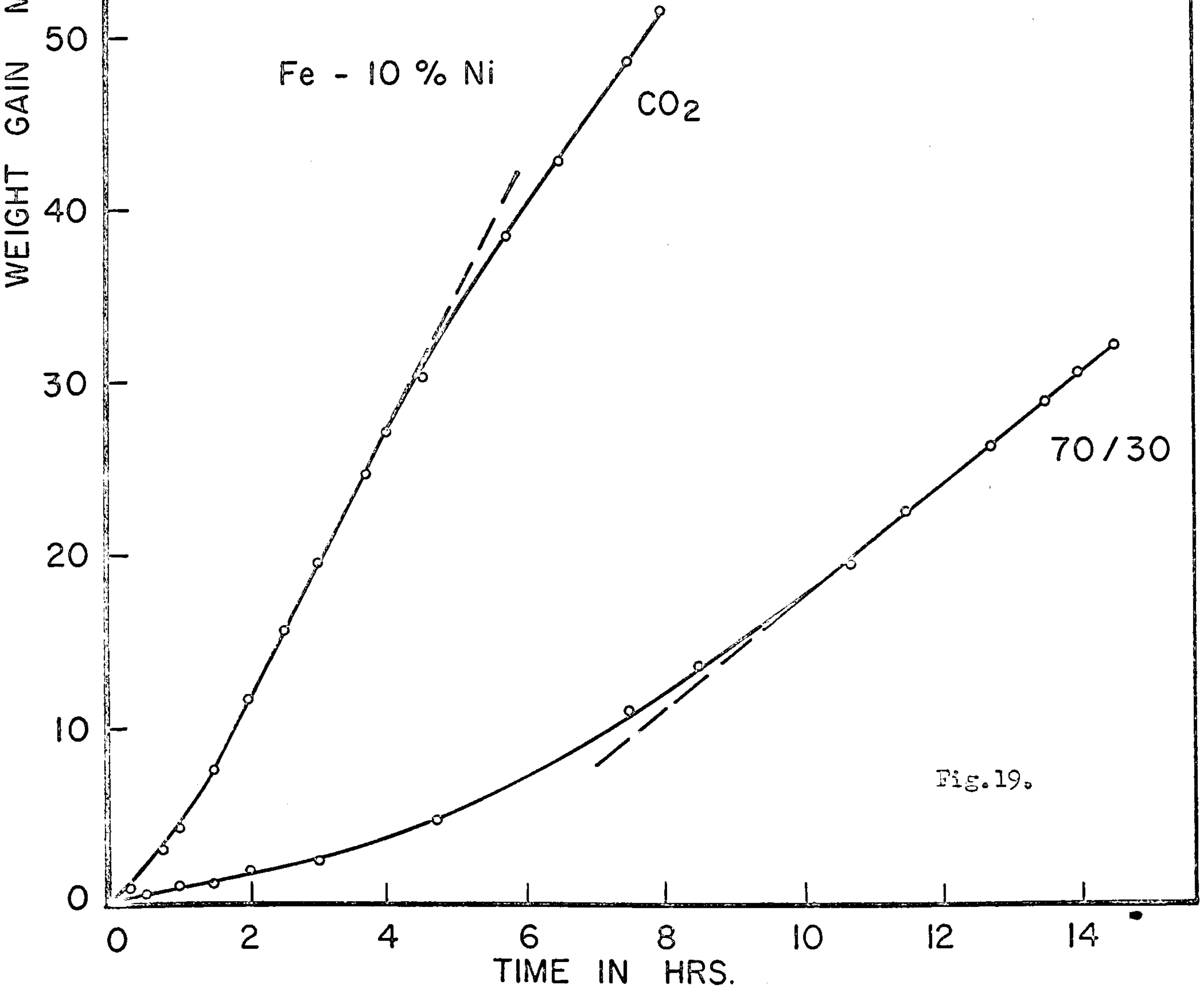
Fe - 10 % Ni
CO₂
70 / 30
0
10
20
30
40
50
0
2
4
6
8
10
12
14
TIME IN HRS.

Fig.19.

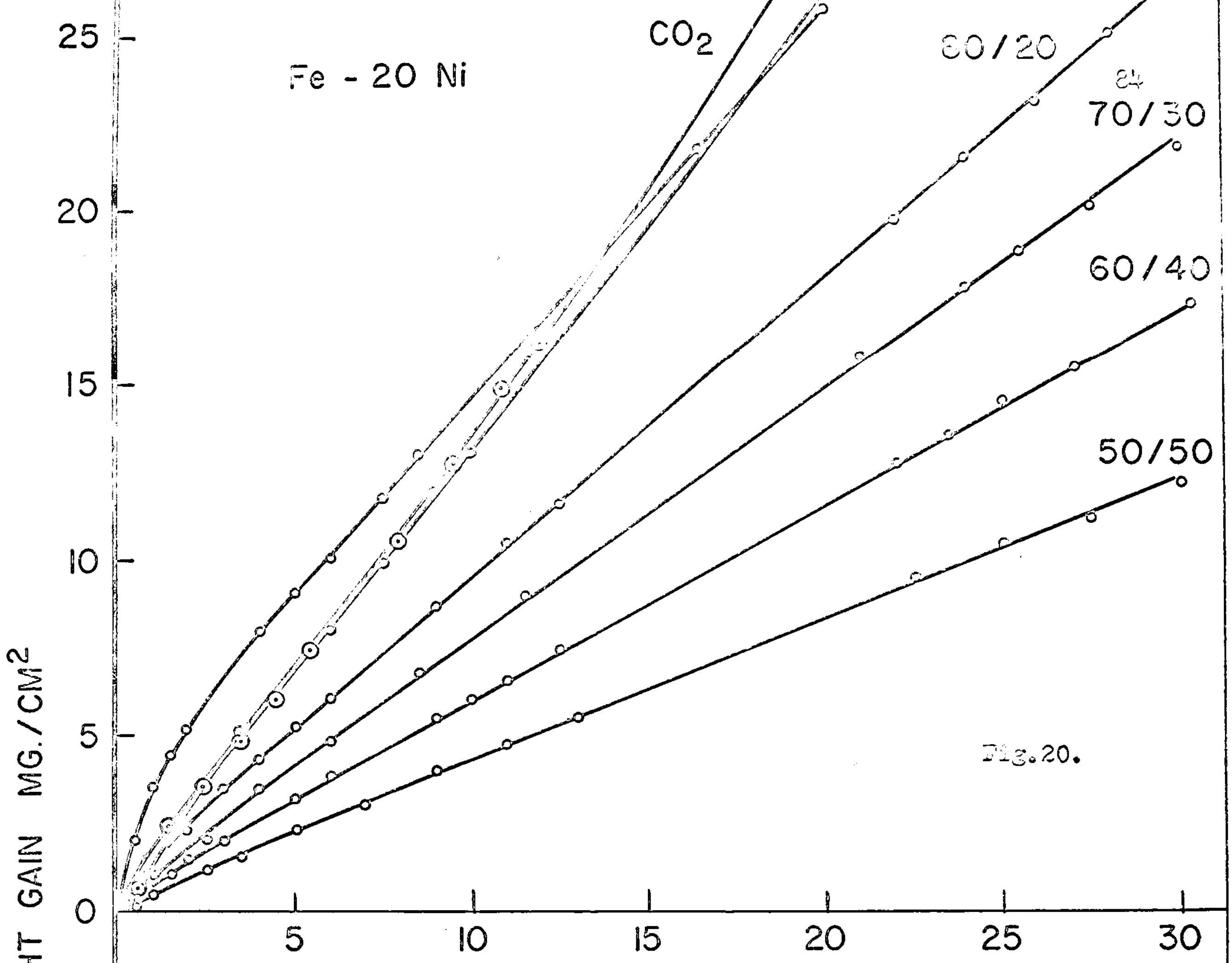
Fe - 20 Ni
CO$_2$
80/20
70/30
60/40
50/50
WEIGHT GAIN MG./CM^2
0
5
10
15
20
25
5
10
15
20
25
30

Fig.20.

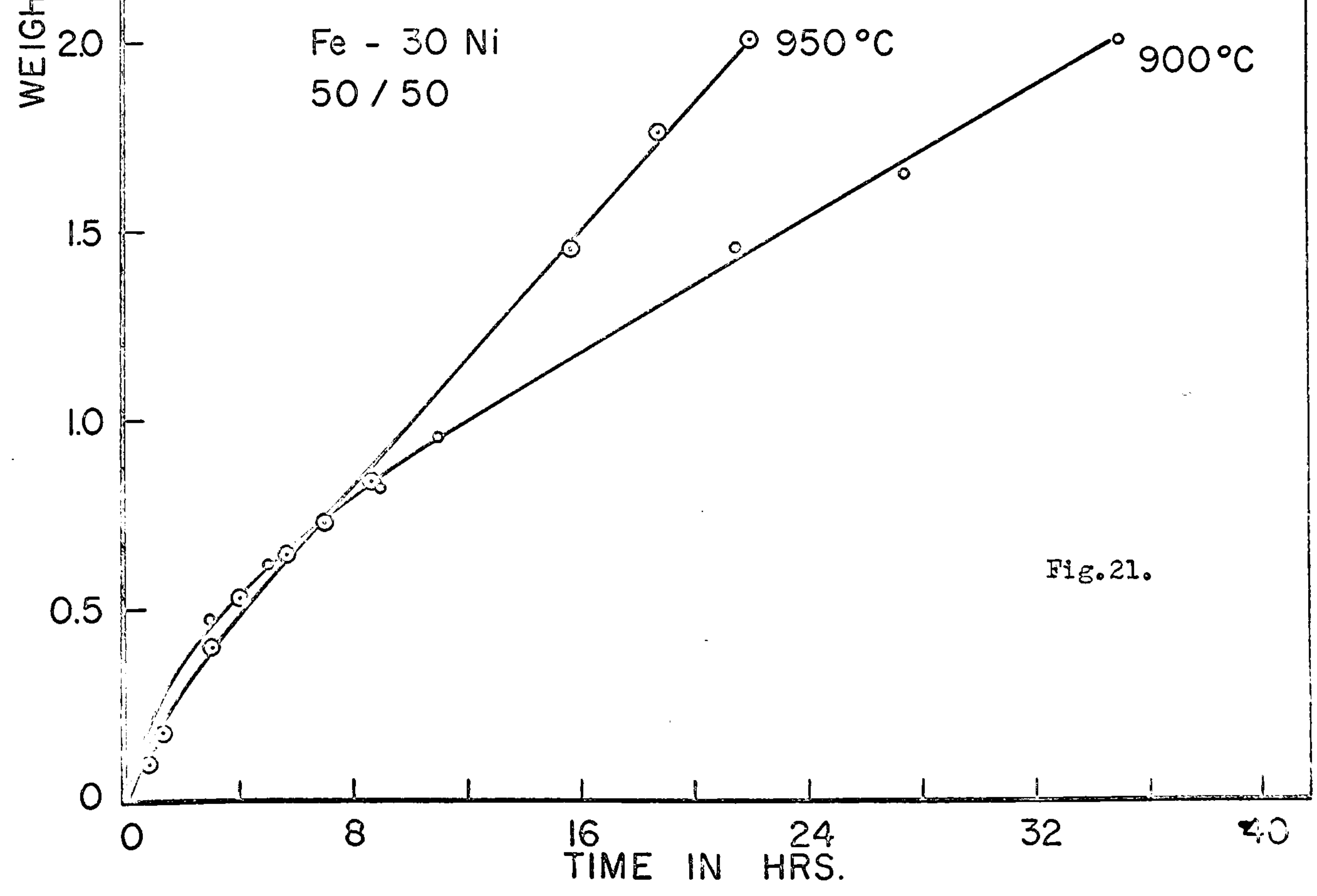
Fe - 30 Ni
50 / 50
950°C
900°C
0
0.5
1.0
1.5
2.0
0
8
16
24
32
40
TIME IN HRS.

Fig.21.

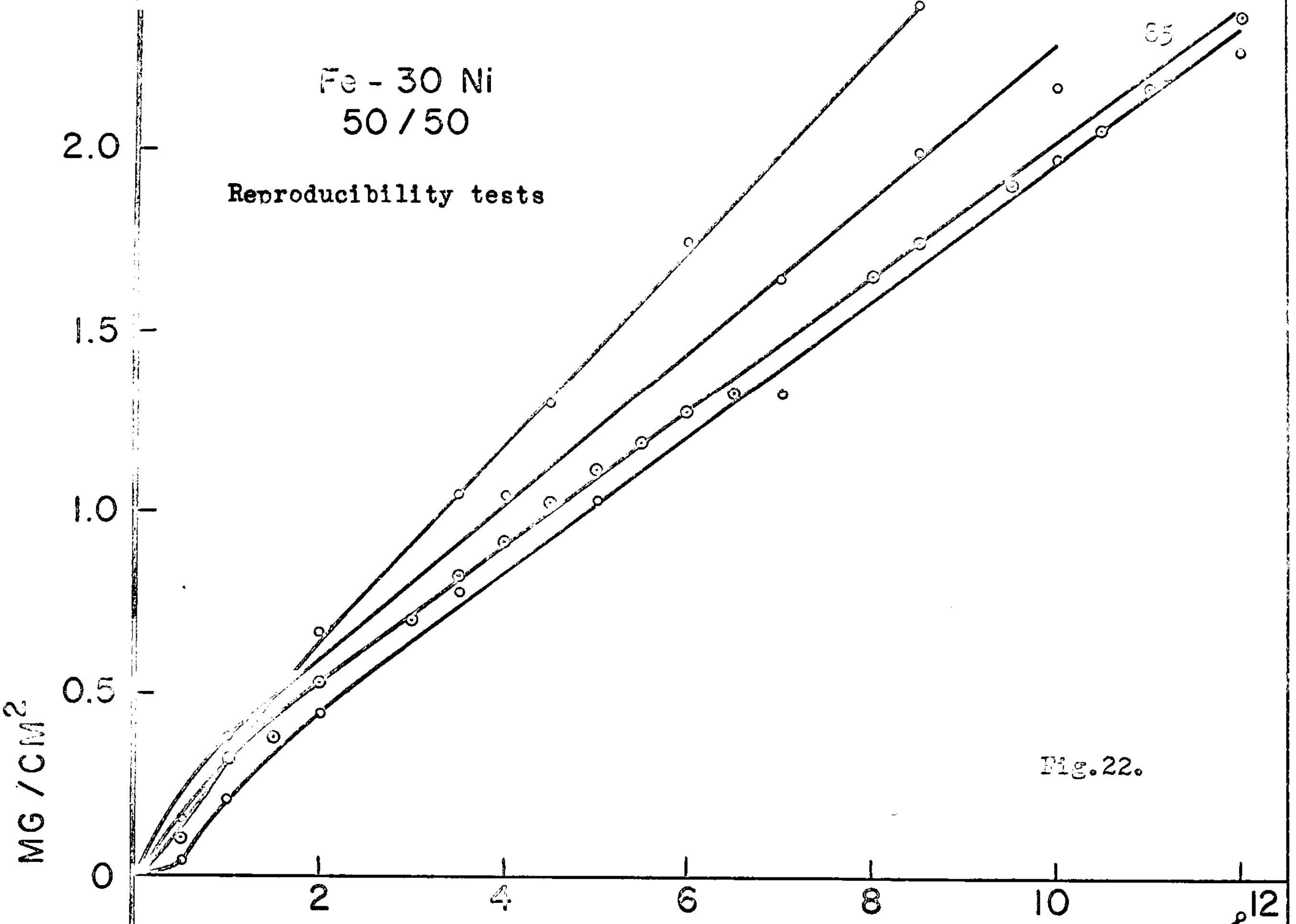
Fe - 30 Ni
50/50
Reproducibility tests
85
MG/CM^2
0
0.5
1.0
1.5
2.0
2
4
6
8
10
12

Fig.22.

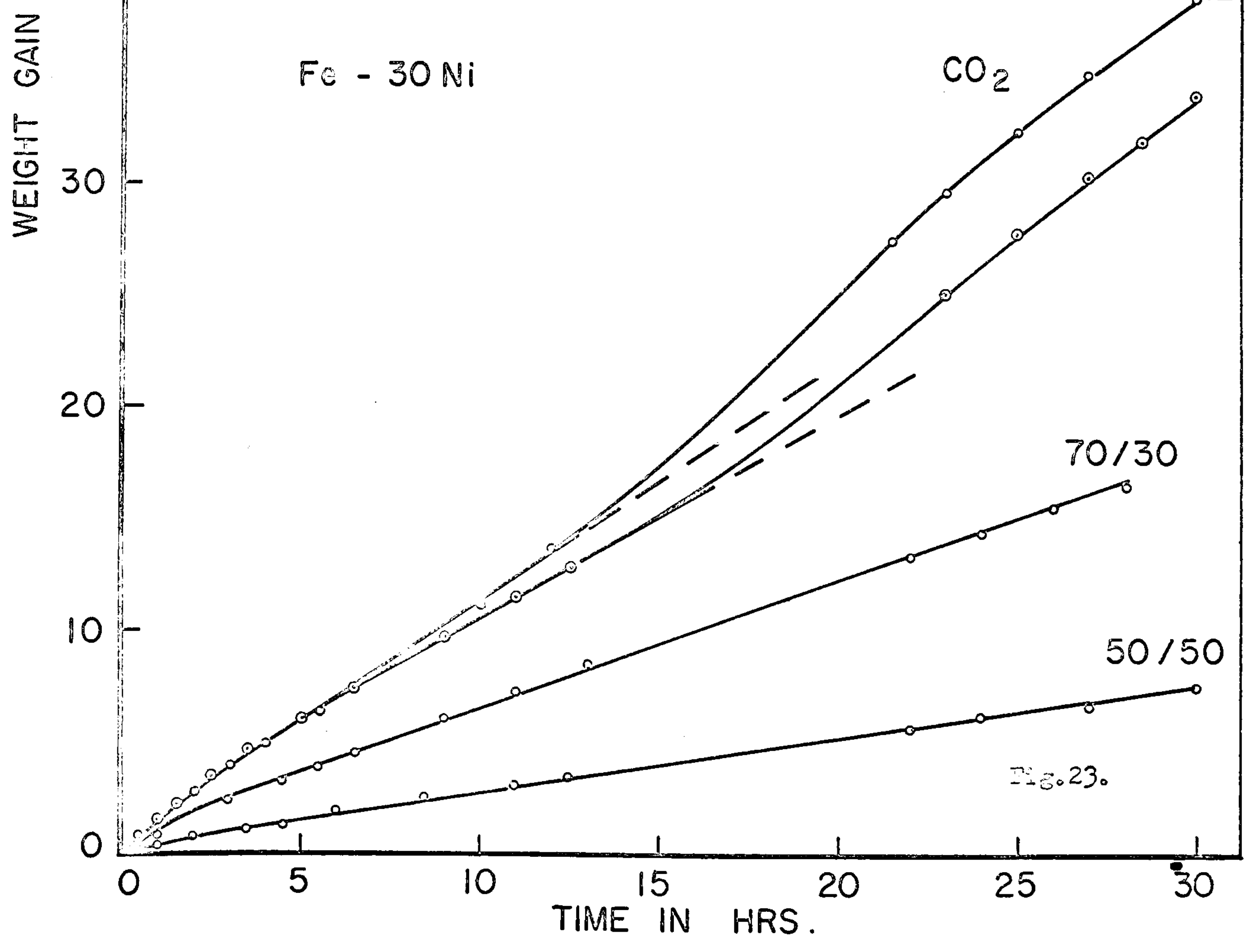
WEIGHT GAIN
Fe - 30 Ni
CO$_2$
70/30
50/50
0
10
20
30
0
5
10
15
20
25
30
TIME IN HRS.

Fig.23.

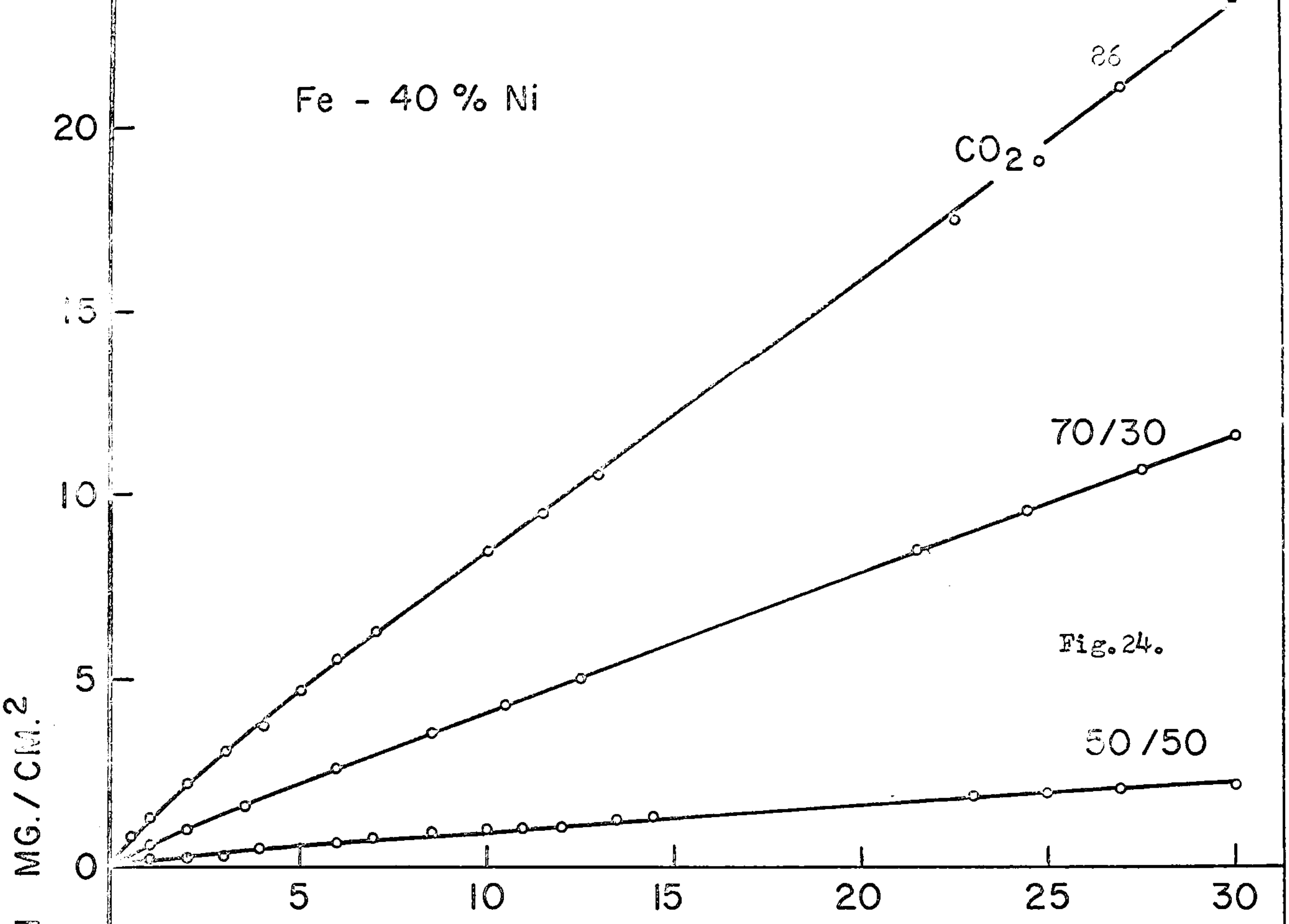
Fe - 40 % Ni
CO2
70/30
50/50
WEIGHT GAIN MG./CM.2
0
5
10
15
20
5
10
15
20
25
30

Fig.24.

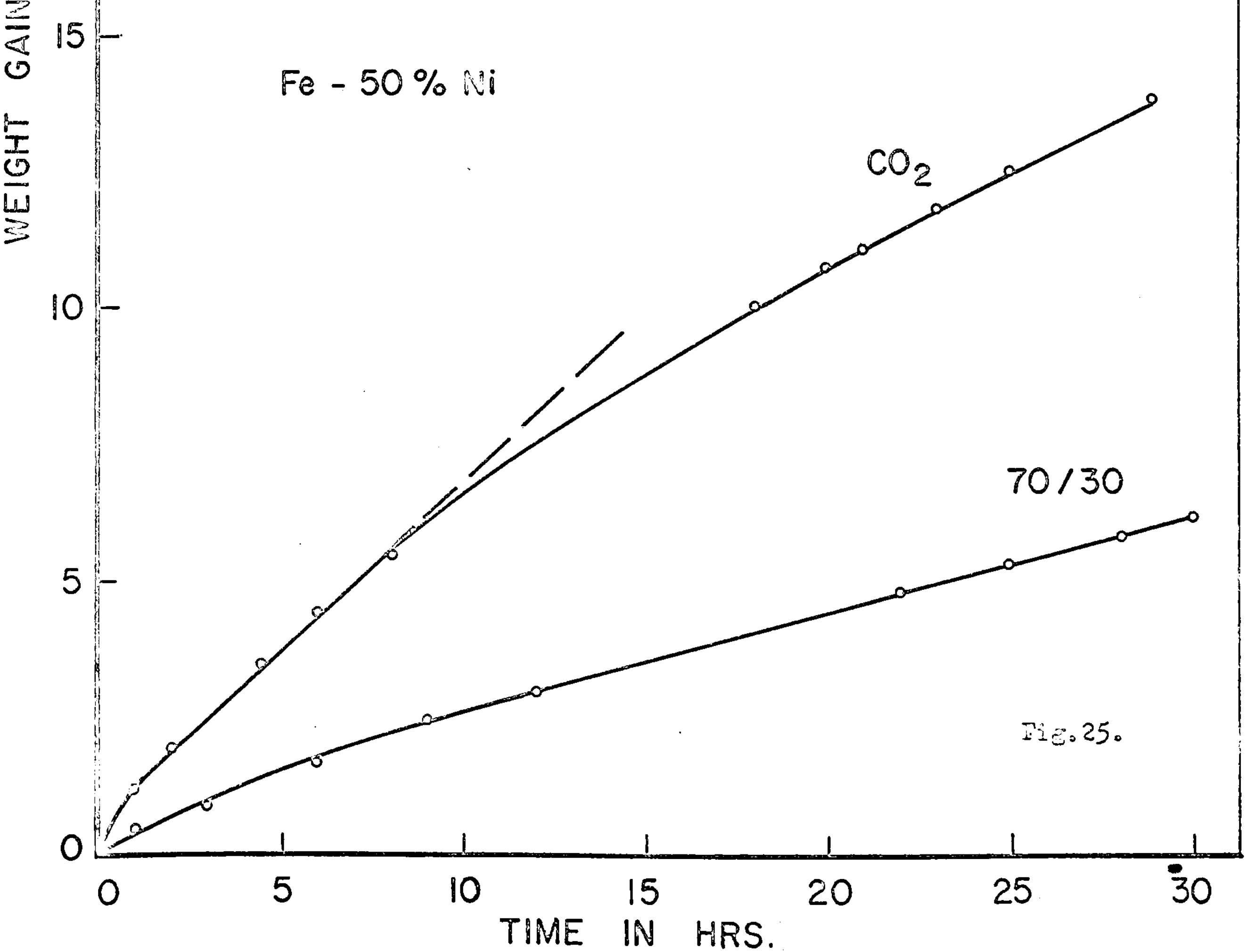
Fe - 50 % Ni
CO2
70/30
0
5
10
15
0
5
10
15
20
25
30
TIME IN HRS.

Fig.25.

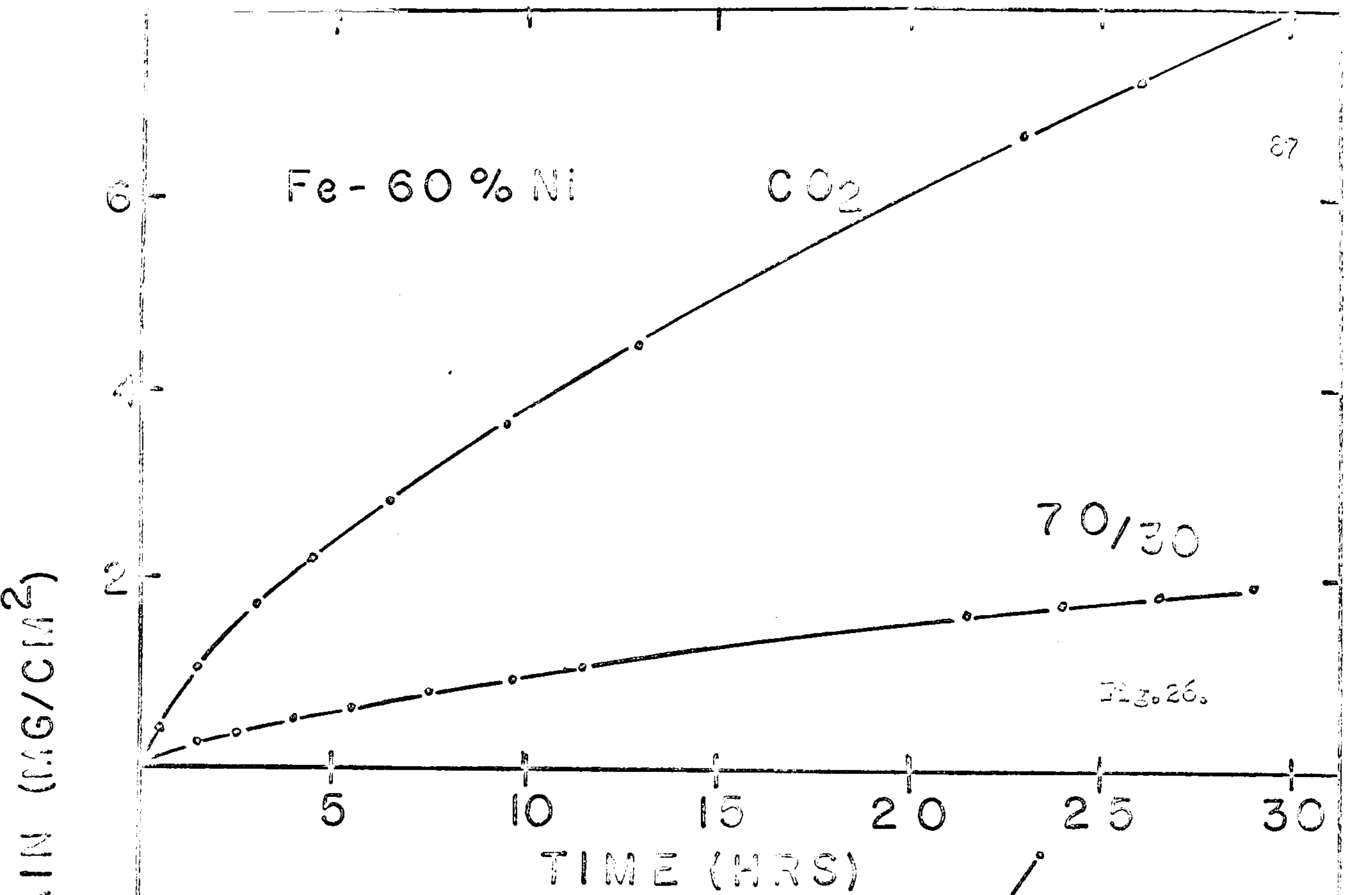

Fig.26.

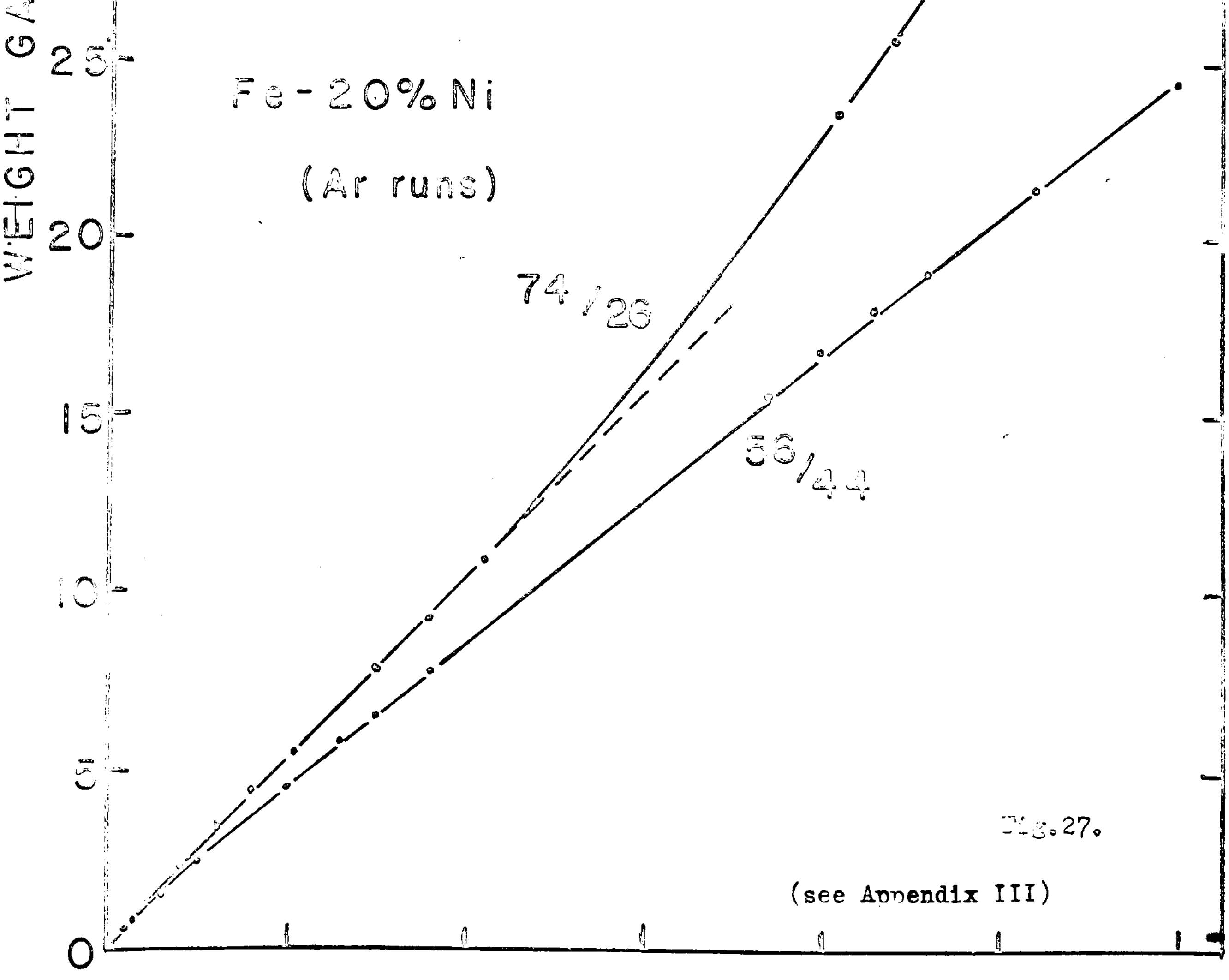

Fig.27.

(see Appendix III)

drawn through the experimental points, and are reported in Table III. Several tests were repeated in order to determine the reproducibility of the data. The average values for these rate constants are included in the table. The poorest reproducibility was associated with the iron - 30% nickel alloy oxidized in 50% carbon dioxide. From these curves, the error in the linear rate constant was computed to be ± 12% from the average. Therefore, for singular tests, the rate constant was assumed to be the average value, and a ± 12% error limit was applied to this value.

The kinetic data for pure iron, iron - 10% nickel, and iron - 50% nickel approached parabolic behaviour after a period of linear oxidation. The scale thicknesses were less than 100 microns before this transition. The iron - 60% nickel alloy, oxidized in carbon dioxide, did not exhibit linear behaviour and the data for this alloy in 70% carbon dioxide could be described by both a linear and parabolic rate law for the experimental test time.

The linear rate constant for the iron - 50% nickel alloy oxidized in carbon dioxide was estimated from the initial portion of the curve on the basis of a log - log plot. The best straight line was drawn through the points which gave an exponent closest to unity. For the points indicated, this exponent was 0.85.

The reaction kinetics for alloys containing more than 60% nickel were not determined.

Throughout the course of the kinetic investigation, it was determined that the spring target could be consistently read to ± 0.03mm on the cathetometer scale. Since the force constant of the spring was 3.6 mg/mm, the error associated with any experimental point is approximately

TABLE III

Linear Rate Constants

Alloy (wt.%Ni)	Gas Composition (CO_2/CO)	K_L (mg/cm^2-hr)
Fe	50.50	5.60 ± 0.68
Fe	70/30	14.2 ± 1.72
Fe	CO_2	31.0
Fe	CO_2	27.2
		average 29.1 ± 3.50
10%	50/50	0.5 ± 0.06
10%	70/30	3.1 ± 0.37
10%	CO_2	8.0 ± 0.96
20%	50/50	0.39 ± 0.05
20%	60/40	0.56 ± 0.07
20%	70/30	0.72 ± 0.09
20%	80/20	0.87 ± 0.10
20%	CO_2	1.10
20%	CO_2	1.24
20%	CO_2	1.17
		average 1.17 ± 0.14
30%	50/50	0.27
30%	50/50	0.21
30%	50/50	0.19
30%	50/50	0.19
		average 0.21 ± 0.03

TABLE III

(Cont'd)

Linear Rate Constants

Alloy (wt.%Ni)	Gas Composition (CO_2/CO)	K_L (mg/cm^2-hr)
30%	70/30	0.57 ± 0.07
30%	CO_2	0.93
30%	CO_2	1.06
		average 0.99 ± 0.12
30%(900°C)	50/50	0.043 ± 0.005
30%(950°C)	50/50	0.08 ± 0.01
40%	50/50	0.07 ± 0.01
40%	70/30	0.39 ± 0.05
40%	CO_2	0.75 ± 0.09
50%	70/30	0.18 ± 0.02
50%	CO_2	0.61 ± 0.07

0.03mg/cm^2 for specimens having about 3.5cm^2 surface area.

6.3 Oxide Structure

The oxide structures were determined by a combination of optical and X-ray diffraction techniques at room temperature. In all alloy oxidation tests, an external scale and a subscale were formed.

The scales formed on pure iron and alloys containing up to 40% nickel consisted entirely of wustite with the exception of alloys containing 30 and 40% nickel oxidized in carbon dioxide. These scales contained precipitates of magnetite, as shown in Figs. 28 and 29. The subscales were wustite in all cases. The scales on the iron - 50% nickel alloy oxidized in 70% carbon dioxide and carbon dioxide were wustite with a uniform precipitation of magnetite, as illustrated in Fig. 30 and 31. The appearance of magnetite is believed to be a result of the decomposition of wustite on cooling to room temperature. The external scale on the 60% nickel alloy oxidized in carbon dioxide was magnetite. The subscale consisted of magnetite near the alloy - oxide interface, and wustite in the interior of the alloy separated by a region of wustite containing precipitated magnetite. The external scale on this alloy oxidized in 70% carbon dioxide consisted of wustite plus precipitated magnetite, similar to the 50% nickel alloy shown in Fig. 30. The scale and subscale of a 70% nickel alloy oxidized in carbon dioxide consisted of a nickel bearing spinel, determined by comparing the lattice parameter with data reported in reference 79. The scale on a 90% nickel alloy oxidized in carbon dioxide was nickel monoxide, and the subscale was not identified.

The scale structures on the materials investigated are summarised in Table IV.

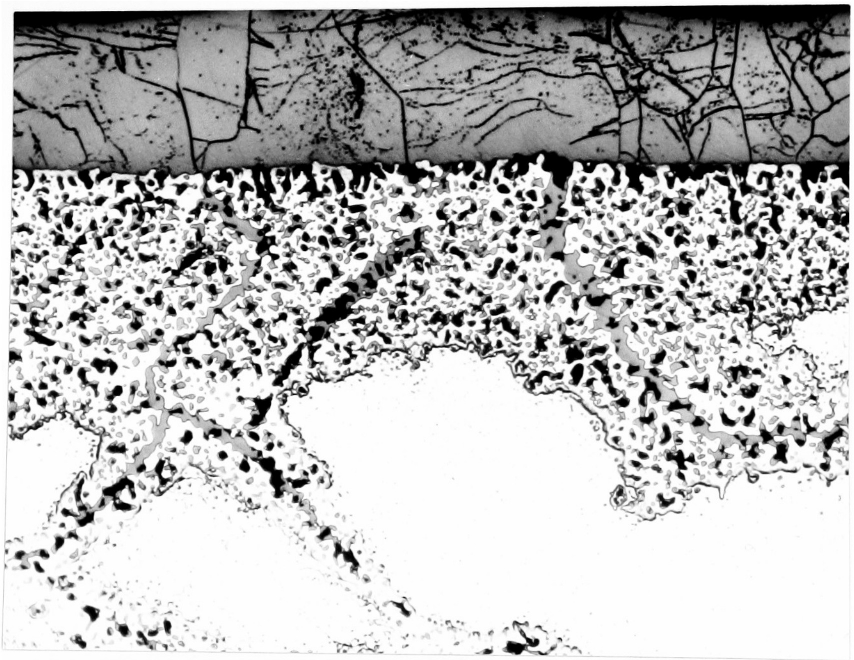

Fig.28. Fe-30%Ni oxidized for 24 hrs. in CO_2. Etched in 2% nital. 210X

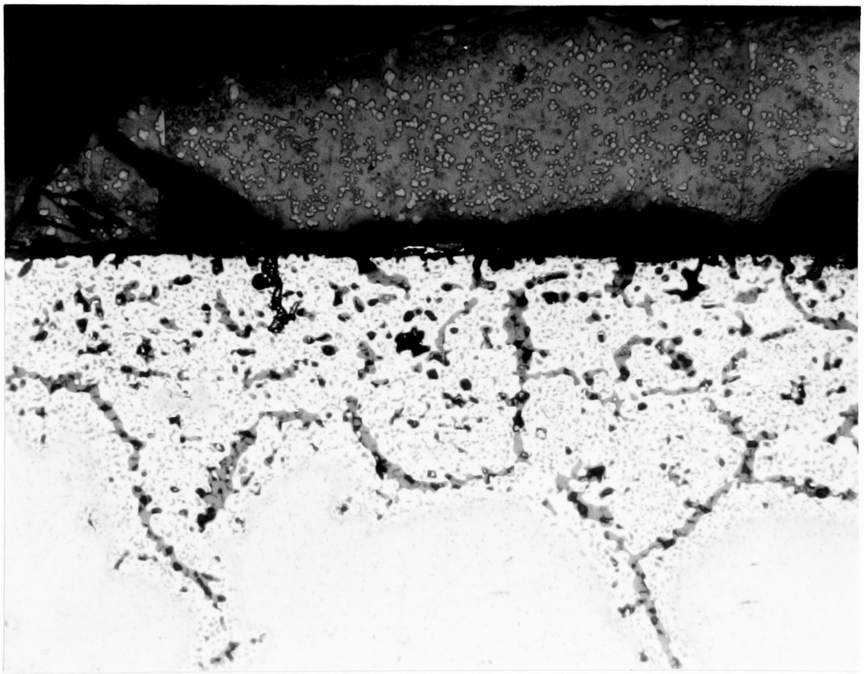

Fig.29. Fe-40%Ni oxidized for 24 hrs. in CO_2. Etched in 2% nital. 210X

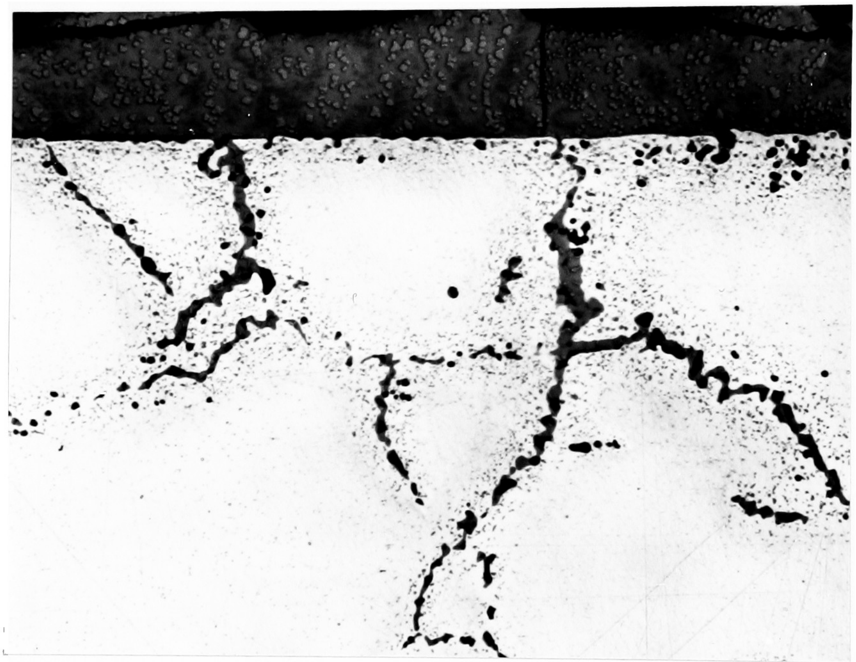

Fig.30. Fe-50%Ni oxidized for 24 hrs. in CO_2. Etched in 2% nital. 210X

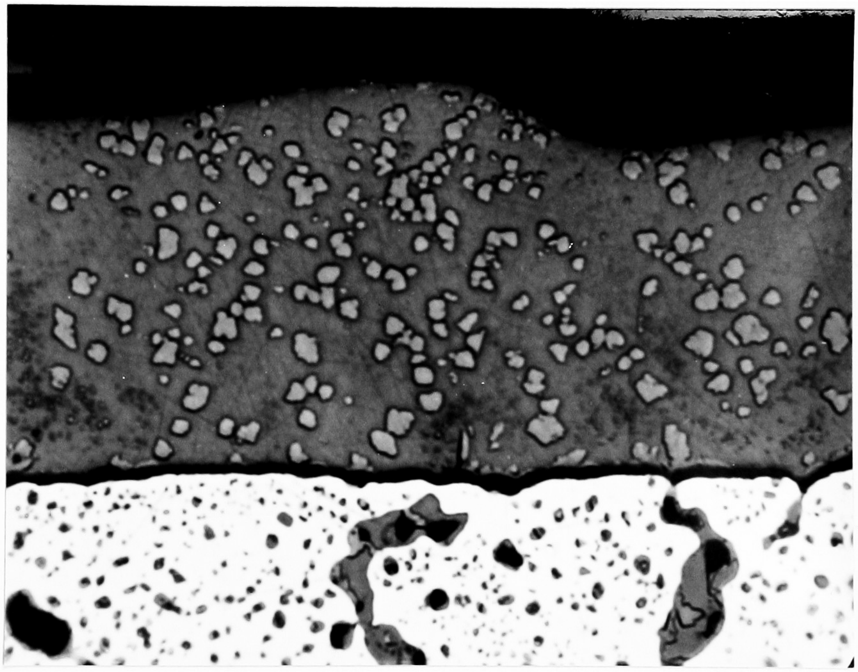

Fig.31. Fe-50%Ni oxidized for 24hrs. in CO_2. Etched in 2% nital. 700X

TABLE IV

Oxide Structures

The scales and subscales on pure iron and the iron - 10% and 20% nickel alloys were wustite in all gas compositions. The following table summarizes structures for alloys containing greater than 20% nickel.

Alloy (wt.%Ni)	Gas Composition CO_2/CO	Oxide Structure Subscale	 Scale
30%	50/50	FeO	FeO
30%	70/30	FeO	FeO - Fe_3O_4ppte
40%	50/50	FeO	FeO
40%	70/30	FeO	FeO
40%	CO_2	FeO	FeO - Fe_3O_4ppte
50%	70/30	FeO	FeO - Fe_3O_4ppte
50%	CO_2	FeO - Fe_3O_4ppte	FeO - Fe_3O_4ppte
60%	70/30	FeO	FeO - Fe_3O_4ppte
60%	CO_2	FeO - Fe_3O_4	Fe_3O_4
70%	CO_2	$Ni_xFe_{3-x}O_4$	$Ni_xFe_{3-x}O_4$
90%	CO_2		NiO

X - Ray Diffraction Data

Alloy (wt.%Ni)	Gas Composition (CO_2/CO)	Oxide (Scale)	a_o (Å)
20%	CO_2	FeO	4.30

TABLE IV

(Cont'd)

X - Ray Diffraction Data

Alloy (wt.%Ni)	Gas Composition (CO_2/CO)	Oxide (Scale)	a_o (Å)
20%	CO_2	FeO	4.30
40%	CO_2	FeO - Fe_3O_4ppte	4.29 - 8.39
60%	70/30	FeO - Fe_3O_4ppte	4.29 - 8.42
60%	CO_2	Fe_3O_4	8.39
70%	CO_2	$Ni_xFe_{3-2}O_4$	8.37
90%	CO_2	NiO	4.19

6.4 Oxide Morphology

A photo micrograph of the surface topography typical of the scales formed on all materials in all gas compositions is shown in Fig.32. It can be seen that the oxide - gas interface is rugged, and that the scale appears to grow macroscopically in a direction perpendicular to the specimen surface but microscopically in crystallographic directions as indicated by the steps and facets in the micrograph.

In cross section, the scales formed on alloys containing up to 50% nickel appear to be compact and nearly pore free. Any porosity in the scales is probably a result of the mechanism of scale growth. It is conceivable that two adjacent step ledges, advancing towards each other, may project out from the oxide surface, meet, and coalesce. A pore would result below the oxide bridge. Oxide scales are suseptible to spalling and severe cracking on cooling for alloys containing more than 50% nickel. An example of this behaviour is shown in Fig.33. In all cases, the metal - oxide interface is planar except in regions where subscale particles have coalesced with the external scale.

An interesting effect was noted when the specimens were metallographically polished on silicon carbide papers using water as a lubricant. In most cases, the scales appeared to be extremely porous as in Fig.34, however they, were essentially pore free as in Fig.35, when kerosene was used as a lubricant. The scales were severely etched in aqueous ferric chloride and remained pore free, indicating that the polishing action did not involve a surface effect. Subsequently all metallographic polishing was done using kerosene as a lubricant.

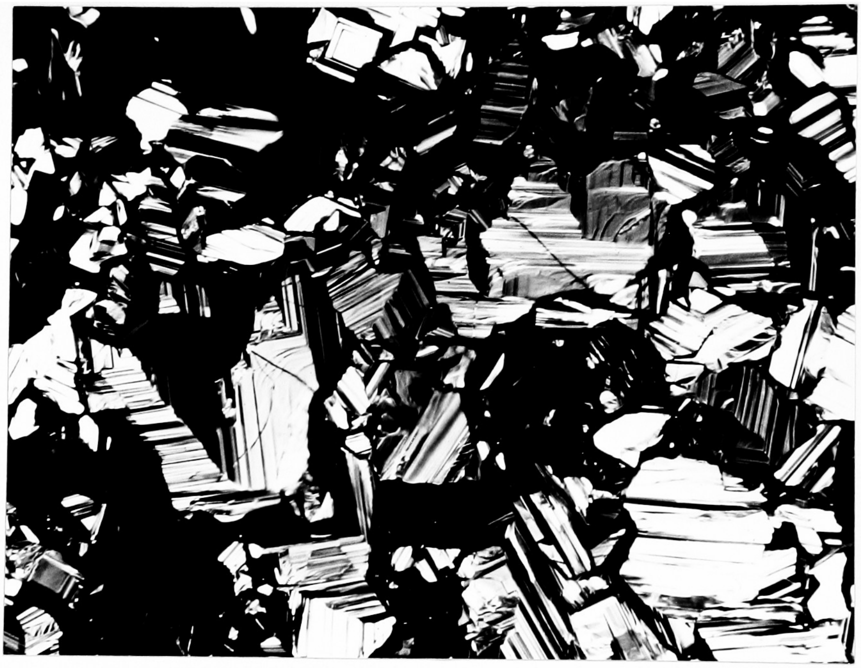

Fig.32. Typical oxide surface topography. Fe-20%Ni oxidized for 24 hrs in CO_2. 200X

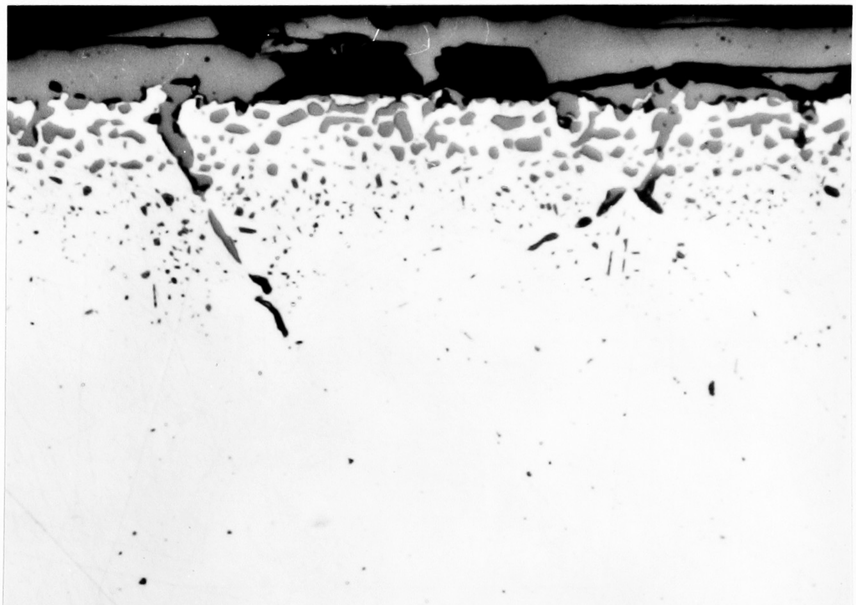

Fig.33. Spalled oxide. Fe-70%Ni oxidized for 48 hrs. in CO_2. 330X

Fig.34. Wustite polished on 600 grit SiC using H_2O as lubricant. 300X

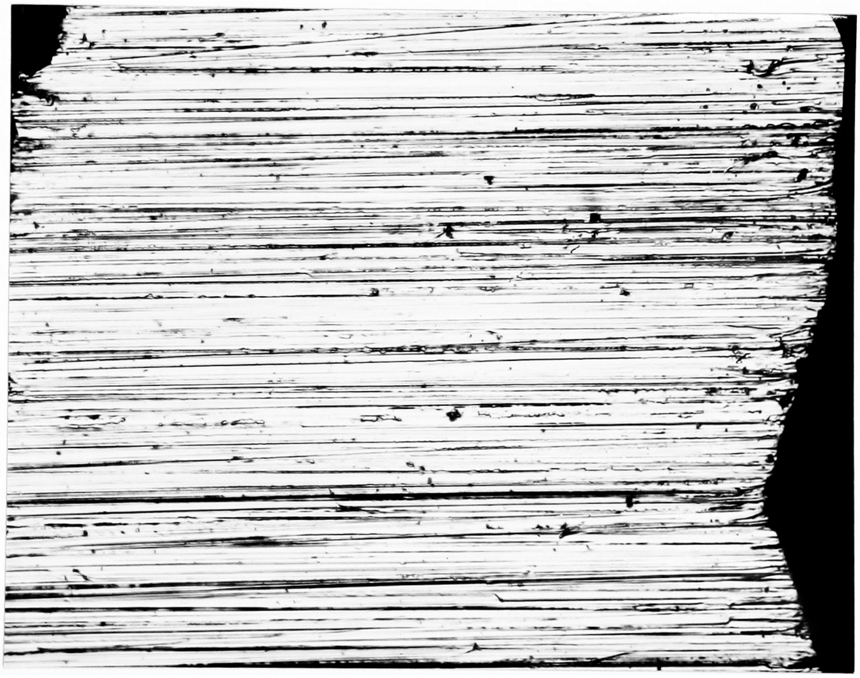

Fig.35. Wustite polished on 600 grit SiC using kerosene as lubricant. 300X

The particle size of the subscale oxide decreases as the nickel content of the alloy increases for a given gas composition, as shown in Fig.36,28,29 ,30 . In fact, the subscale oxide in the iron - 10% nickel alloy oxidized in carbon dioxide is the continuous phase, as shown in Fig.37. Then, a gradual increase in size occurs when the composition exceeds 60% nickel, however, a spinel oxide constitutes the subscale in these cases. The particle size across a given subscale is reasonably uniform except in the vicinity of the subscale - alloy interface. For a given alloy, the subscale precipitation increases as the carbon dioxide composition of the gas phase increases, as illustrated by comparing Figs.38 and 28. In severely oxidized specimens a band adjacent to the metal - oxide interface appears containing a low concentration of oxide particles. This band is readily apparent in Fig.37.

There is a definite tendency for subscale oxide to precipitate at grain boundaries as can be seen in the photomicrographs already presented. The effect becomes more pronounced relative to the lattice precipitation with increasing nickel concentration and lower carbon dioxide contents in the gas phase. At nickel concentrations greater than 60%, a reversal occurs as in shown in Fig.33. No tendency for boundary precipitation was observed in the 90% nickel alloy. The grain boundary oxide is continuous, except at regions near the penetration front. As shown in Fig.39, the oxide nucleates in the boundary ahead of the advancing tip and grows until it coalesces with the tip forming a continuous boundary film. In all specimens, there is a region of lattice precipitation adjacent to the boundary oxide and ahead of the advancing subscale front.

There is also the problem of the apparent porosity in the subscale

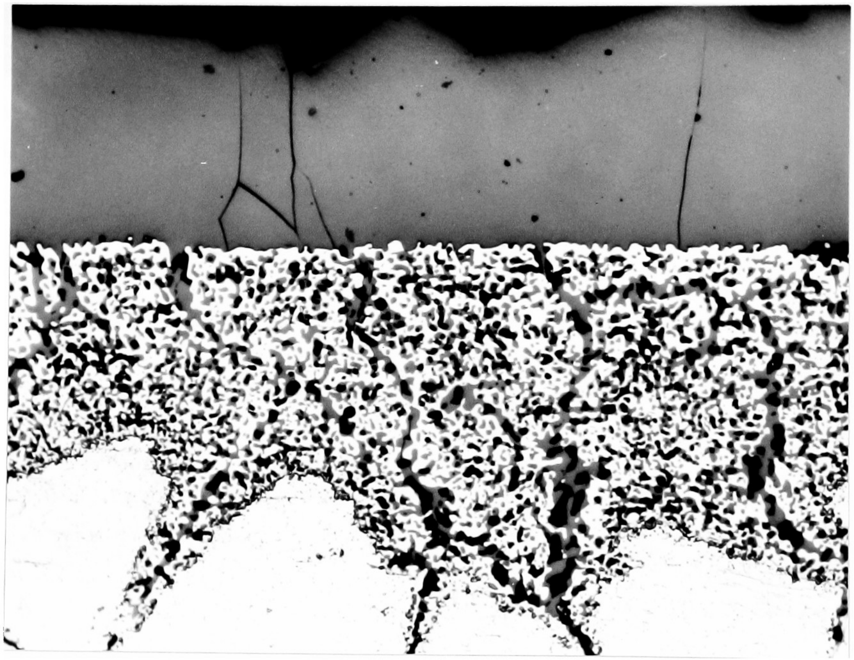

Fig.36. Fe-20%Ni oxidized for 24 hrs. in CO_2. Etched in 2%nital. 210X

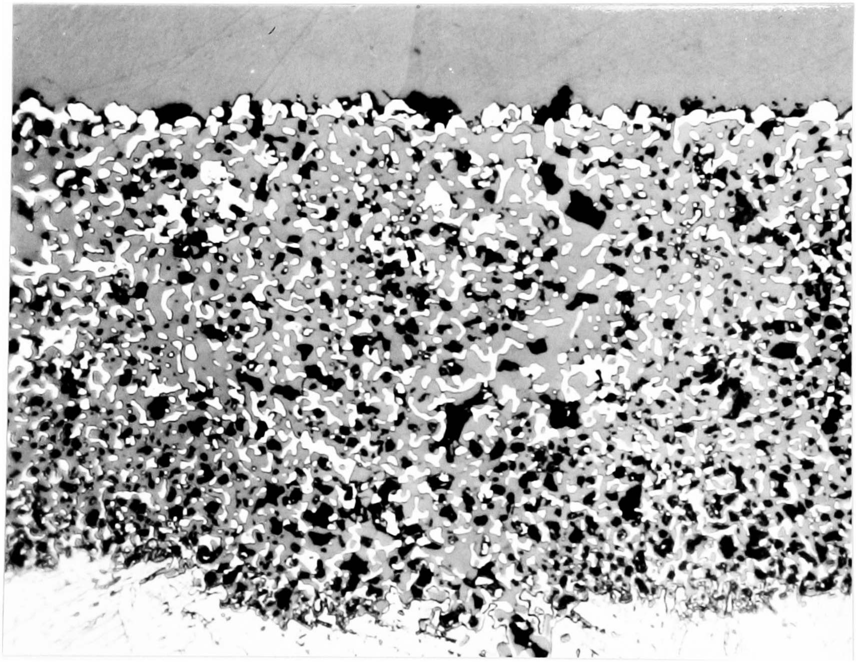

Fig.37. Fe-10%Ni oxidized for 6 hrs. in CO_2. Etched in 2% nital. 465X

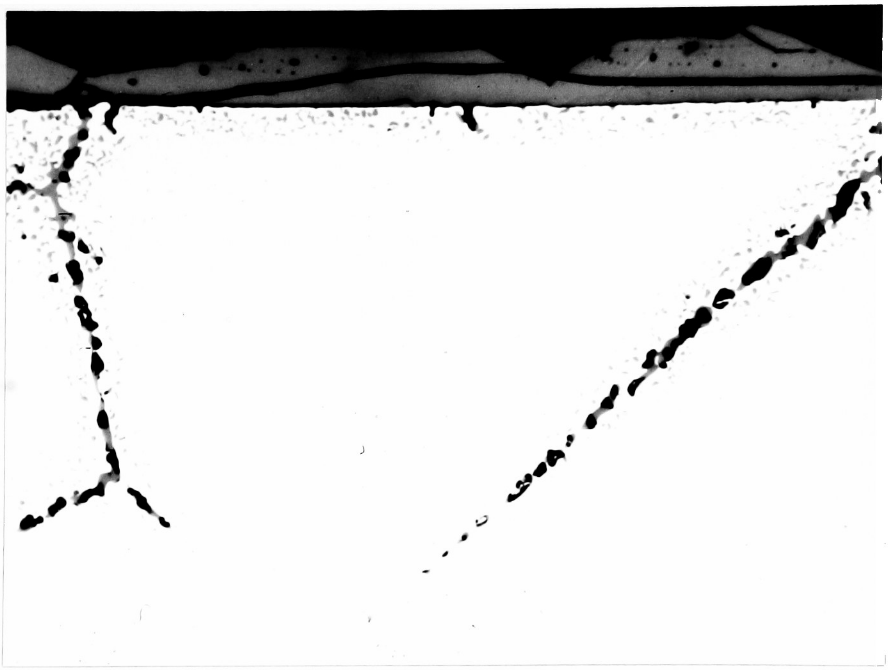

Fig.38. Fe-30%Ni oxidized in 50% CO_2. 530X - 24 hrs

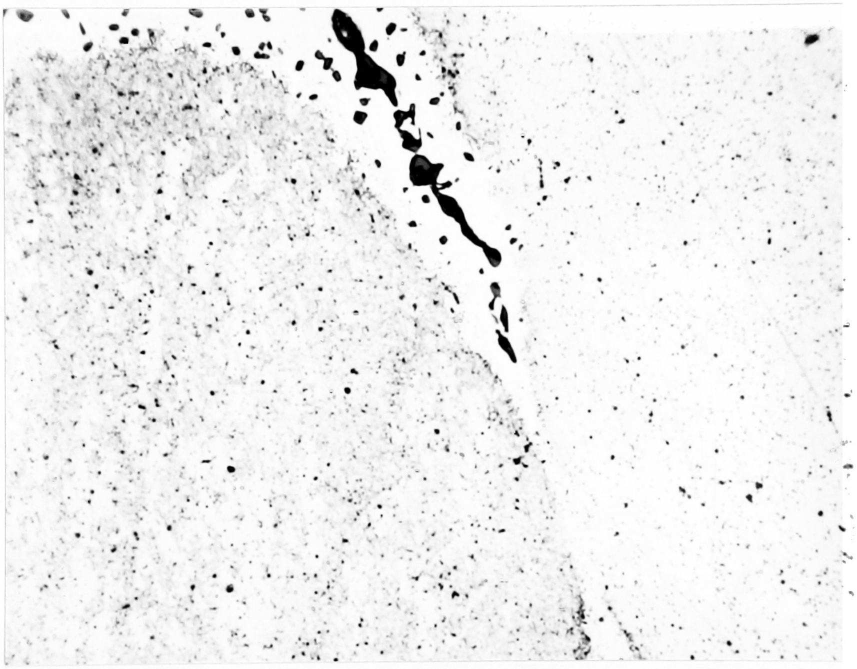

Fig.39. Nucleation of grain boundary oxide. Fe-30%Ni oxidized for 30 hrs. in 50% CO_2. 580X

oxide. This appears to be a result of the mechanical polishing operation, as shown in Figs.40(a) and 40(b). After diamond polishing for 30 seconds, a few pores are visible. Examination of the same area after a 4 minute polishing period, demonstrates that the amount of porosity has increased considerably. It is concluded that both subscales and external scales are relatively pore free, and any real porosity does not influence the reaction mechanisms.

6.5 Oxide Growth Rates

The rates of external scale growth and subscale and grain boundary penetration were determined for several alloys in order to establish the time dependence of the processes and to obtain an order of magnitude for subscale and grain boundary penetration rates. Thickness measurements were made about the periphery of a specimen. Complications arose in the alloys which had been oxidized in carbon dioxide due to the rugged nature of the oxide - gas and subscale - alloy interfaces. In these cases, measurements were taken at planar regions of the scale and at subscale regions between grain boundary sites. These results are shown graphically in Figs.41 to 46. The points on the graph represent the average value; and the errors were determined from the standard deviation.

In all cases, the subscale penetration rates followed a parabolic time dependence, with the exception of the 10% nickel alloy oxidized in carbon dioxide. The grain boundary precipitation front also followed a parabolic time dependence for the two cases investigated. The rate constants for these determinations are given in Table V. The scales thickened at a linear rate for iron-20% and 30% nickel alloys oxidized in 50% carbon dioxide, but at a parabolic rate for 10% and 30% nickel alloys oxidized

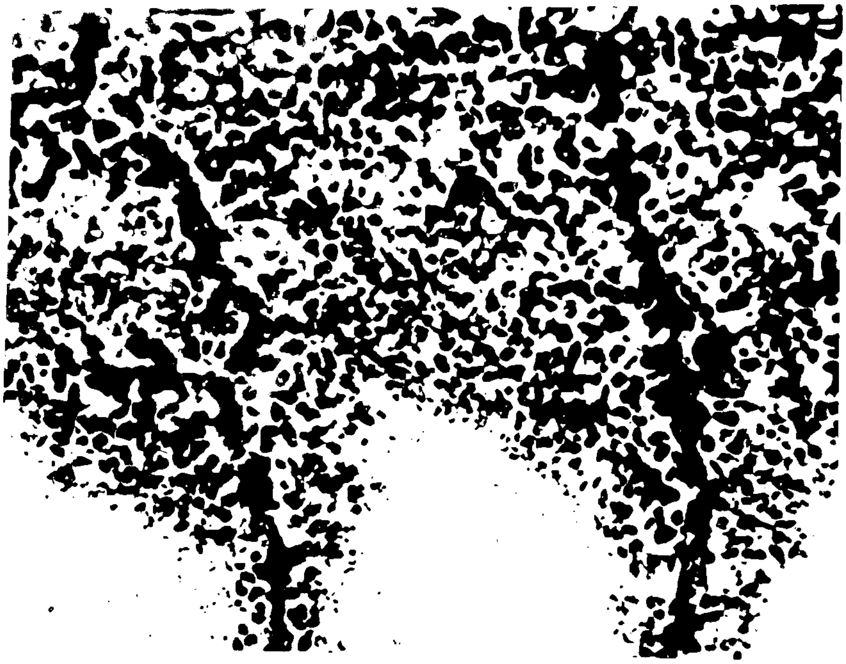

Fig.40(a). Subscale region mechanically polished for 30 seconds with 1 micron diamond paste. Fe-20%Ni oxidized for 24 hrs. in CO_2. 465X

Fig.40(b). Subscale region mechanically polished for 4 minutes with 1 micron diamond paste. Fe-20%Ni oxidized for 24 hrs. in CO_2. 465X

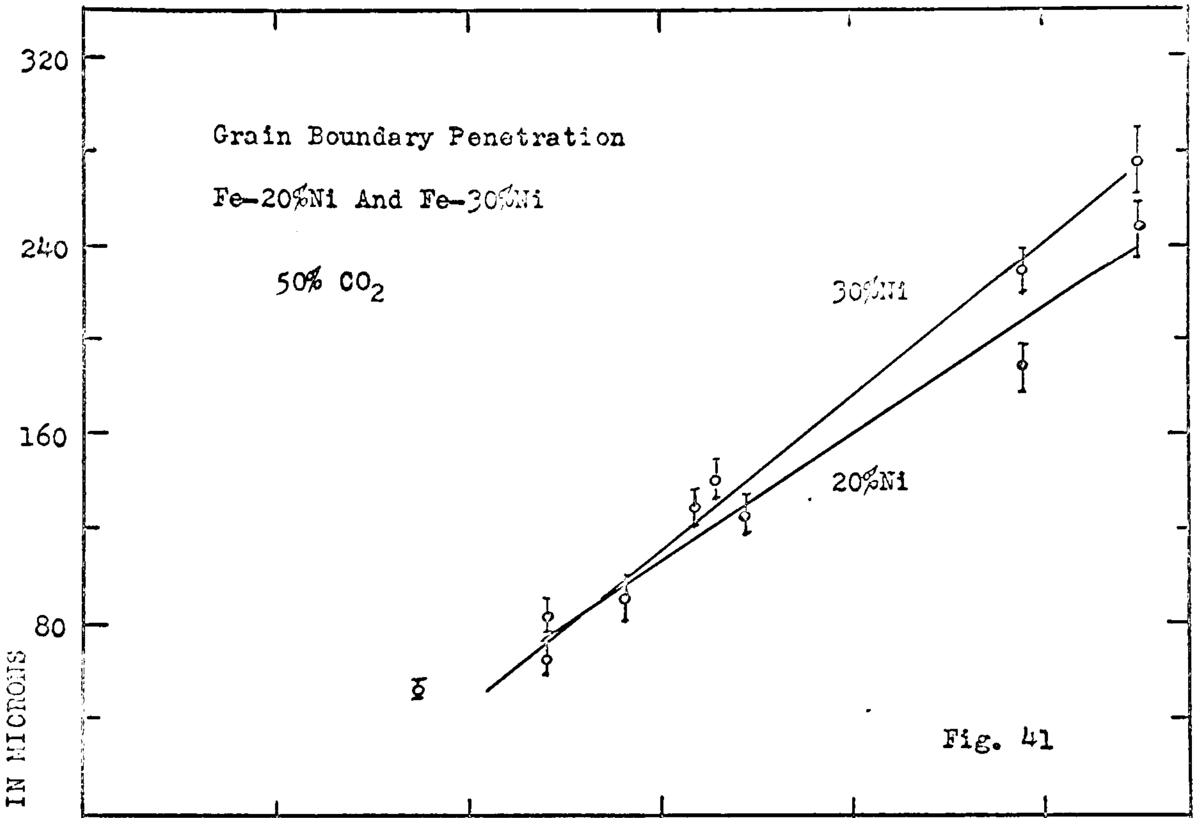
320
240
160
80
DISTANCE IN MICRONS
Grain Boundary Penetration
Fe-20%Ni And Fe-30%Ni
50% CO$_2$
30%Ni
20%Ni

Fig. 41

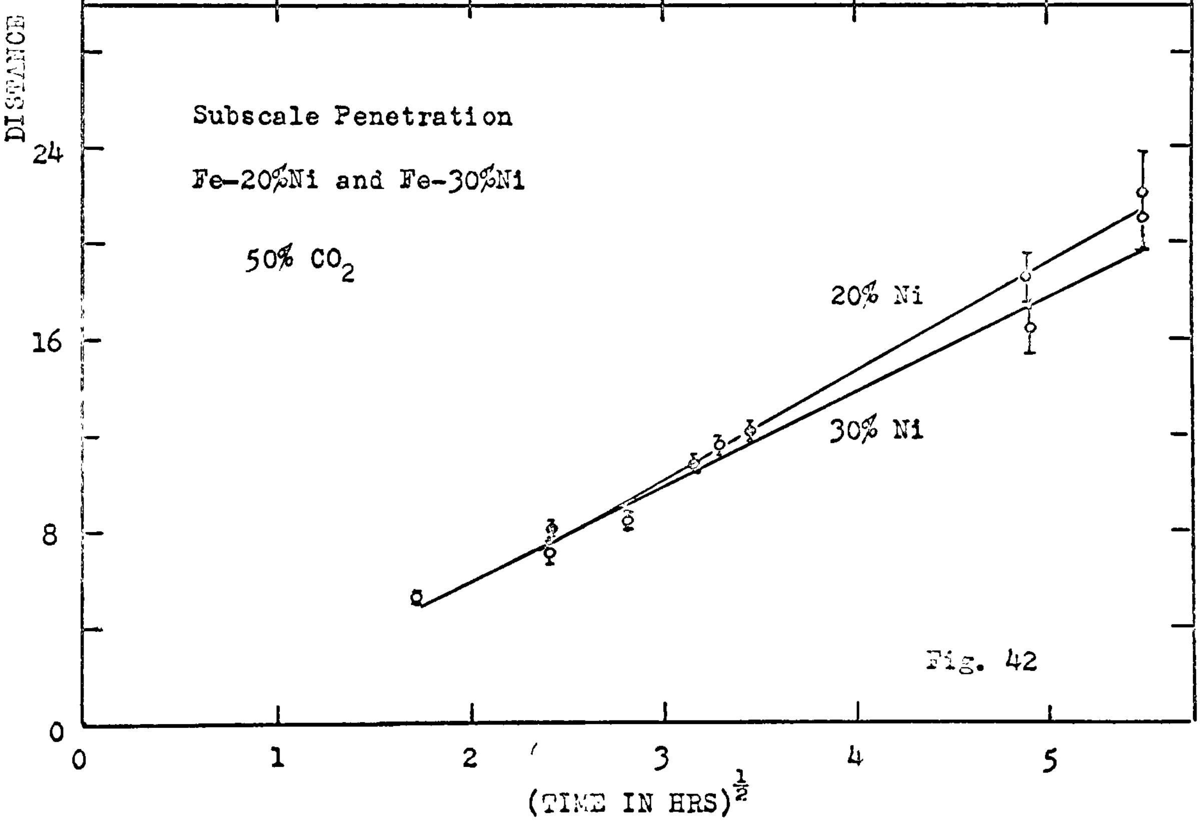
24
16
8
0
0
1
2
3
4
5
(TIME IN HRS)$^{\frac{1}{2}}$
Subscale Penetration
Fe-20%Ni and Fe-30%Ni
50% CO$_2$
20% Ni
30% Ni

Fig. 42

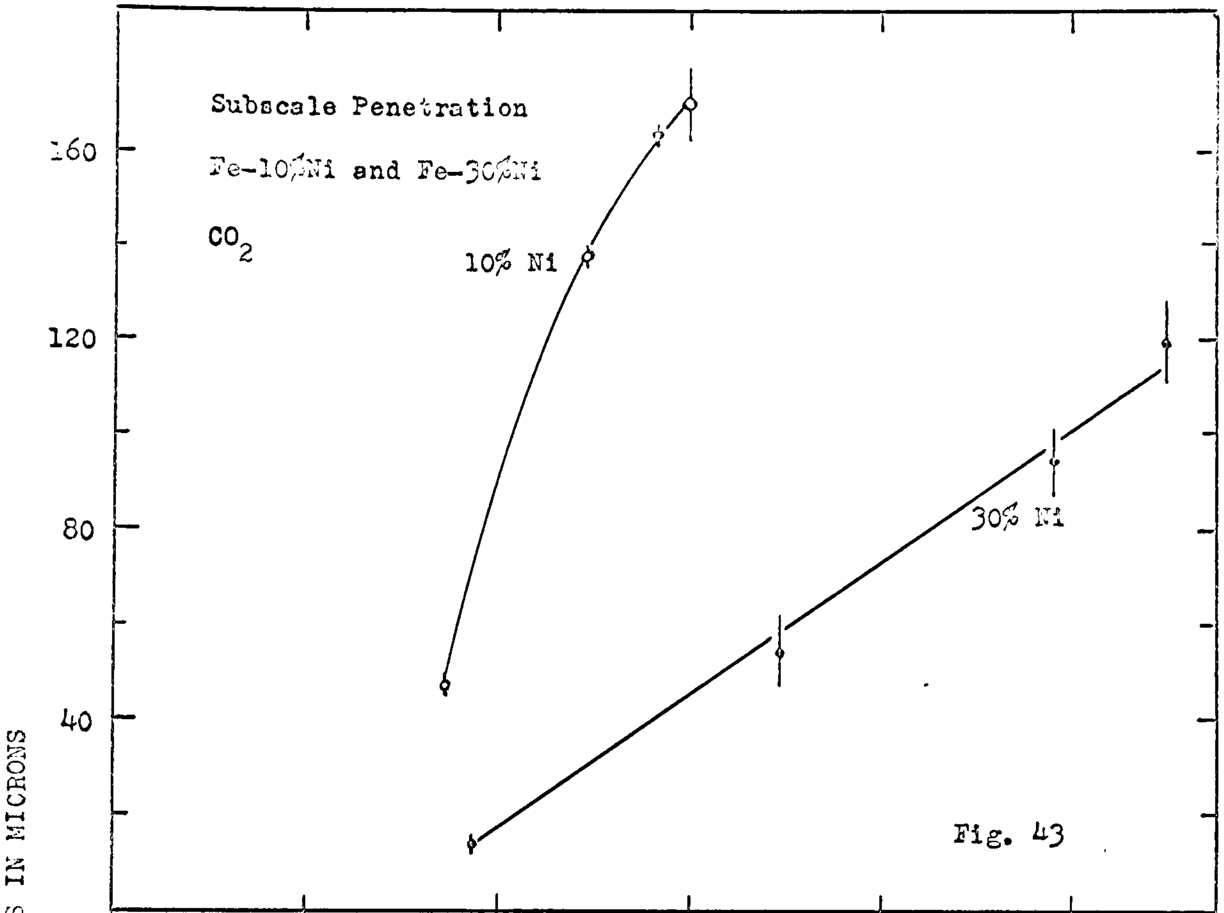
Subscale Penetration
Fe-10%Ni and Fe-30%Ni
CO_2
10% Ni
30% Ni
160
120
80
40
THICKNESS IN MICRONS

Fig. 43

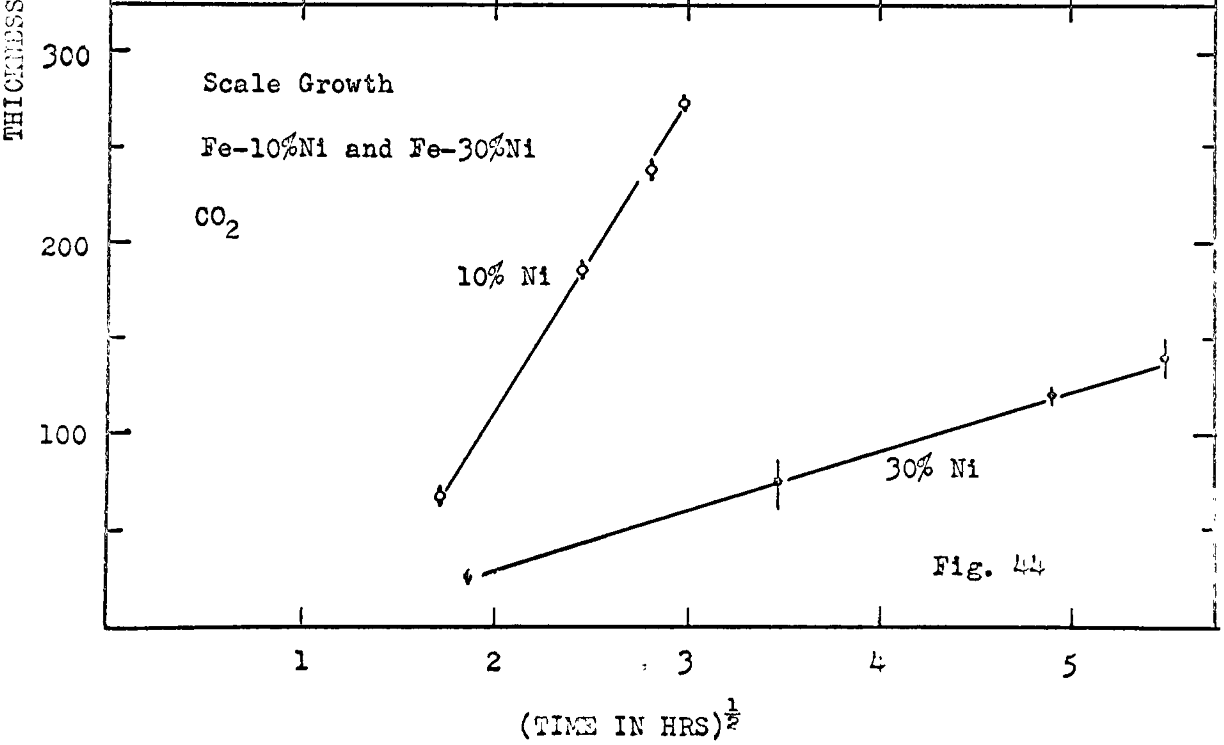
Scale Growth
Fe-10%Ni and Fe-30%Ni
CO_2
10% Ni
30% Ni
300
200
100
1
2
3
4
5
(TIME IN HRS)$^{\frac{1}{2}}$

Fig. 44

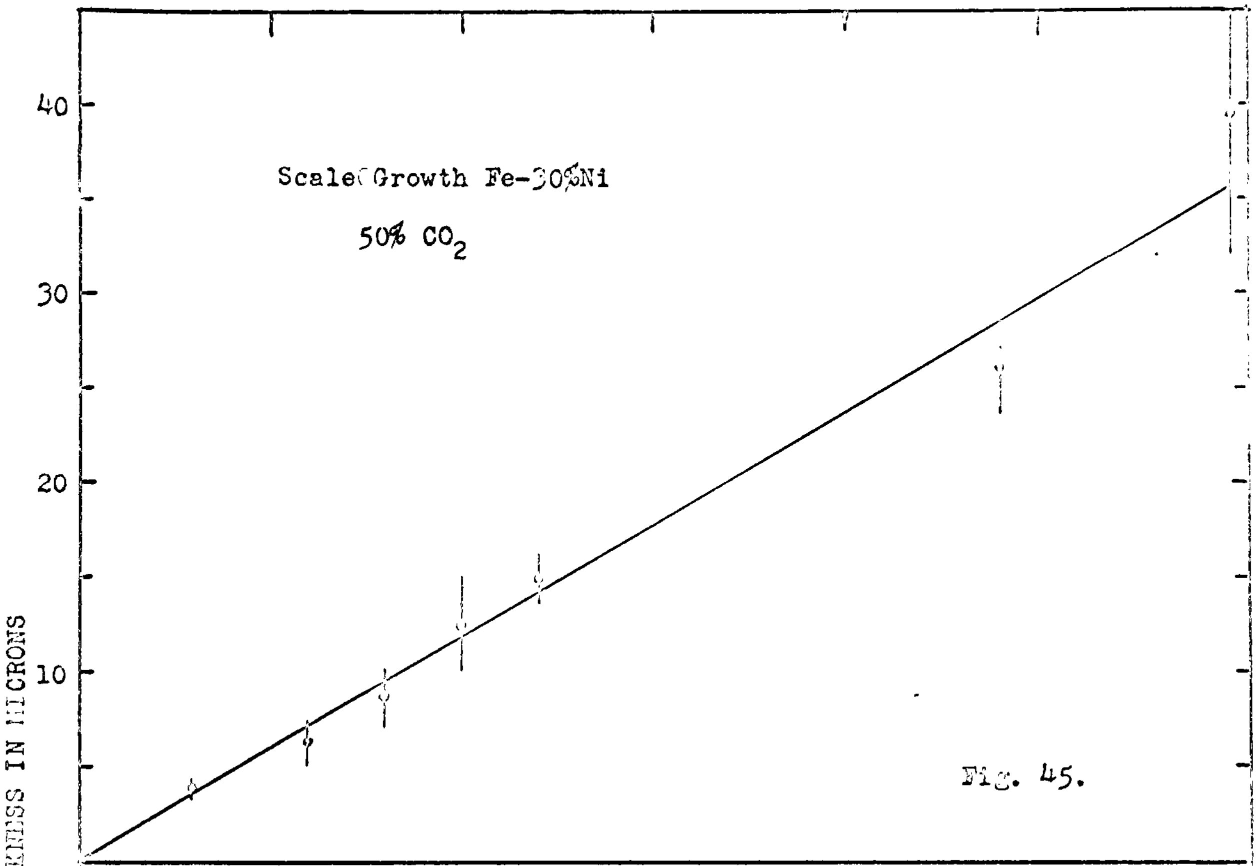
Scale Growth Fe-30%Ni
50% CO_2
40
30
20
10
THICKNESS IN MICRONS

Fig. 45.

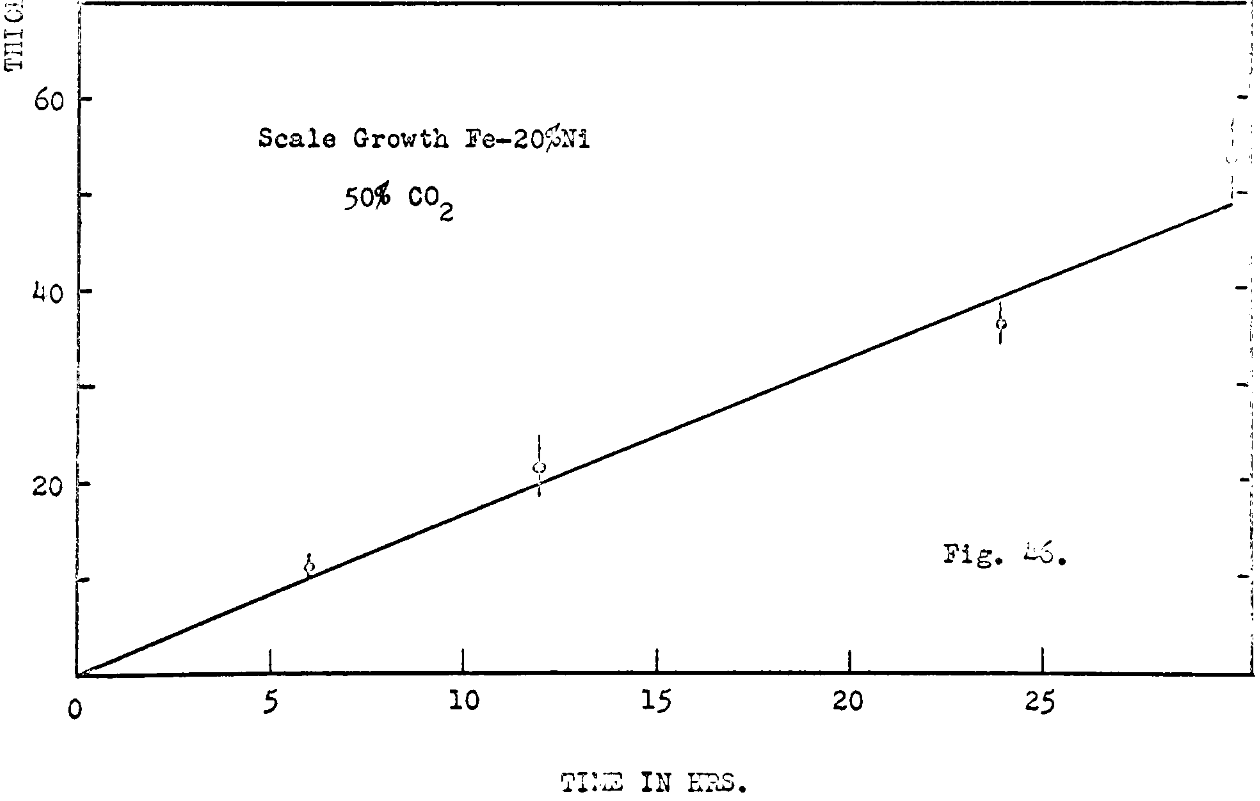
Scale Growth Fe-20%Ni
50% CO_2
60
40
20
0
5
10
15
20
25
TIME IN HRS.

Fig. 46.

TABLE V

Subscale and Grain Boundary Penetration Rates

Alloy (wt%Ni)	Gas Composition CO_2/CO	K_p(subscale) cm^2/sec	K_p(grain boundary) cm^2/sec
20%	50/50	6.1×10^{-11}	8.1×10^{-9}
30%	50/50	4.7×10^{-11}	1.1×10^{-8}
30%	CO_2	2×10^{-9}	

in carbon dioxide. No explanation can be given for the different results on scale growth rates.

Oxide growth kinetics were determined for a few alloys only, however, it may be stated qualitatively that the scale growth and subscale penetration rates decrease with an increase in nickel content; the grain boundary penetration rates gradually increase for up to 50% nickel additions.

6.6 Electron Probe Microanalyses

Attempts were made to determine the concentration gradients in the subscale region and unoxidized metal, The results obtained are not reliable in a quantitative sense. The main difficulty associated with these measurements occurs as a result of the close proximity of the subscale oxide particles. It was virtually impossible to cross the subscale without the electron beam being atop oxide particles for less than 75% of the time. The same problems are encountered in point counting. The results of three traverses are given in Fig.47. Emphasis is placed on the nickel scans for the following reason. On traversing from the alloy interior to the alloy - scale interface, the only contribution to an increase in X-ray intensity will be due to nickel enrichment in the metal phase. If the beam crosses an oxide precipitate, the intensity will fall to background, since nickel has a very low solubility in the oxide. Scanning the subscale results in peaks and valleys in the intensity curve, and the only solution is to join the peaks with a smooth curve. The situation is different for iron since crossing the oxide may result in an increase or decrease in intensity depending on the iron concentration in the metal phase. Furthermore, the intensity will decrease if the electron beam traverses a hole in the subscale region. As a result, the iron scan is more difficult to analyse. The nickel gradients at the subscale - alloy interface are

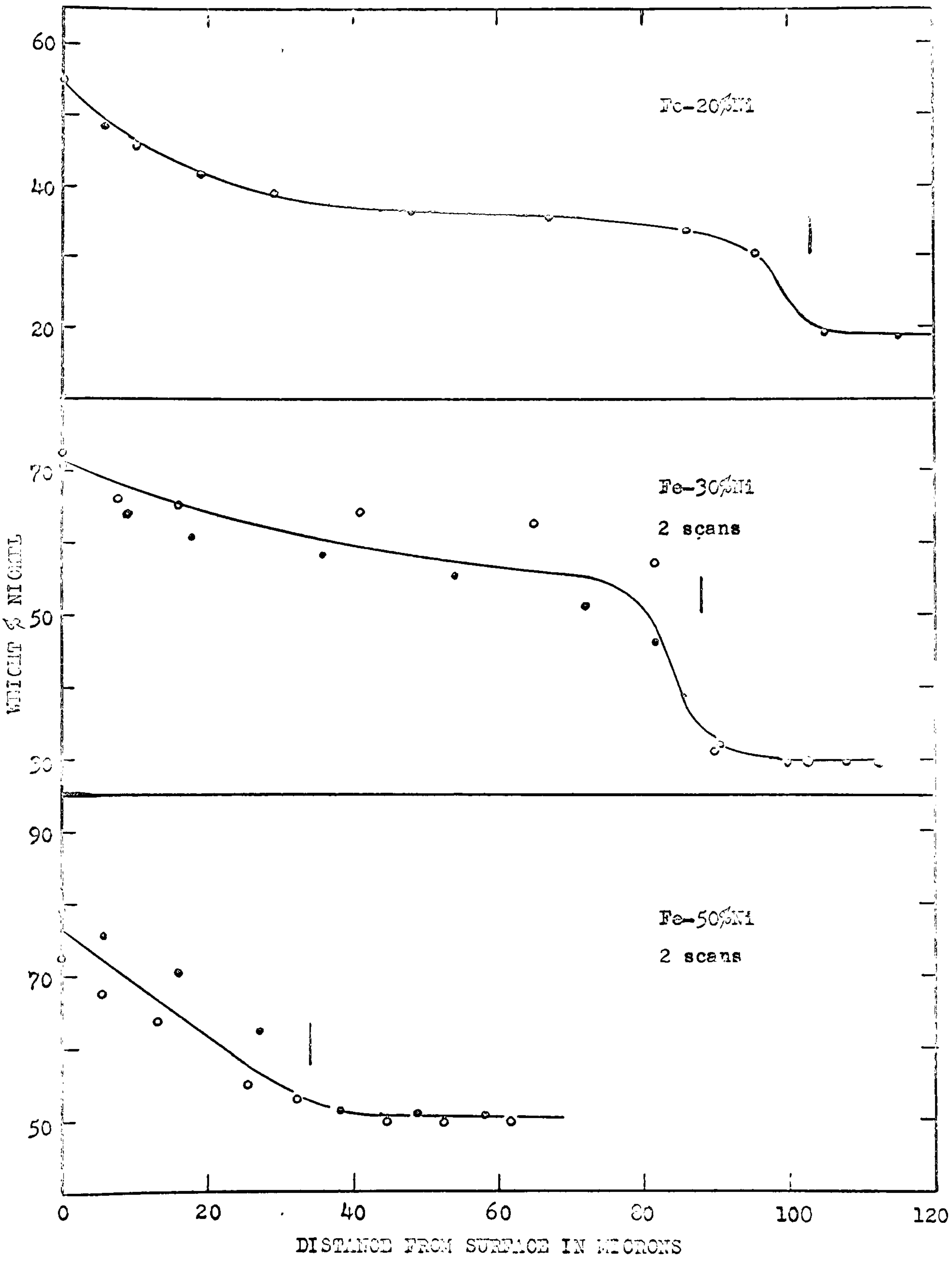

Fig.47. Electron probe scans

steep for alloys with appreciable subscale development, as shown for the iron 20% and iron - 30% nickel alloys in Fig.47, compared to gradients in materials with smaller amounts of precipitation as illustrated by the iron - 50% nickel alloy. The possibility exists that there may be steep gradients at each particle in the subscale which cannot be detected, and the scans only represent an averaging effect. Nickel gradients were always detected in regions in which there were oxide precipitates adjacent to the grain boundary oxide. Negligible gradients were detected in alloy regions where there was no precipitation, at either the subscale - alloy or grain boundary oxide - alloy interfaces. No gradients could be detected in the subscale alloy phase when traversing in a direction parallel to the surface.

The nickel concentrations at the metal - oxide interface could be readily obtained from the taper sections described in the previous chapter. These values were obtained by point counting at different areas. Eight to ten readings were taken at each area and the average obtained are reported in Table VI for the alloys investigated. The values were reproducible to ± 2% nickel. The errors reported were determined from the arithimetic deviation from the mean.

It is of interest to know if the interface compositions vary as a function of time for given experimental conditions. As can be seen in Table VI, after an initial period, a constant value is attained for at least the two cases investigated. These observations are considered representative of all experimental tests. The surface concentrations are impossible to determine for shott times since the enrichment layer below the surface is so thin that the analysis would give some average value as a result of electron penetration into the specimen.

TABLE VI

Electron Probe Microanalysis: Interface Concentrations

Alloy (wt.%Ni)	Gas Composition (CO_2/CO)	Oxidation Time (hrs)	Average Concentration (wt.%Ni)
10%	70/30	14.5	40
10%	CO_2	6	48.7
20%	50/50	24	38
20%	60/40	30	51
20%	70/30	24	52.5
20%	80/20	30	53.2
20%	CO_2	21	55.9
20%	CO_2	24	55.4
30%	50/50	3	45.5
30%	50/50	6	50.2
30%	50/50	12	48
30%	50/50	30	49.5
30%	70/30	24	57
30%	CO_2	12	65.6
30%	CO_2	24	68.1
40%	50/50	24	60.3
40%	20/30	24	65.5
40%	CO_2	24	75.2
50%	70/30	24	69
50%	CO_2	24	79.9

CHAPTER VII

DISCUSSION

7.1 Introduction

The use of carbon dioxide - carbon monoxide atmospheres facilitated the adjustment of oxygen potentials to values below the dissociation pressures of the higher oxides of iron. This lead to the formation of wustite as the sole reaction product for alloys containing 0-50% nickel. Since the diffusivity of iron in wustite is large, 5×10^{-6} cm^2/sec at 1000°C,[50] and nickel behaves as a noble element, the conditions are such that a non-planar interface may develope in accordance with the previously discussed Wagner mechanism.[31]

However, linear oxidation kinetics were observed for long exposures. In all cases, oxygen dissolved in the metal phase and subsequently diffused into the interior resulting in the precipitation of internal oxide. Therefore, the basic assumptions of the Wagner model are violated, namely, that diffusion in the alloy phase is rate controlling, and that oxygen migration is confined to plastic flow of the oxide.[31] Thus, this mechanism definitely does not apply to oxidation of iron - nickel alloys under the present experimental conditions.

The oxidation mechanism of iron - nickel alloys in carbon dioxide - carbon monoxide atmospheres is complicated by the number of processes which occur at the reaction temperature. Iron is selectively oxidized and depleted at the metal - oxide interface. The scale thickens by diffusion of iron ions to the oxide - gas interface where reaction with adsorbed oxygen takes place. Since, the total uptake of oxygen is directly proportional to time, a chemisorption reaction is rate controlling. Justification will be presented for this viewpoint.

Furthermore, the alloys oxidised internally. Since the diffusivity of oxygen in wustite is negligible, the oxygen supply originated from the dissociation of oxide at the metal - oxide interface. Consequently, the linear reaction rates and the internal oxidation phenomena will be discussed in separate sections in terms of the theory previously presented and other pertinent data.

7.2 Linear Oxidation Kinetics

7.2.1 General Discussion

It is apparent from the kinetic results that the linear rate curves do not extrapolate to the origin. The data for pure iron and the iron - 10% nickel alloy indicated an induction period before the onset of linear rates. In each case, linear behaviour occurred after a weight gain of approximately 8 - 12 mg/cm^2. The other alloys oxidized at decreasing rates before onset of linear kinetics. In view of the number of processes occurring in the early stages of the reaction, an attempt is not made to account for the initial reaction rates deviating from linear behaviour. These characteristics have been observed previously for the oxidation kinetics of iron in carbon dioxide atmospheres[68, 70].

When deviations occur following linear kinetics, the rates approach parabolic kinetics, Figs. 16 to 19. Relatively thick scales were observed on pure iron and the 10% nickel alloy, Fig. 48. For these cases, it is assumed that diffusion of iron ions through the thick wustite scales become the rate controlling reaction step. Smeltzer[70] and Pettit[68] have demonstrated that the transition from linear to parabolic oxidation kinetics

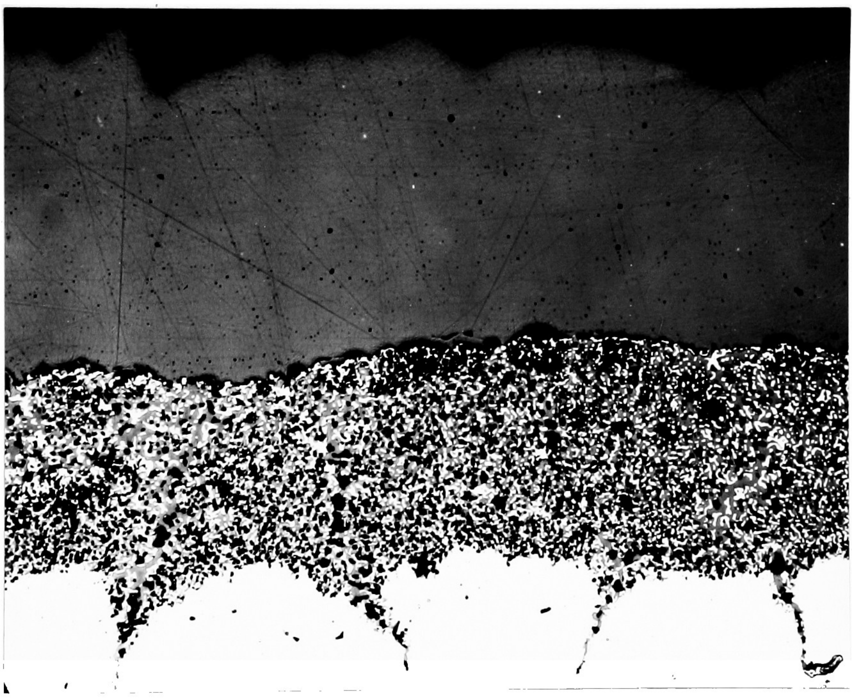

Fig.48. Fe-10%Ni oxidized for 8 hrs. in CO_2. 150X

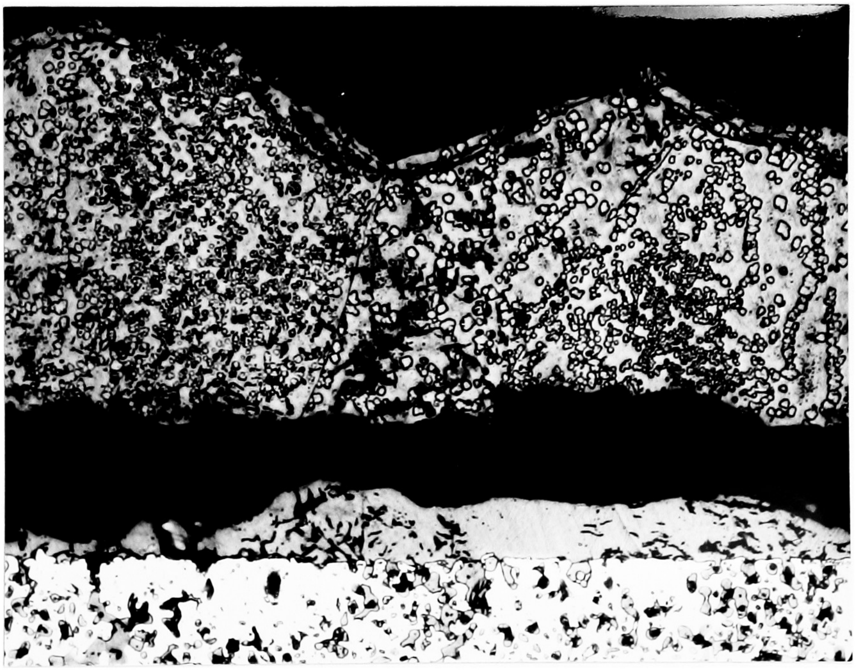

Fig.49. Mechanical failure of the oxide scale: Fe-30%Ni oxidized for 24 hrs. in CO_2. 300X

for iron is associated with the transition from a chemisorption reaction to a reaction governed by diffusion of iron in wustite.

Two additional factors may account for the transition from linear to parabolic oxidation kinetics when the internal scale is relatively thin. First, diffusion in the alloy phase may play a predominant role. For example, it is suggested that iron diffusion in the 50% nickel alloy plays a predominant role during parabolic oxidation in carbon dioxide Fig.25. Secondly, a different oxide may be formed, in which diffusion rates are much slower than in wustite. For example, iron diffusion in magnetite is 10^{-4} times less rapid than in wustite. Accordingly, the parabolic growth of the spinel oxide observed on the 60% nickel alloy oxidized in carbon dioxide, Fig.26, may be associated with this behaviour.

There were exceptions to these observations for alloys containing 20% and 30% nickel oxidized in carbon dioxide. In six out of seven tests, the oxidation rates gradually increased after linear oxidation. Examination of an iron 30% nickel alloy illustrated that the scale was detached from the metal phase at various positions along the alloy - oxide interface. A new oxide layer was formed on these exposed areas, Fig.49. Accordingly, the rate increases are associated with mechanical failure of the oxide scale and subsequent oxidation of the exposed areas.

It should be mentioned that linear reaction rates would be observed if steady state diffusion through a resistance layer of constant thickness, either in the solid phase or the gas phase, is rate controlling. A solid phase layer can be eliminated since regions of constant external scale or internal subscale thicknesses were not observed. Diffusion of the oxidizing gas through a boundary layer film adjacent to the oxide surface is the other rate controlling possibility. Assuming that the rate of transport of carbon dioxide gas across a boundary layer film was rate controlling, the calculated rate of oxidation for pure iron was approximately 30 times greater than the observed rate. Since the values used in this calculation are approximately of the same order of magnitude for iron - nickel alloys, the above result applies to oxidation of the alloys. Details of the calculation are given in Appendix 1.

The possibility of gaseous diffusion determining the reaction rate may be checked by determining the activation energy for oxidation. The Arrhenius temperature coefficient for the oxidation of an iron 30% nickel alloy in a 50% carbon dioxide atmosphere was determined by plotting the logarithm of the rate constants for the temperatures of 900°, 950°, and 1000°C versus the reciprocal of the absolute temperature. This plot is shown in Fig.50. An activation energy of 1 - 3 kcal. would be expected for a gaseous diffusion process, whereas a value of 21 kcal. is found experimentally. Gas diffusion, therefore, does not act as a rate determining step in the oxidation mechanism.

7.2.2. Oxidation Rate as a Function of Gas Composition

The linear rates may now be discussed in terms of the oxidation model presented in the theoretical chapter. Equation 4 - 10 was derived on the basis that a chemisorption reaction determined the oxidation rate. Therefore, the proposed mechanism can be verified if plots of K_L versus $(1 - a_o^{eq}/a_o^{s})\ P_{CO_2}$ satisfy the data. Since it was shown that this expression is equivalent to equation 3 - 16 of Smeltzer, equation 3 - 9 of Pettit et al., and equation 3 - 21 of Turkdogen, experimental values of K_L versus P_{CO_2} should obey a linear relationship. In this way, the data

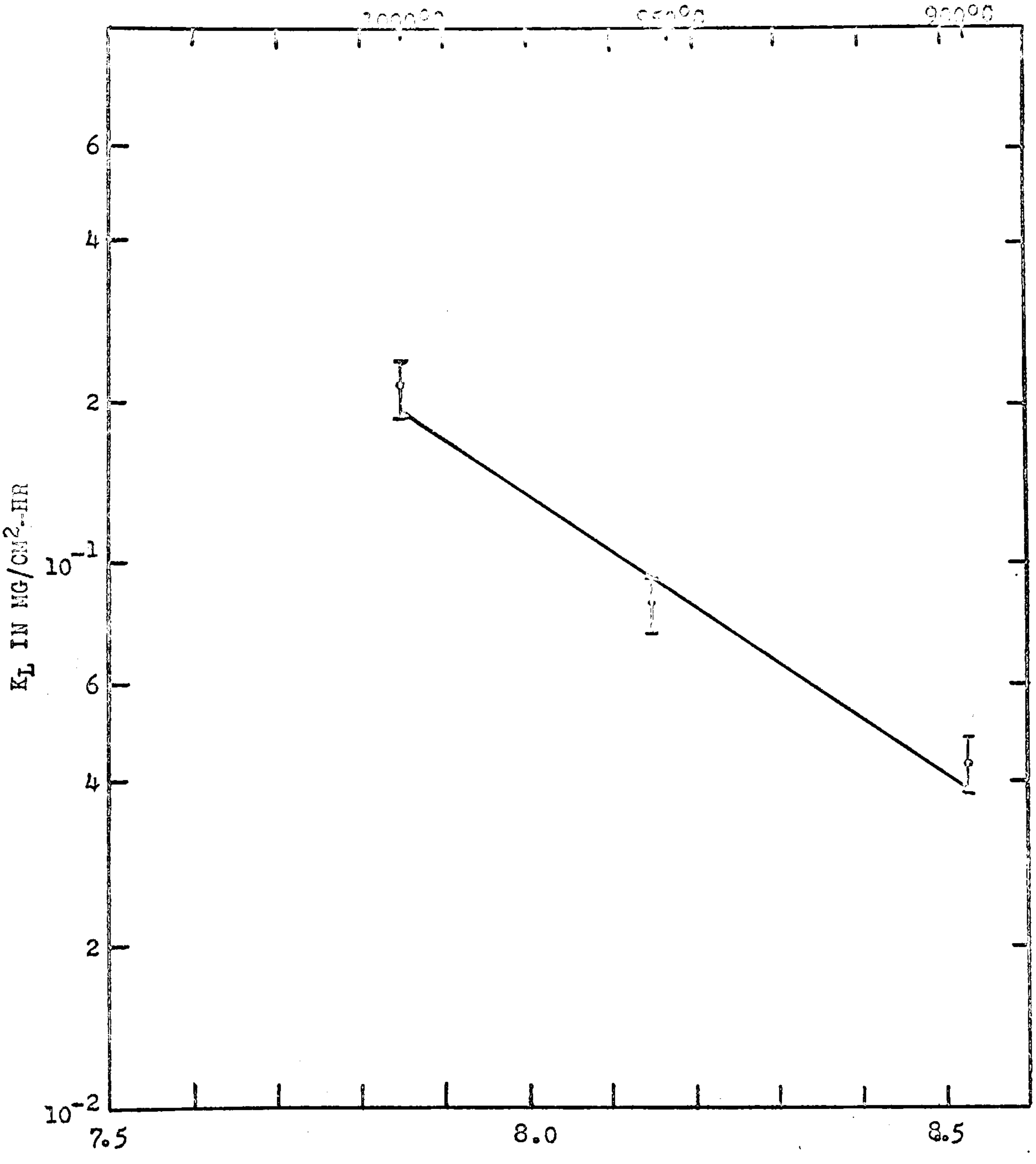

Fig. 50. Arrhenius temperature coefficient for the oxidation of an Fe-30% Ni alloy in 50% CO_2.

may be presented in the simplest form.

The results are shown in Figs. 51 and 52 for pure iron and iron - 10% nickel, and iron - 20, 30, 40, 50% nickel alloys. The dissociation pressures for wustite equilibrated with iron - nickel alloys were taken from the results of Rieder and Smeltzer[95] and Bryant and Smeltzer[104]. These investigators utilized electrochemical measurements on solid galvanic cells to determine the activity of oxygen in wustite equilibrated with alloys containing up to 80% nickel. The results can be described by the theoretical equation with the exception of the results for the iron - 10% nickel alloy. The deviations of the kinetic results for this alloy from the theoretical equation may be caused partially by the inaccurate evaluations of the linear rate constants. Furthermore, the subscale for specimens oxidized in carbon dioxide was a continuous phase which would complicate the oxidation process, Fig.37.

The value for the oxygen activity in the gas phase in equilibrium with wustite, a_o , appears in equation 4 - 10. This term is equivalent to $P_{CO_2}{}^{1}$ in equation 3 - 16 and equation 3 - 9. For wustite scales on pure iron, the equilibrium value is assumed to be given by the dissociation pressure of wustite in equilibrium with the metal phase, since it is argued that there is no iron concentration gradient across the oxide, when oxidation is determined by the slow chemisorption rate determining step.[68, 70] Complications arise when the same approach is taken for iron - nickel alloys.

It is apparent from the electron probe data that the nickel concentration increases from the initial bulk content to a higher value at the interface, Table VI. When the dissociation pressures of wustite in equilibrium with alloys characteristic of these increased concentrations are

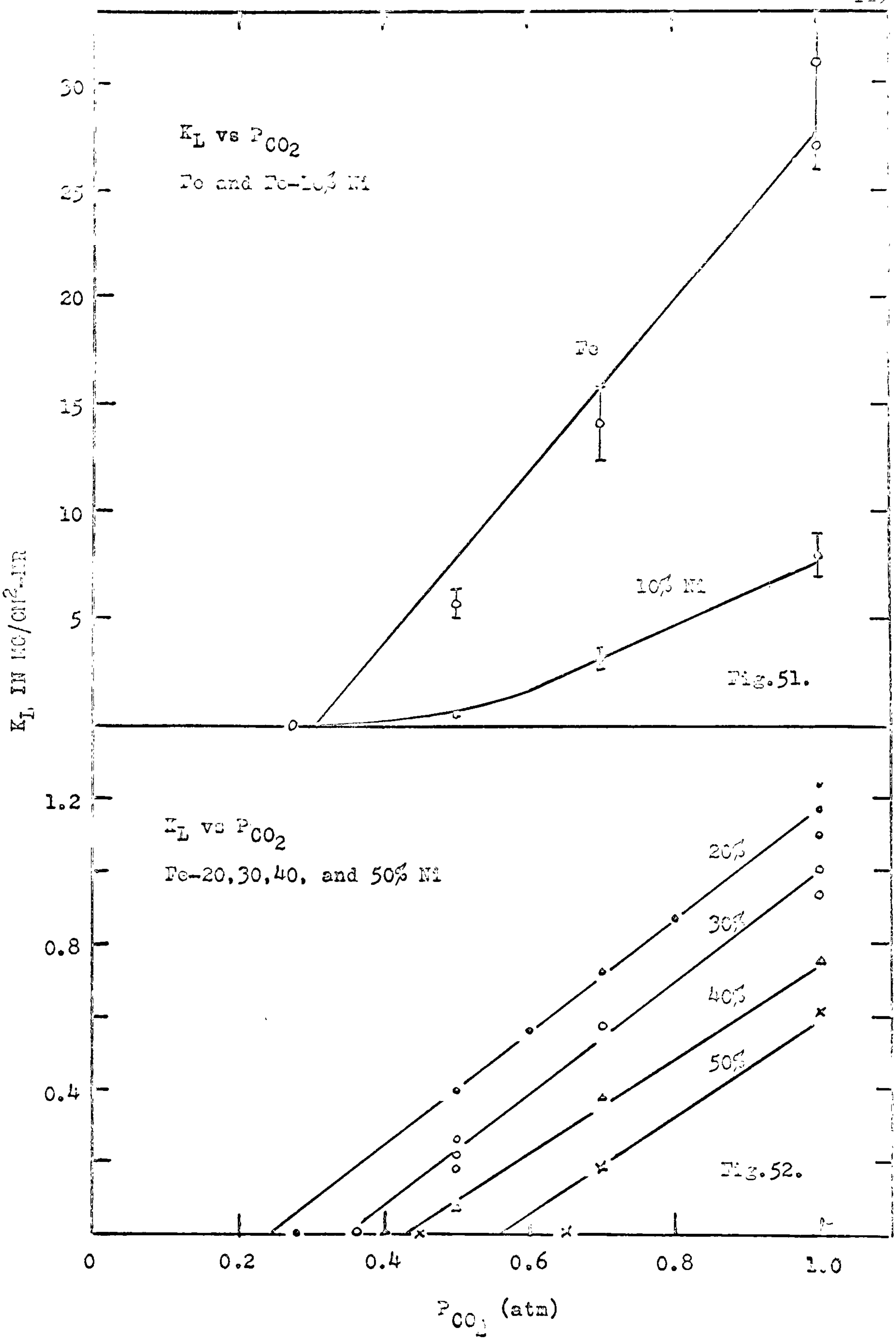
K_L vs P_{CO_2}
Fe and Fe-10% Ni
Fe
10% Ni
Fig.51.
30
25
20
15
10
5
K_L vs P_{CO_2}
Fe-20,30,40, and 50% Ni
20%
30%
40%
50%
Fig.52.
1.2
0.8
0.4
0
0.2
0.4
0.6
0.8
1.0
K_L IN MG/CM^2-HR
P_{CO_2} (atm)

used for a_o , the required linear relationships between K_L and $(1 - a_o / a_o^{s}) P_{CO_2}$ are not obtained. Good agreement is obtained only when the dissociation pressures for the alloys containing the bulk nickel concentration are used for a_o .

It can be seen from Fig.51 and 52 that the lines extrapolated to the abscissa, representing the equilibrium oxygen activities between the alloy and wustite phases, intersecting this axis at the equilibrium $P_{CO_2}^{1}$ values for pure iron and for the iron - 20, 30, 40 and 50% nickel alloys. In the case of the 50% nickel alloy, the line intersects the axis at a value between that given by references 95 and 104. It appears then that although metal is enriched at the metal - oxide interface, the rate of oxygen uptake at the oxide - gas interface is determined by the initial bulk concentration of the alloy and the partial pressure of carbon dioxide in the gas phase.

These findings demonstrate that the composition of the oxide at the oxide - gas interface does not significantly alter from the composition of the oxide formed during the initial stages of the reaction. As shown in Fig.8, iron can be supplied to the external scale from the metal surface and from the alloy interior via diffusion in the grain boundary oxide. Therefore, the supply of iron is rapid enough to maintain gas decomposition control owing to the rapid diffusivity of iron in wustite.[50]

However, in order for local equilibrium conditions to apply at the scale - metal interface where the metal phase is of enriched nickel concentration, it is necessary that nickel diffuse into the scale. Since the solubility of nickel in wustite is less than 2 atomic per cent, the diffusivity of nickel ions may be small making it difficult for the oxide to equilibrate with the alloy phase across the entire scale. This is compatible with the results of Wagner[105] concerning the reduction of chromium doped wustite. In this case chromium was enriched in the oxide at the metal - oxide interface. In a recent investigation, Wood has determined that iron diffused further than nickel in iron oxides formed on stainless steels.[106] Therefore, it is possible that a steep nickel gradient may exist in wustite at the metal oxide interface. The composition at the outer oxide surface would not alter from the initial value to a measurable degree.

In this respect, it was noted that the microhardnesses of the internal oxide precipitates and the external scale were different as shown in Fig.53. Oxide precipitates in the subscale regions exhibited smaller hardness values. If nickel solution in the oxide increased its' plasticity. these measurements indicate a deficit of nickel in the external scale. It was not possible to determine the nickel concentrations in the scale with the electron probe since intensity measurements were of the same order of magnitude as background. Scans across a number of scales did not reveal concentration gradients, with respect to both iron and nickel.

Hence, one can only conclude that the dissociation pressure for wustite equilibrated with the alloy of initial nickel concentration is a good approximation in equation 4 - 10, in view of the experimental agreement.

Magnetite precipitated in the wustite scales upon quenching the specimens from the reaction temperature. These findings indicate an oxygen gradient in the internal scale. If the entire scale was in equilibrium with the alloy. magnetite would not be expected to precipitate on quenching, since the scale composition would be given by the tie line connecting the alloy composition with the wustite phase field. In order for

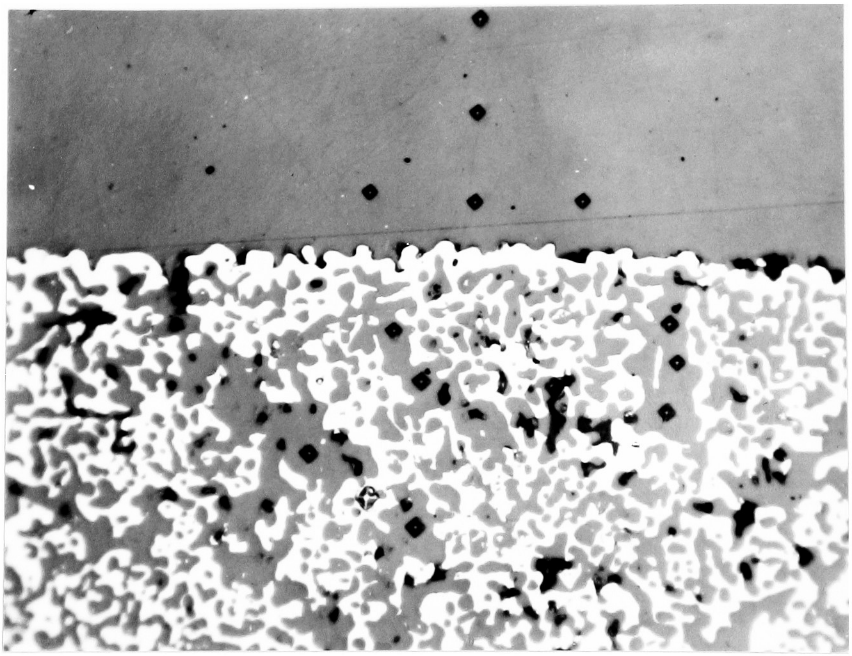

Fig.53. Microhardness of external and internal oxide. Fe-20%Ni oxidized for 24 hrs. in CO_2. 465X.

magnetite to precipitate, the scale composition would be given by a point at the wustite - magnetite phase boundary. Accordingly, the curvature of the wustite - magnetite phase boundary surface in the ternary system must be displaced towards higher iron concentrations at lower temperatures to the extent that the two phase region, wustite - magnetite, is entered on cooling.

7.2.3. Oxidation Rate as a Function of Nickel Concentration

The oxidation rate dependence on the initial alloy nickel concentration is shown in Fig.54. The magnitude of the linear oxidation rate constant decreases with increasing nickel contents in the alloys. If the positive hole concentration, $[\oplus]$, in wustite was known as a function of iron concentration in the alloy phase, and $\ominus_v$, the fraction of vacant oxygen sites on wustite, was known as a function of oxide and gas composition, the observed kinetics could be discussed in terms of the general equation 4 - 9 on a quantitative basis. Since these relationships are unknown, one can only comment on the shape of the curves which would be generated by this expression.

If wustite is equilibrated with pure iron, one can write,

$$Fe + 2\oplus + Fe_{\square} = nil \qquad 7\text{-}1$$

and

$$\oplus^2 = \frac{1}{K(a_{Fe})^{2/3}} \qquad 7\text{-}2$$

Iron nickel-alloys exhibit nearly ideal behaviour and a similar equilibrium expression would be expected for the equilibration of wustite with iron - nickel alloys. Substitution for the positive hole concentration

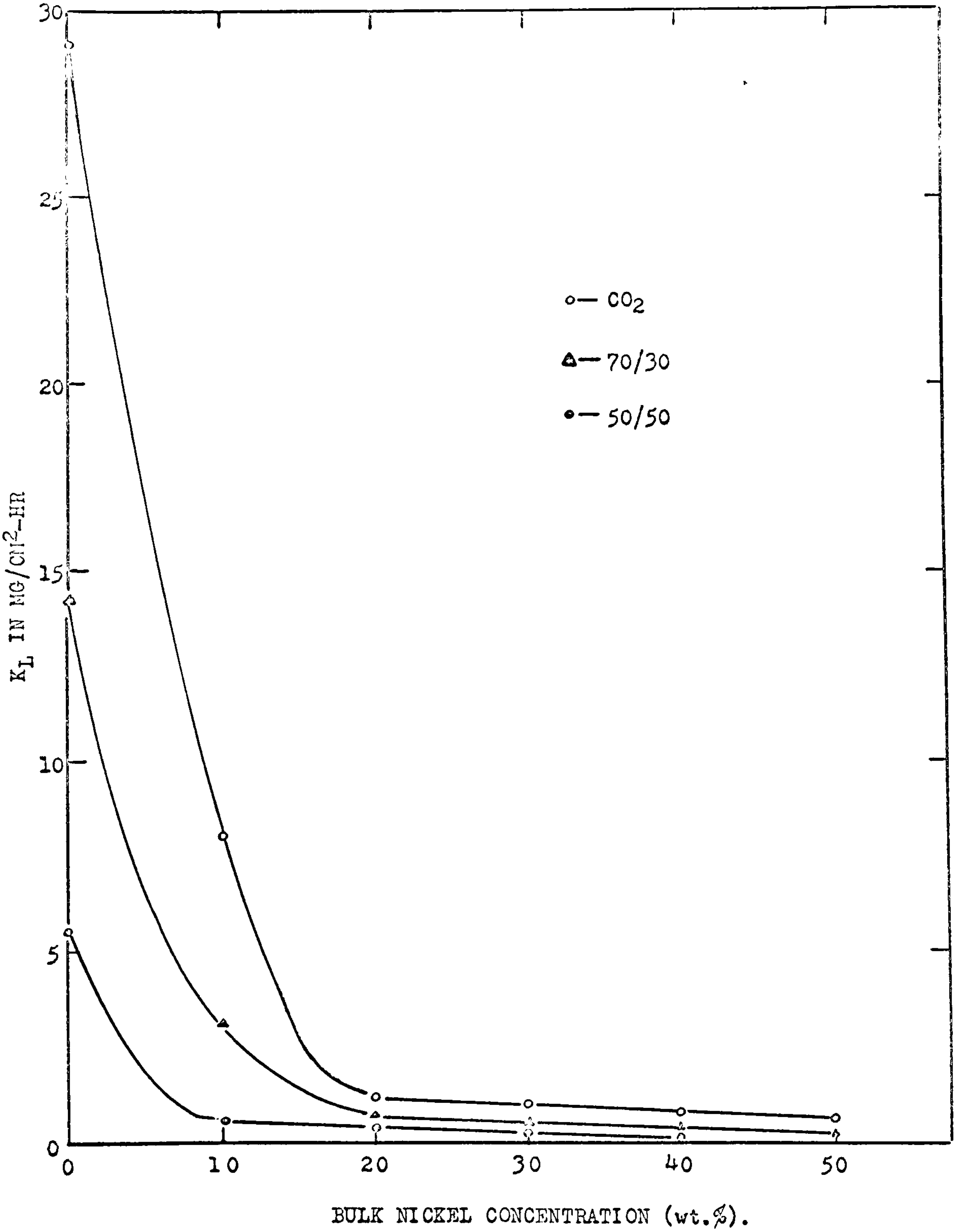

Fig. 54. Linear rate constant versus bulk nickel concentration

in the general equation 4 - 9 would yield on expression of the form,

$$K_L = \frac{k_1 k_3 \Theta_v}{\frac{k_2}{K(a_{Fe})^{2/3} P_{CO}} + k_3} \left[1 - \frac{a_o^{eq}}{a_o^{g}} \right] P_{CO_2} \qquad 7\text{-}3$$

If one assumes that the individual reaction rate constants, the equilibrium constant, K, and the fraction of vacant oxygen adsorption sites are constants independent of nickel concentration in the alloys, plots of K_L versus alloy concentration for each gas composition yield a family of curves of the same form as those shown in Fig. 54. Despite this feature, application of equation 7 - 3 to the linear oxidation kinetics may only be assessed when the influence of nickel contents in the alloy and oxide on the kinetic and equilibrium reaction parameters has been determined quantitatively.

7.4 Internal Oxidation of Iron - Nickel Alloys

7.4.1. General Discussion

The general features of the internal oxidation process have been outlined in the experimental results section. The subscale formed in iron-nickel alloys is similar to that in copper - platinum, copper - palladium and nickel-platinum alloys investigated by Thomas.[30] This investigator reported that small amounts of noble metal could be detected in the external scales, and suggested that small additions of noble element to the oxide may increase the dissociation pressure of the oxide.

Since the same oxide, wustite, is formed both internally and externally in iron - nickel alloys, the dissociation pressure of the oxide at the metal - oxide interface must be greater than the dissociation pressure of oxide formed internally. Also the oxygen activity attains its maximum value where the noble metal content of the alloy is of maximum value. Since the noble metal content is highest at the metal - oxide interface and decreases across the subscale attaining bulk value at the subscale alloy interface, an oxygen pressure or oxygen activity gradient exists across the subscale. This activity gradient represents the driving force for internal oxidation. These conclusions are supported by experimental findings. The dissociation pressure of wustite in equilibrium with iron - nickel alloys increases with increasing nickel content[95, 104]. Also, the electron probe data of this investigation, Table VI, demonstrate that the nickel concentration is highest at the metal - oxide interface and decreases with distance through the subscale. Therefore, the oxygen activity gradient represents the driving force for internal oxidation of iron-nickel alloys.

Thomas[30] described the internal oxidation processes in terms of the inward diffusion of oxygen on its concentration gradient. For this concentration gradient to exist, it must be assumed that the solubility of oxygen increases with increasing noble metal content. In the theoretical section, it was demonstrated that this approximation is not valid for iron - nickel alloys, equation 4-35. The solubility of oxygen was shown to decrease with increasing nickel concentration on a purely thermodynamic basis. Accordingly, the binary diffusion equations of the Thomas model cannot be applied since the oxygen gradient would be directed toward the metal - oxide interface in the subscale region. This characteristic would require the impossible condition for the considered binary diffusion equations of up-hill diffusion of oxygen on a concentration gradient.

As described in the theoretical section, a different approach was taken in order to account for internal oxidation in the iron - nickel system, incorporating the principles of multicomponent diffusion. Using this analysis, the concentration gradients of other components and possible interactions between diffusing species are taken into account.

7.4.2 Subscale Morphology

For the model advanced in the theoretical section, equations were deduced for subscale penetration under the assumption that oxygen dissolved in the alloy phase and diffused into the matrix along a planar front. This implied that oxygen diffusivity in the grain boundaries was of the same order of magnitude as in the metal lattice, although examination of the subscale morphology illustrated that the grain boundary precipitation advanced beyond the lattice precipitation front, Fig. 28 to 30. This is believed to be a result of preferential nucleation at grain boundary sites and not indicative of a preferential grain boundary diffusion process.

There are several experimental observations which support the premise that oxygen diffuses inwards along a uniform front. Examination of iron - 30% nickel alloys oxidized in 50% carbon dioxide revealed that the depth of grain boundary penetration relative to the lattice penetration at 1000°C was equal to and in some areas greater than this ratio at 900°C, see Fig. 38 and Fig. 55. This would not be expected if a preferential grain boundary diffusion process was operative. Similar conclusions were made by Thomas[30] for copper - noble metal alloys.

Several attempts were made to reveal an oxygen concentration profile using microhardness and etching techneques. Significant phenomena were observed when cross-sections of oxidized specimens were etched in

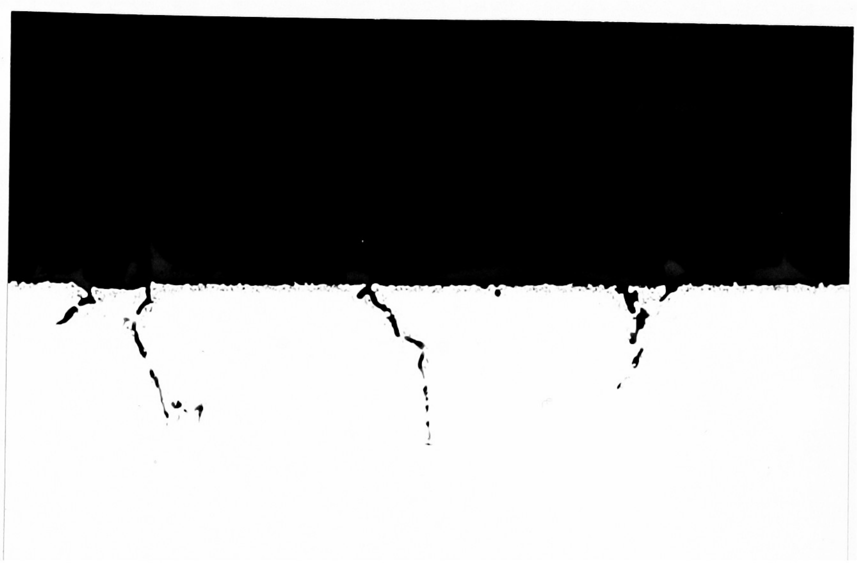

Fig.55. Fe-30%Ni alloy oxidized for 24 hrs. in 50% CO_2 at 900°C. 430X

aqueous ferric chloride. A high density band of etch pits appeared at depths beyond the grain boundary penetration in all specimens. A typical band structure is shown in Figs. 56 (a) and 56 (b). These etch pits would arise due to selective etching of alloy where dislocations intersect the surface. The large density of dislocations required for this type of pitting must be associated with the penetration of oxygen into the alloy since no other process is occurring at these observed depths. Confirmation for this viewpoint was obtained by showing that the motion of the band front followed a parabolic time dependence, Fig. 57. The parabolic rate constant for an iron - 30% nickel alloy oxidized in 50% carbon dioxide was determined to be 2.0 x 10^{-8}cm^2/sec which is the same order of magnitude of the diffusion coefficient for oxygen in iron which is approximatly 3 x 10^{-8}cm^2/sec.[41] Assuming that the pit band is associated with oxygen diffusion, its planar front offers confirmation to the assumption that oxygen diffuses inwards along a uniform front. Accordingly, grain boundary precipitation is not a result of preferential boundary diffusion.

Anslie[108] has reported a mechanism which will account for these observations. If an atom can diffuse both interstitially and substitutionally, the latter via a vacancy mechanism, the interstitials may diffuse ahead of the substitutionals and enter vacant lattice sites, creating an undersaturation of vacancies. Ainslie determined that small undersaturations can promote dislocation down climb with subsequent emission of vacancies in order to relieve the undersaturation. Therefore, in undersaturated regions, a high dislocation density results. These considerations have been shown to be valid for diffusion of sulphur in iron[108] and the mechanism is feasible in the present situation especially since oxygen is a large

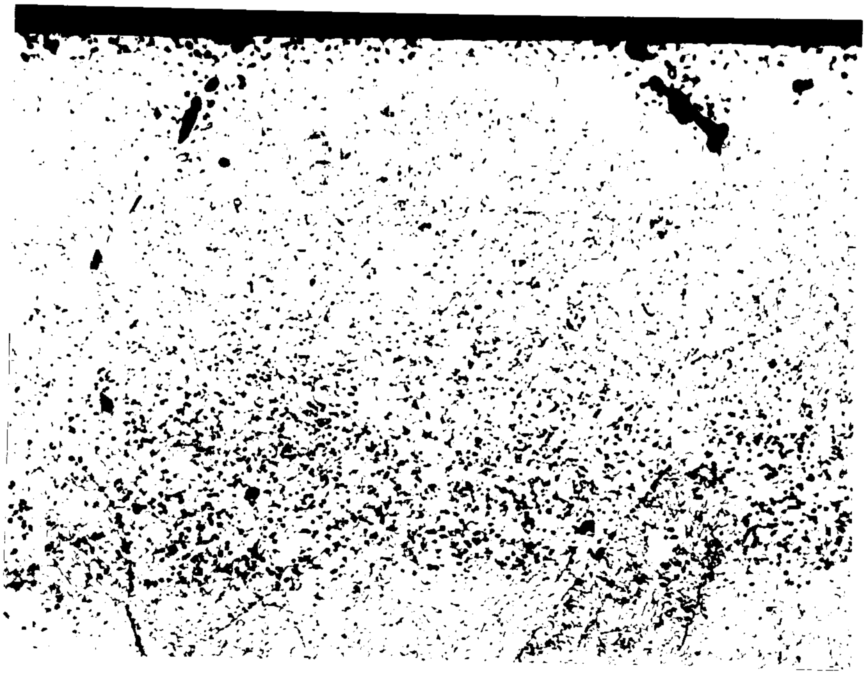

Fig.56(a). Etch pit band in an Fe-30%Ni alloy oxidized for 8 hrs. in 50% CO_2. 465X

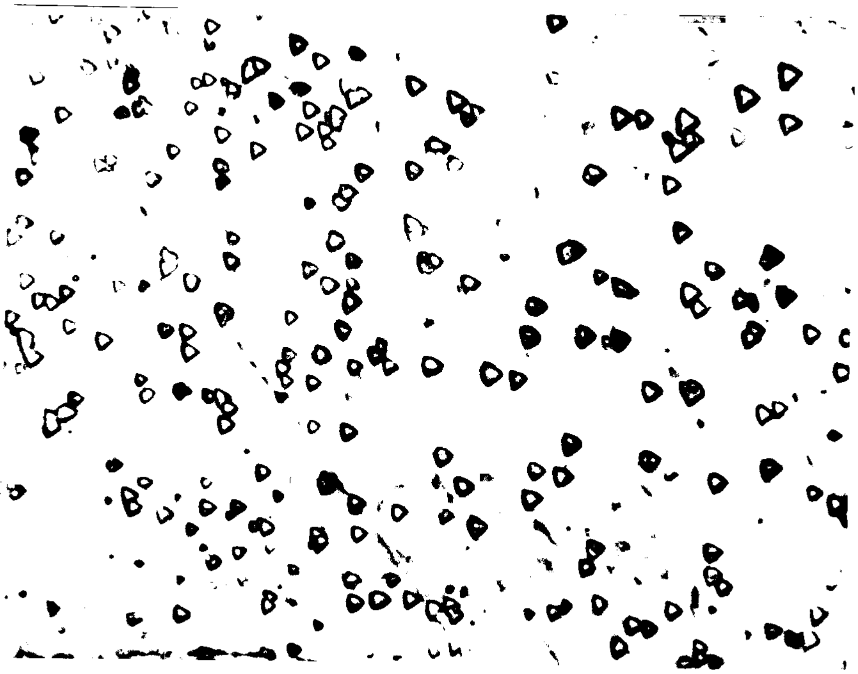

Fig.56(b). Etch pit morphology in Fig.56(b). 2300X

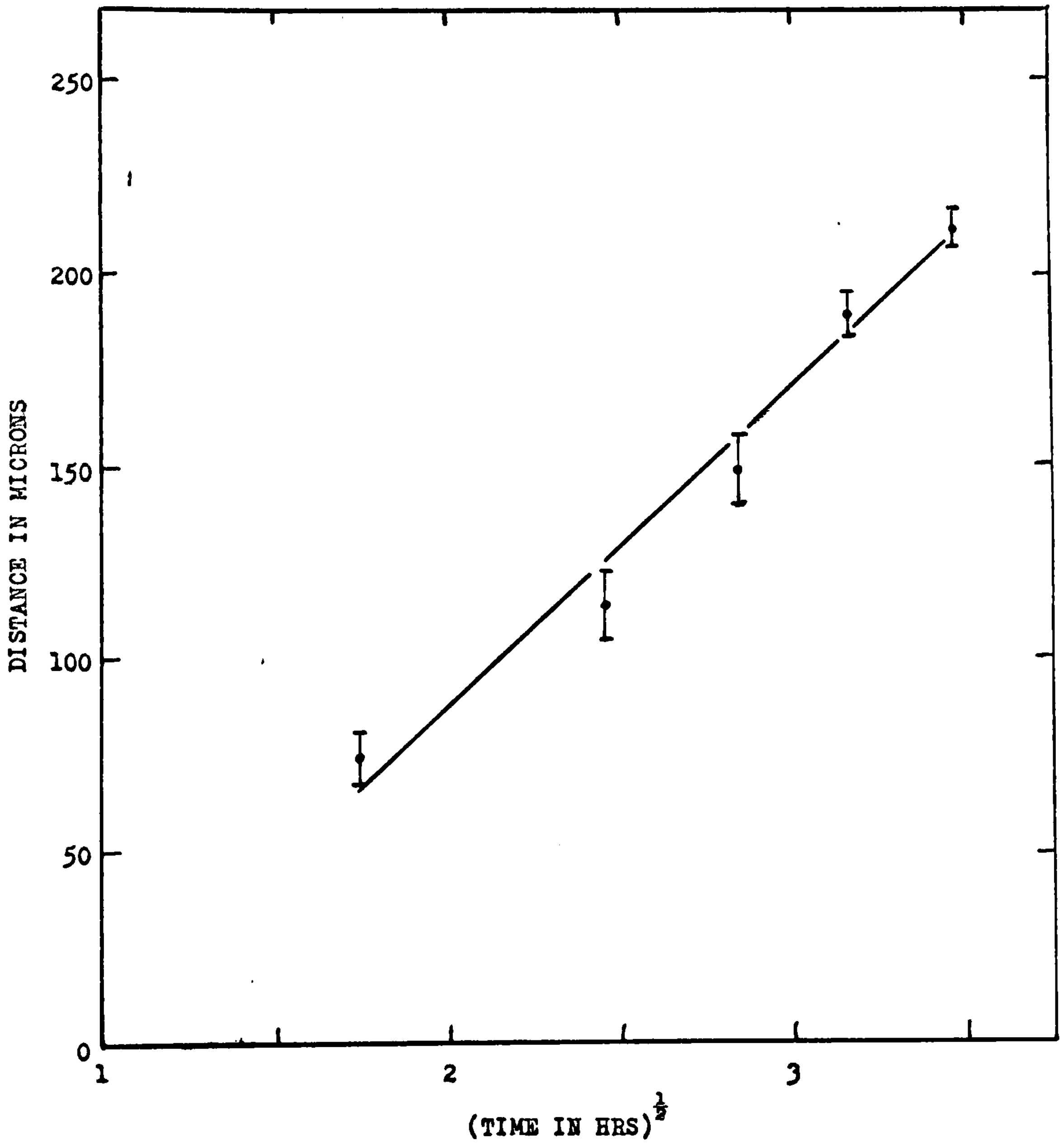

Fig.57. Etch pit band penetration rate for Fe-30%Ni alloy oxidized in 50% CO_2.

interstitial species. In view of these observations, it is assumed that oxygen penetrates the alloy uniformly and the preferential grain boundary precipitation is a nucleation effect. Lower supersaturation leads to precipitation of oxide at grain boundaries compared to that required to nucleate and precipitate oxide in the alloy lattice.

7.4.3 Generation of Supersaturation in Iron-Nickel Alloys

Equation 4-17 and equation 4-18 can be used to demonstrate that oxygen supersaturation is generated in the alloy as a result of the presence of the nickel gradient. When the degree of oxygen supersaturation is sufficient to satisfy the critical concentration product for nucleation, oxide is precipitated. That is, the nickel gradient establishes the alloy composition in a two phase region in the ternary iron - nickel - oxygen phase diagram. Substitution of appropriate values into equations 4-17 and 4-18 allows one to map the diffusion path on the ternary phase diagram. This is referred to as the virtual path by Kirkaldy[26].

Values for the various parameters can be obtained from the literature and electron probe data with the exception of the off-diagonal diffusion coefficient D_{12}. It is necessary in this instance to assume an approximate value. An estimated value of D_{12} was obtained by using the quantity of oxygen fluxed into the alloy to produce a given amount of oxide using equation 4-19, neglecting the oxygen term. In this manner, D_{12} was estimated to be 10^{-12} cm^2/sec.

A virtual path calculation was carried out for an iron-30% nickel alloy oxidized in 50% carbon dioxide. From the electron probe data, the concentration of nickel at the interface was .07 moles/cm^3, and the oxygen concentration was expressed as the ratio C_1/C_1^s where C_1^s is the saturation value at the interface. The saturation value for oxygen was taken to be 10^{-5} moles/cm^3. The diffusion coefficient of nickel in iron-nickel was taken from the data of O/gilvie,[109] and the oxygen coefficient from that of Bohnenkamp and Engell[41] and Schenck et al,[64] $D_{11} \sim 10^{-8} cm^2/sec$. In this calculation, it was assumed that the oxygen solubility is independent of alloy composition.

The calculated virtual path is shown in Fig.58. It can be seen that the diffusion path does enter the two phase wustite alloy region. Moreover, the oxygen profile at some given time before precipitation can be described by plotting the oxygen concentration versus distance from the metal - oxide interface, using equation 4-17. This profile is shown in Fig.59. It can be seen from this plot that oxide precipitation will occur to a greater depth at grain boundaries, as observed in the cross-sections, if the critical oxygen concentration required for nucleation is less for the grain boundary regions than the metal lattice. Thus the degree of supersaturation is influenced by the nickel concentration distribution whereas the depth of oxygen penetration is influenced by the oxygen diffusivity in the alloy phase. These two factors imply that the rate of subscale penetration into the alloy lattice is largely dependent upon the diffusivity of nickel and that rate of subscale formation along the grain boundaries is mainly dependent on the oxygen diffusivity.
The rate constants for lattice and grain boundary precipitation in the iron - 20% and 30% nickel alloys oxidized in 50% carbon dioxide reported in Table V and Fig.42, qualitatively agree with these considerations. These alloys were selected for detailed measurements since the precipitation fronts could be measured faily accurately, and the internal oxide did not occupy a large proportion

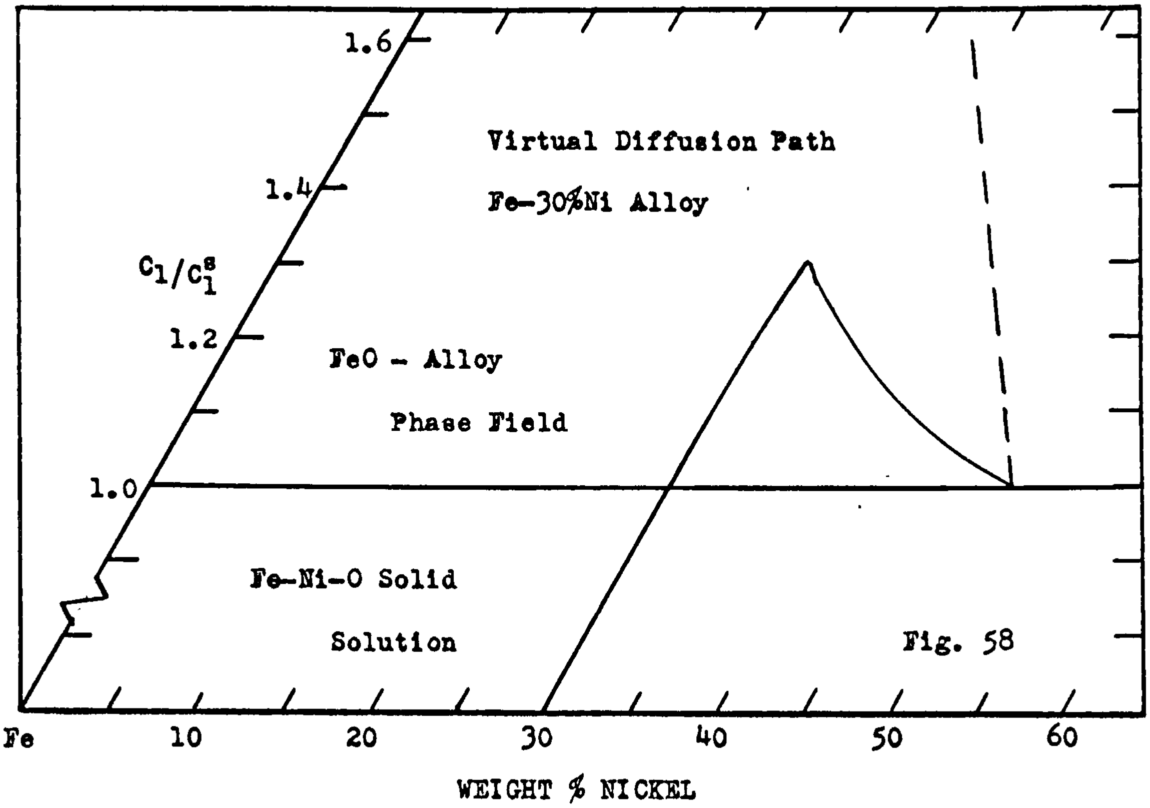
Virtual Diffusion Path
Fe-30%Ni Alloy
C_1/C_1^s
1.6
1.4
1.2
1.0
FeO - Alloy
Phase Field
Fe-Ni-O Solid
Solution
Fe
10
20
30
40
50
60
WEIGHT % NICKEL

Fig. 58

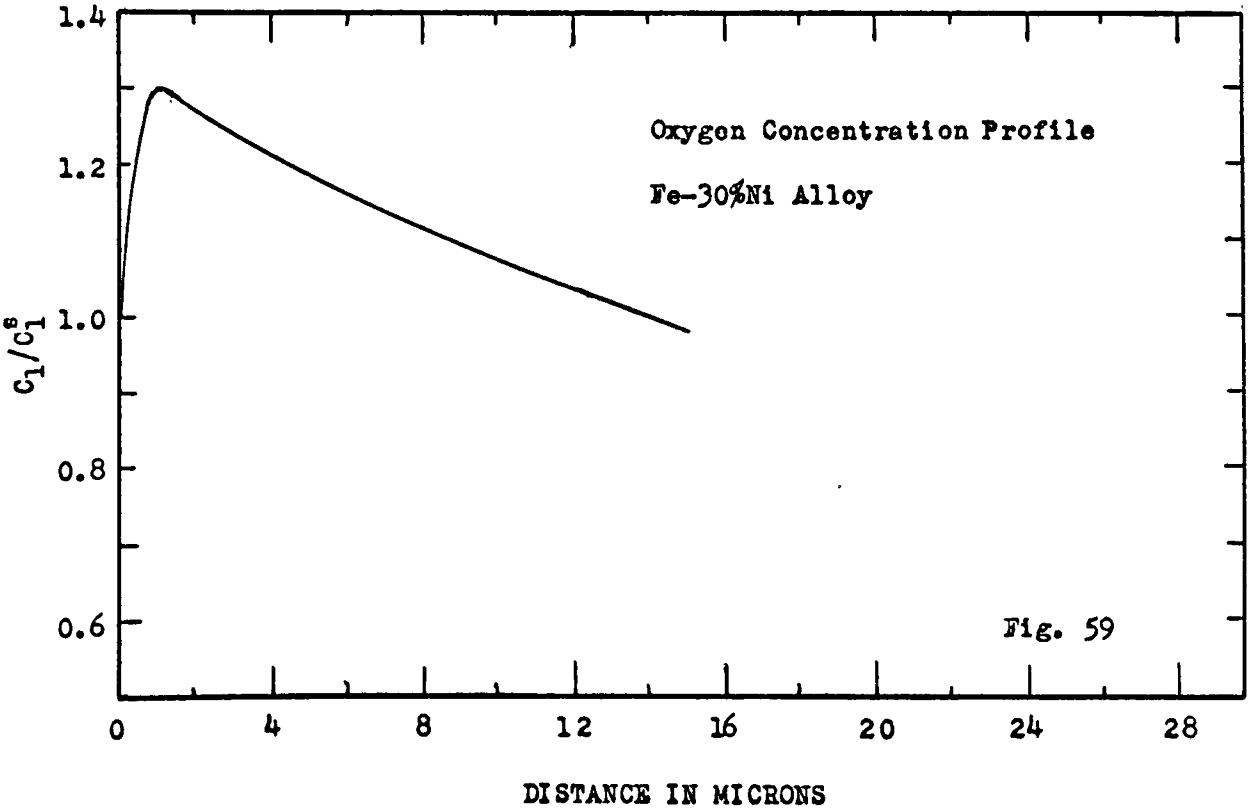
Oxygen Concentration Profile
Fe-30%Ni Alloy
C_1/C_1^s
1.4
1.2
1.0
0.8
0.6
0
4
8
12
16
20
24
28
DISTANCE IN MICRONS

Fig. 59

of the subscale region which is required by the theory, since it was assumed that precipitates do not interfere with diffusion processes.

7.4.4 Verification of the Theoretical Developments

In the theoretical section, expressions were developed to determine the amount of oxygen which diffuses into the alloy phase. This calculated amount of oxygen may be compared to that found experimentally to test the applicability of the multicomponent diffusion model.

The actual amounts of oxygen present as internal oxide in the iron - 20% and 30% nickel alloys oxidized in 50% carbon dioxide were determined from the experimental penetration curves given in Fig. 42. In both cases, the oxide particle size was uniform across the subscale and this phase represented approximately 20% of the volume. Neglecting the small variable concentration of wustite, the concentration of oxygen, C_o^{Fe} is 0.08 moles/cm^3 of wustite. The observed weight of oxygen is then,

$$W_o = 0.2 \; x \; C_o^{FeO} \; A \qquad 7\text{-}4$$

where x is the subscale thickness in cm., and A is the surface area considered. In the calculations $A = 1$ cm^2. Since the penetration of subscale follows a parabolic relationship, $x = \sqrt{K_p t}$,

$$W_o = 0.2 \; (K_p)^{\frac{1}{2}} \; C_o^{FeO} \; t^{\frac{1}{2}} \qquad 7\text{-}5$$

Utilizing the determinations of the parabolic constants from the penetration curves, experimental weights of oxygen as oxide in the alloys are,

$$W_o \; (20\% \; Ni) = 1.2 \times 10^{-7} \; t^{\frac{1}{2}} \; \text{moles/cm}^2/\text{sec}^{\frac{1}{2}} \qquad 7\text{-}6$$

and

$$W_o \; (30\% \; Ni) = 1.1 \times 10^{-7} \; t^{\frac{1}{2}} \; \text{moles/cm}^2/\text{sec}^{\frac{1}{2}} \qquad 7\text{-}7$$

As theoretically predicted, the rates of subscale penetration obey parabolic relationships. The above values for uptake of oxygen may now be compared to those obtained using equation 4-38 after appropriate substitution. Values previously given for the diffusion constants of oxygen and nickel were employed for D_{11} and D_{22}; C_{21} and N_2 were determined from the electron probe data, Table VI, assuming an alloy density of 8 gm/cm^3, $\mathcal{E}_{12}$ was estimated to be 10, on the basis that $D_{12}/D_{11} \simeq 10^{-4}$ and $D_{12}/D_{11} \simeq \mathcal{E}_{12} N_1$, where $N_1 = 2 \times 10^{-5}$.

The calculated values are,

$$W_o \text{ (20\% Ni)} = 0.2 \times 10^{-8} \; t^{\frac{1}{2}} \text{ moles/cm}^2/\text{Sec}^{\frac{1}{2}} \qquad 7\text{-}8$$

and

$$W_o \text{ (30\% Ni)} = 0.7 \times 10^{-9} \; t^{\frac{1}{2}} \text{ moles/cm}^2/\text{sec}^{\frac{1}{2}} \qquad 7\text{-}9$$

Utilizing equation 4-25, and assuming that the solubility of oxygen in the alloys is the same as pure iron and independent of nickel concentration the calculated values are,

$$W_o \text{ (20\% Ni)} = 0.9 \times 10^{-7} \; t^{\frac{1}{2}} \text{ moles/cm}^2/\text{sec}^{\frac{1}{2}} \qquad 7\text{-}10$$

and

$$W_o \text{ (30\% Ni)} = 0.9 \times 10^{-7} \; t^{\frac{1}{2}} \text{ moles/cm}^2/\text{sec}^{\frac{1}{2}} \qquad 7\text{-}11$$

It is apparent from these calculations, that the expression describing the solubility of oxygen in the alloys based on the Gibbs - Duhem relationship, equation 4-37, is a crude approximation. Agreement is better when it is assumed that the oxygen solubility approaches that for pure iron. The importance of the Gibbs - Duhem result is associated with equation 4-35, which predicts a decrease in oxygen solubility with increasing nickel contents.

Examination of Figs.36, 28, 29, and 30 illustrates that the amount of oxygen present as internal oxide decreased with increasing nickel concentration for a given gas composition. At surface compositions of 70% to 80% nickel the reduction in oxide concentration was quite dramatic. The difference in the nickel concentration gradient $(C_{21} - C_{20})$ decreases only slightly with increasing nickel concentration, Table VI. However, as a result of the reduction of the oxygen saturation concentration with nickel concentration, equation 4-35, this reduction in precipitation is expected. Oxygen solubility must decrease rapidly at nickel concentrations of the order of 70 - 80%.

For a given bulk nickel content and increasing carbon dioxide pressures, the amount of subscale increased; compare Fig.28 with 38. However, in these cases, the increase in precipitation is a result of an increase in the nickel gradient $(C_{21} - C_{20})$ in equation 4-25, as shown in Table VI.

Although numerous approximations were necessary, the theoretical relationships support the proposed mechanism of internal oxidation. To derive these relationships, it was assumed that the parameteres D_{12}, ε_{12}, D_{11}, D_{22} were independent of concentration, and that the nickel concentration gradient could be approximated to an error function relation. This latter consideration could not be examined because electron probe scans across the subscale illustrated that the precipitation reaction greatly modified the nickel profile in cases were there was copious precipitation. An error function solution was approached when the precipitation was minimized, such as in the case for the 50% nickel alloy oxidized in carbon dioxide, Fig.47.

7.4.5 Additional Features of Internal Oxidation

The above mechanism for internal oxidation is based on the influence of a nickel gradient on the penetration of oxygen into the alloy. Since specimens heated in carbon dioxide - carbon monoxide atmospheres at a potential just below that required for external oxidation did not oxidize internally, an experiment was designed to determine the effect of the presence of a steep nickel gradient in the alloy.

An approximately 3 micron layer of pure nickel was electroplated on an iron - 10% nickel alloy from a standard Watts solution. The specimen was exposed to a 50% carbon dioxide atmosphere for 10 hours. The result of this test is shown in the taper section in Fig.60. The nickel plate-alloy interface is visible in the micrograph. It is apparent that oxide has precipitated in the alloy phase behind this interface. This observation supports the argument that oxygen supersaturation in the presence of a nickel gradient attains the critical value required for oxide precipitation. However, this conclusion must be accepted with reservation because the oxygen potential in the nickel plate may be sufficiently high enough to oxidize this particular alloy. However, this latter consideration does not explain the occurrence of oxide as precipitates in the alloy. Accordingly, the observations may be regarded as additional tentative support for the conclusion that oxide precipitation in the alloy occurs in the presence of a nickel gradient.

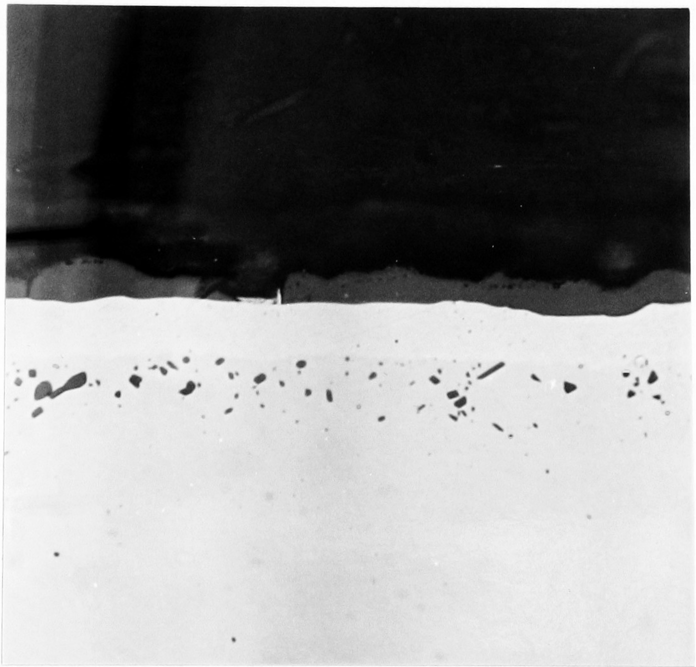

Fig.60. Ni - plated Fe - 10% Ni alloy exposed for 10 hrs. in 50% CO_2. 820X

CONCLUSIONS

1. Iron and iron - nickel alloys have been oxidized in carbon dioxide - carbon monoxide atmospheres at 1000°C. Linear reaction rates were observed for iron and alloys containing up to 50% nickel. Internal oxidation occurred in all alloys investigated. For alloys containing up to 50% nickel, wustite was the only oxide formed and its composition was dependent upon the nickel contents of the alloys. A spinel oxide formed on alloys containing greater than 50% nickel.

2. The basic postulates of a theoretical model previously advanced by Wagner for oxidation of these alloys were violated as a result of the occurrence of linear reaction rates and internal oxidation.

3. A kinetic equation was derived for linear oxidation of iron and iron - nickel alloys based on the assumption that dissociation of carbon dioxide at the oxide gas interface was the rate controlling reaction. Several equations reported in the literature to describe the linear oxidation kinetics of iron were shown to be equivalent to the derived equation.

4. The kinetic expression predicted a direct proportionality between the rate constant and partial pressure of carbon dioxide which was observed for pure iron and iron - 20, 30, and 40% nickel alloys.

5. Electron probe microanalytical analyses demonstrated the presence of large nickel gradients in the metal phase below the metal - scale interface of the iron - nickel alloys.

6. An internal oxidation model was presented based upon the principles of diffusion in multicomponent metallic systems to account

for the effects of metal concentration gradients at the alloy - oxide interface on oxygen solution and oxide precipitation in the alloys.

7. Equations, based on the above model, adequately described supersaturation of oxygen prior to precipitation of oxide and the amount of oxygen present as internal oxide.

8. Subscale morphologies were presented illustrating the preferential precipitation of oxide at grain boundaries. The internal oxidation model satisfactorily accounted for this effect, assuming that greater supersaturation was required for lattice precipitation compared to grain boundary oxide formation.

9. The rates of subscale formation at grain boundaries and within grains were dependent on the diffusivity of nickel and oxygen in the alloy phase.

10. Several fundamental parameters are required in order to test the theoretical relationships on a quantitative basis.

APPENDIX I

If gaseous diffusion of carbon dioxide is rate controlling, the oxidation rate will be given by the rate of transfer of gas to the oxide surface. Consider the largest observed oxidation rate, namely, for pure iron in carbon dioxide. From the linear rate constant, the oxygen uptake is $\frac{29 \times 10^{-3}}{16} \cdot \frac{1}{3600} = 5 \times 10^{-7}$ gm-atoms O/cm^2/sec. One gram - molecule of carbon dioxide supplies one gram - atom of oxygen according to,

$$CO_2 \rightarrow O + CO \qquad \text{A - 1}$$

The rate of carbon dioxide diffusion to the surface is given by, [111],

$$N_{CO_2} = \frac{D}{RTl} \cdot N_v \cdot (P_{CO_2} - P_{CO_2}^{i}) \qquad \text{A - 2}$$

where $N_v = 0.664 \left(\frac{lV\rho}{u}\right)^{0.5} \left(\frac{u}{\rho D}\right)^{0.33}$ and V, ρ, u are the gas velocity, density and viscosity respectively, D is the gaseous diffusion coefficient and l is the specimen length. Substituting appropriate values,

$$N_v = 0.664 \left(\frac{1.5 \times 0.6 \times 0.43 \times 10^{-3}}{450 \times 10^{-6}}\right)^{0.5} \left(\frac{450 \times 10^{-6}}{0.43 \times 10^{-3} \times 1.5}\right)^{0.33}$$

$$= 0.55$$

where $V_{max} = 2V_{average}$ has been substituted for the gas velocity. Therefore,

$$N_{CO_2} = \frac{1.5 \times 0.55 \times 0.75}{82.05 \times 1273 \times 1.5} = 3.9 \times 10^{-6} \text{gm-atoms O/cm}^2\text{/sec}$$

The oxidation rate should be 8 times larger than observed for the case of pure iron. The alloy oxidation rate is approximately 30 times less than pure iron, therefore, observed rates differ by 100-500 times.

APPENDIX II

In the internal oxidation model, it is assumed that the metal - oxide interface is stationary. This assumption is based on the premise that the volume of wustite precipitated in the alloy lattice compensates for the volume of iron reacted to form external oxide. The thicknesses of iron - 20% and 30% nickel alloy plates, oxidized in 50% carbon dioxide for various time intervals, are compared to the initial values in the table below. The initial dimensions, determined with a metric micrometer, are accurate to ± 15 microns. The final dimensions were obtained with a calibrated filar microscope eyepiece; the errors are the standard diviation.

ALLOY (wt% Ni)	TIME (hrs)	INITIAL THICKNESS (microns)	FINAL THICKNESS (microns)	INTERFACE MOVEMENT (microns)
20	6	650	616 ± 7	17
20	12	670	663 ± 6	3.5
20	24	580	552 ± 5	14
20	30	670	645 ± 2	13
30	3	660	624 ± 7	18
30	6	630	608 ± 8	11
30	10	650	625 ± 2	13
30	24	580	575 ± 5	2.5
30	30	610	590 ± 6	10

The results indicate that the metal - oxide interface recedes only during the initial stages of reaction; and then, it remains essentially stationary as oxidation continues. Assuming that a thin layer of oxide is formed prior to the precipitation of internal oxide, it is concluded that the interface recedes slightly as iron is selectively removed from the alloy; then, it becomes stationary as a result of subscale development.

APPENDIX III

Two kinetic experiments were carried out on an iron - 20% nickel alloy, in which argon was substituted for carbon monoxide. The results are reported graphically in Fig.27, page 87. The kinetic data can be adequately described by straight lines. The reaction rate decreases as the argon concentration is increased. It is concluded that the chemisorption model applies; and that the effect of argon is to dilute the oxidizing gas. Similar results have been reported for pure iron.[68]

BIBLIOGRAPHY

1. Hauffe, K., Oxydation von Metallen u. Metallegierungen, Berlin: Springer, 1956.

2. Kubaschewski, O., and Hopkins, B. E., Oxidation of Metals and Alloys, London: Butterworths, 1962.

3. Evans, U. R., The Corrosion and Oxidation of Metals, New York: St. Martin's Press, 1960.

4. Benard, J., Oxidation des Metaux, Paris: Gauthier - Villars, 1962 - 1964, (2 v.).

5. Wagner, C., von Baumback, H. H., and Dunwald, H., Z. Phys. Chem., (B), 22, 226 (1933).

6. Wagner, C., and Dunwald, H., Z Phys. Chem., (B), 22, 212 (1933).

7. Wagner, C., Hauffe, K., and Gundermann, J., Z. Phys. Chem., (B), 37, 148 (1937).

8. Pilling, N. B., and Bedwarth, R. E., J. Inst. Met., 29, 529 (1923).

9. Tammann, G., Z. anorg. Chem., 111, 78 (1920).

10. Wagner, C., and Gruenewald, K., Z. Phys. Chem., (B), 40, 455 (1938).

11. Cabrera, N., and Mott, N. F., Rep. Progr. Phys., 12, 163 (1948).

12. Hauffe, K., and Ilschner, B., Z. Electrochem., 58, 382 (1954).

13. Grimley, T. B., and Trapnell, B. M. W., Proc. Roy. Soc., (A), 234, 405 (1956)

14. Uhlig, H., Acta Met., 4, 541 (1956)

15. Wagner, C., Z. Phys. Chem., (B), 21, 25 (1933).

16. Wagner, C., Atom Movements, A.S.M., Cleveland, 1951, p.153.

17. Nagel, K., and Wagner, C., Z. Phys. Chem., (B) 25, 71 (1934).

18. Wagner, C., Z. Phys. Chem., (B), 32, 447 (1936).

19. Carter, R. E., and Richardson, F. D., Trans. A.I.M.E., 203, 336 (1955)

20. Turkdogan, E. T., McKewan, W. M., and Zwell, L., J. Phys. Chem. 69, 327 (1965).

21. Hoar, T. P., and Price, L. E., Trans. Faraday Soc., 34, 867 (1938).

22. Jost, W., Diffusion in Solids, Liquids and Gases, New York: Acedemic Press, (1952).

23. Smeltzer, W. W., Haering, R. R., and Kirkaldy, J. S., Acta Met. 9, 880 (1961).

24. Akram, K. H., and Smeltzer, W. W., Can. Met. Quart., 1, 41 (1962).

25. Clark, J. B., and Rhines, F. N., Trans. A.S.M. 51, 199 (1959).

26. Kirkaldy, J. S., and Brown, L. C., Can. Met. Quart., 2, 89 (1963).

27. Moreau, J. and Benard, J., Rev. Met., 59, 161 (1962).

28. Valensi, G., C. R. Acad. Sci., Paris, 203, 1252 (1936)

29. Wagner, C., J. Electrochem. Soc., 99, 369 (1952).

30. Thomas, D. E., J. of Metals, 3, 926 (1951).

31. Wagner, C., J. Electrochem. Soc., 103, 571 (1956).

32. Rapp, R. A., Acta Met., 9, 730 (1961).

33. Maak, F., Z. Metallk., 52, 538 (1961).

34. Smith, C. S., J. Inst. Metals 46, 49 (1931).

35. Blazey, C., ibid, 46, 353 (1931).

36. Frohlich, K. W., Z. Metallk., 28, 368 (1936).

37. Rhines, F. N., Trans. A.I.M.E., 137, 246 (1940).

38. Rhines, F. N., and Grobe, A. H., ibid, 147, 318 (1942).

39. Leroux, J. A. A. and Raub, E., Z. anorg. Chem., 188, 205 (1930).

40. Norbury, A. L., J. Inst. Metals, 39, 145 (1928).

41. Bohnenkamp, K., and Engell, H. J., Arch. Eisenhuttenw, 35, 1011 (1964).

42. Rhines, F. N., Johnson, W. A., and Anderson, W. A., Trans A.I.M.E., 147, 205 (1942).

43. Darken, L. S., ibid, 150, 157 (1942).

44. Meijering, J. L., and Druyvesteyn, M. J., Philips Res. Rep., 2, 81 (1947): 2, 260 (1947).

45. Wagner, C., Z. Elektrochem, 63, 772 (1959).

46. Bohm, G., and Kahlweit, M., Acta Met., 12, 641 (1964)

47. Paidassi, J., Trans A.I.M. E. 197, 1570 (1953).

48. Gulbransen, E. A., and Ruka, R., J. Metals N.Y. 188, 1500 (1950).

49. Gulbransen, E. A., and Hickman, J. W., Trans A.I.M.E. 171, 306 (1947).

50. Himmel, L. Mehl, R. F., and Birchenall, C. E., J. Metals, N.Y., 5, 827 (1953).

51. Davies, M. H., Simnad, M. T., and Birchenall, C. E., J. Metals, N. Y., 5, 1250, (1953): 3, 889 (1951).

52. Pfeil, L. B., J.I.S.I. 119, 501 (1929): 131, 237 (1931).

53. Engell, H. J., Arch. Eisenhuttenw., 28, 109 (1957).

54. Marion, F., Docum. metall., 24, 87 (1955).

55. Darken, L. S., and Gurry, R. W., J. Am. Chem. Soc., 67, 1398 (1945).

56. Kubaschewski, O., and Brasher, D. M., Trans. Faraday Soc., 55, 1200 (1959).

57. Moreau, J. and Cagnet, M., Rev. Metall., 55, 1091 (1958).

58. Vernon, W. H. J., Calnan, E. A., Clews, C. J. B., and Nurse, T. J., Proc. Roy. Soc., (A), 216, 375 (1953).

59. Paidassi, J., Acta Met., 6, 184 (1958).

60. Winterbottom, A. B., J.I.S.I., 165, 9 (1950).

61. Stanley, J. K., von Hoene, J., and Huntoon, R. T., Trans. A.I.M.E., 43, 426 (1951).

62. Portevin, A., Pretet, E., and Jolivet, H., Rev. Metall., 31, 101, 186, 219, (1934).

63. Paidassi, J., Ing. guim., 10, 5 (1951).

64. Schmahl, N. G., Baumann, H., and Schenck, H., Arch. Eisenhuttenw. 29, 147 (1958).

65. Fischbeck, K., Neundeubel, L., and Salzev, F., Z. Elektrochem. u. angew. physik. Chem. 40, 517 (1934).

66. Hauffe, K., and Pfeiffer, H., Z. Metallk, 44, 27 (1953).

67. Pfeiffer, H., and Laubmeyer, C., Z. Elektrochem., 59, 579 (1955).

68. Pettit, E., Yinger, R., and Wagner, J. B. Jr., Acta Met., 8, 617 (1960).

69. Kobayaski, H., and Wagner, C., J. Chem. Phys., 26, 1609 (1957).

70. Smeltzer, W. W., Trans. A.I.M.E., 218, 674 (1960).

71. Kubaschewski, O., and von Goldbeck, O., Z. Metallk., 39, 158 (1948).

72. Gulbransen, E. A., and Andrew, K. F., J. Electrochem. Soc., 104, 451 (1957).

73. Moore, W. J. and Lee, J. K., Trans. Faraday Soc., 48, 916 (1952).

74. Moore, W. J., and Lee, J. K., J. Chem. Phys. 19, 255 (1951).

75. Sartell, J. A., and Li, C. H., J. Inst. Met., 90, 92 (1961 - 1962). Trans. A.I.M.E., 221, 158 (1962).

76. Wlodek, S. T., Rep. R62FPD140, G. E. Co., Erandale, Ohio.

77. Engle, H. J., Hauffe, K., and Ischner, B., Z. Elektrochem, 58,

478 (1954).

78. Uhlig, H., Pickett, J., and MacNairn, J., Acta Met. 7, 111, (1959).

79. Braber, M. J. and Birchenall, C. E., Corrosion, 14, 179t (1958).

80. Foley, R. T., J. Electrochem. Soc., 109, 1202 (1962).

81. Scherl, E., and Kiwitt, K., Arch. Eisenhuttenw., 3, 405, (1936).

82. Sachs, K., J.I.S.I., 185, 348 (1957).

83. Sachs, K., Metallurgia, 54, 109 (1956).

84. Stead, J. E., J.I.S.I., 94. 243 (1916).

85. Foley, R.T., and Guare, C. J., J. Electrochem Soc., 106, 936 (1959).

86. Foley, R.T., Dreck, J. U., and Fryxell, R. E., ibid, 102, 440 (1955).

87. Foley, R.T., Guare, C. J. and Schmidt, H. R., ibid, 104, 413 (1957).

88. Foley, R. T., ibid, 108, 216 (1961).

89. Foley, R. T., ibid, 109, 278 (1962).

90. Kennedy, J. W., Calvert, L. D., and Cohen, M., Trans. A.I.M.E., 215, 64 (1959).

91. Yearian, H. J., Boren, H. E., Jr., and Warr, W. E., Corrosion, 12, 561t (1956).

92. Koh, P. K., and Caugherty, B., J. Appl. Phys., 23, 427 (1952).

93. Benard, J. and Moreau, J., Rev. Met., 47, 317 (1950).

94. Brabers, M. J., Heickeger, W. J., and Birchenall, C. E., Chimie Physique, 53, 810 (1956).

95. Roeder, G. A., and Smeltzer, W. W., J. Electrochem. Soc., 111, 1074 (1964).

96. Onsager, L., Ann. N.Y., Acad. Sci., 46, 241 (1945).

97. Kirkaldy, J. S., Can. J. Phys., 36, 907 (1958).

98. Kirkaldy, J. S., ibid, 35, 435 (1957).

99. Purdy, G. R., private communication.

100. Kitchener, J. A., Bockris, I. O. M., Gleiser, M., and Evans, I. W., Acta Met. 1, 93 (1953).

101. Kirkaldy, J. S., and Purdy, G. R., Can. J. Phys. 40, 208 (1962).

102. Samuels, L. E., J. Inst. Metals, 81, 471 (1952 - 1953), 85, 51 (1956 - 1957).

103. Birks, L. S., Electron Pobe Microanalysis N.Y./London, Interscience 1963.

104. Bryant, P., and Smeltzer, W. W., To be published.

105. Levin, R. L., and Wagner, J. B. Jr., Trans. A.I.M.E., 233, 159 (1965).

106. Wood, G. C., Hobby, M. G., and Vaszko, B., J.I.S.I., 202, 685 (1964).

107. Wagner, C., Thermodynamics of Alloys, Addison - Wesley, (1952), p.53.

108. Ainslie, N. G., Hoffman, R. E., and Seybolt, A. U., Acta Met., 8, 523 (1960).

109. Goldstein, J. I., Hanneman, R. E., and Ogilvie, R. E., Trans. A.I.M.E. 233, 812 (1965).

110. Kirkaldy, J. S., private communication.

111. Schlichting, H., Boundary Layer Theory, (translation by J. Kestin), McGraw-Hill Book Co., N.Y., 1960.